17 *B*-physics

17.1 Introduction

The rate of *B*-hadron production at the LHC is enormous thanks to the large hadronic cross-section for *b*-quark production and the high luminosity of the machine ($L = 10^{33}\,\mathrm{cm}^{-2}\mathrm{s}^{-1}$ even at so-called low luminosity). About one collision in every hundred will produce a *b*-quark pair, which is a considerably better signal-to-noise ratio than at lower-energy hadron machines such as the Tevatron. In ATLAS, an inclusive-muon trigger with a p_{T} threshold of 6 GeV will make an initial selection of *B*-events. Using this inclusive selection, about 25% of the muon-trigger events will contain *b*-quarks. In the first year of operation, some $2.3\text{x}10^{10}$ *b*-quark pair events will be selected for more detailed analysis in the LVL2 trigger and event filter, that are focused on the selection of specific classes of final states. This event rate will be higher than in any accelerator presently operating, or in any accelerator in operation before the start-up of the LHC.

Although the main focus of the ATLAS physics programme is the search for and study of physics beyond the Standard Model, through the production and decay of new types of particles, an important range of *B*-physics studies is planned, as discussed in this Chapter. In fact, an important aim of the *B*-physics work is to test the Standard Model through precision measurements of *B*-hadron decays that together will over-constrain the CKM matrix, possibly giving indirect evidence for new physics. This programme of work will include the following: precise measurements of *CP* violation in *B*-meson decays, which in the Standard Model is due to a single phase in the CKM matrix; precise measurements of the periods of flavour oscillations in B_s^0 as well as B_d^0 mesons, and of relative decay rates – such measurements constrain the elements of the CKM matrix; searches for and measurements of very rare decays which are strongly suppressed in the Standard Model and where significant enhancements could provide indirect evidence for new physics. Many of the ATLAS measurements will be more precise than those from experiments at lower-energy machines, thanks to the greater available statistics.

At the LHC, the general-purpose experiments ATLAS and CMS will face stiff competition from LHCb, which is a dedicated *B*-physics experiment. However, even though a dedicated experiment can be better optimised for certain event types, ATLAS will be competitive in several channels. ATLAS will thus play an important role in maximising the combined precision of *B*-physics measurements from the LHC.

In the following, the *B*-physics potential of ATLAS is presented. The remainder of this section introduces the framework concerning the production and triggering of *B* hadrons. Section 17.2 discusses *CP*-violation measurements in a number of channels, and also addresses the decay channel $B_s^0 \to J/\psi\phi$ more generally, including a discussion on the measurement of $\Delta\Gamma_s$. B_s^0-oscillation measurements provide information complementary to the *CP*-violation measurements, and the capabilities of measuring the oscillation parameter are described in Section 17.3. Rare decays of the type $B \to \mu\mu(X)$ are described in Section 17.4, and finally, other precision measurements are briefly discussed in Section 17.5.

17.1.1 General features of beauty production in ATLAS

ATLAS will observe decays of *B* hadrons, that are centrally produced in proton–proton collisions at 14 TeV centre-of-mass energy. Events will be selected initially by an inclusive-muon trigger with a p_T threshold of 6 GeV in the pseudorapidity range $|\eta| < 2.4$. Further selections at the trigger level focus on specific final states. For the selected events, the Bjorken *x*-variable of the colliding partons will be between 10^{-4} and 10^{-1} – this range is an order of magnitude broader than in collider experiments at the Tevatron. The mean value of the *B*-hadron transverse momentum with respect to the beam in the statistically dominant channels is 16 GeV or more, which is high enough to justify the perturbative QCD approach [17-1]. At the phenomenological level, the role of higher-order corrections to *b*-quark production may be understood in terms of additional production mechanisms, such as flavour excitation and parton showering [17-2].

At the LHC, many studies can be made of *B*-hadron production. Measurements include *b*-jet differential cross-sections, differential cross-sections of single particles in *b*-jets, production asymmetries, production polarisation, b–$\bar{b}$ correlations, $b\bar{b}g$ final states, doubly-heavy-flavoured hadrons, double *b*-quark-pair production, and prompt J/ψ production. The *B*-hadron production features are discussed in more detail in Chapter 15. It is worth noting that the *B*-production cross-section is not well understood at the phenomenological level, and that predictions are uncertain to a factor of two or more.

17.1.2 Model used for simulation studies

About 1.5 million *B*-hadron events have been simulated using the PYTHIA 5.7 and JETSET 7.4 programs [17-3] for event generation. The flavour-creation, flavour-excitation and gluon-splitting production mechanisms of *b*-quarks were included. The simulations were performed with the CTEQ2L set of parton-distribution functions and the default set of PYTHIA parameters, the most important ones being the *b*-quark mass ($m_b = 5$ GeV) and the factorisation scale ($\mu = p_T^{\text{hard}}$). The fragmentation of *b*-quarks to *B*-hadrons was simulated according to the Peterson function with $\varepsilon_b = 0.007$, as supported by LEP measurements. The choice of parameters was motivated by the fact that the corresponding simulation results reproduce the *b*-quark production cross-section at the Tevatron [17-4].

The total $b\bar{b}$ cross-section is not well defined in PYTHIA when one includes processes other than the lowest-order one for $b\bar{b}$ production, since PYTHIA takes the partons to be massless, and therefore the cross-section diverges when the transverse momentum approaches to zero. However, what is relevant for ATLAS is the part of the cross-section that passes the trigger – this is 2.3 μb when the $b\bar{b}$ events are triggered requiring a muon with $p_T > 6$ GeV and $|\eta| < 2.4$.

About 30% of all the generated events were processed with a detailed detector-simulation program (the remaining events were used for larger-statistics studies using a parametrisation of the detector performance). The simulation software, based on the GEANT 3 package and described in [17-5], was used to simulate the detector response. For most of the events, only the Inner Detector was simulated, since the analyses rely mostly on charged particles reconstructed in the Inner Detector. For the *B*-physics studies presented in this chapter, pile-up (average 2.3 events at low luminosity) was not included in the simulation unless stated explicitly.

Information about particles resulting from all types of secondary interactions inside the Inner Detector was stored if the energy of the incident particle was above 300 MeV (10 MeV for bremsstrahlung). Also, information was stored on particle decays anywhere in the ATLAS detector for use in the study of background muons coming from decays of charged kaons and pions.

Backgrounds which require large rejection factors in the analysis were simulated using a fast Monte Carlo simulation program [17-6]. This included a parametrisation of the detector performance, which was tuned to reproduce the results from reconstruction of fully simulated *B*-physics events in the Inner Detector [17-7]. More detailed information about the production and data samples is given in [17-8].

17.1.3 Trigger

The triggers for *B*-physics studies are described in Chapter 11 and more details can be found in [17-9]; only a brief description is given here.

As indicated above, the LVL1 trigger for all *B*-physics studies in ATLAS will be an inclusive muon trigger, with a transverse-momentum threshold of 6 GeV in the pseudorapidity range $|\eta| < 2.4$. At LVL2, the LVL1 muon is first confirmed before proceeding to a track search in the Inner Detector. The cross-section for $b\bar{b}$ events passing this initial stage of the LVL2 trigger is 2.3 μb. Note that the LVL1 trigger muon, which must be confirmed at LVL2, may come either from the *B*-decay of interest, or from the decay of the other *B*-hadron in the event.

At LVL2, ATLAS expects to trigger on both $J/\psi \to \mu\mu$ and $J/\psi \to ee$. In the case of $J/\psi \to \mu\mu$, the LVL1 trigger muon may come from the J/ψ or from the decay of the other *B*-hadron in the event. A trigger on $J/\psi \to \mu\mu$ may be achieved by requiring a second muon of $p_T > 3$ GeV, using information from the muon chambers in the end-cap and from the Tile hadronic calorimeter in the barrel. The feasibility of such a trigger over the full $|\eta| < 2.5$ region is currently under study. Using the muon chambers alone, it would be possible to trigger over the whole $|\eta| < 2.5$ region down to a p_T threshold of 5 GeV. In the $B_d^0 \to J/\psi\, K_S^0$ analysis, results will be presented for both trigger-threshold possibilities. The dimuon trigger covers rare *B*-decays, $B_{d,s} \to \mu\mu(X)$, in addition to the numerous final states containing J/ψ that are considered in the study of *CP* violation and other topics. With $J/\psi \to \mu\mu$ giving the LVL1 trigger muon, the event may be selected if there is a $p_T > 5$ GeV electron identified at LVL2, even if the second muon from the J/ψ does not pass the LVL2 selection. Such events are useful for *CP*-violation studies with electron tagging; the second muon from the J/ψ decay can be reconstructed in the event filter with relaxed cuts.

The trigger on $J/\psi \to ee$ is implemented at LVL2, using information from the Inner Detector and, in particular, relying on the electron–hadron separation provided by the TRT (see Chapter 10 of [17-9]). With this technique, it will be possible to use an electron p_T threshold of 0.5 GeV (the minimum track p_T reconstructible in the Inner Detector). The $J/\psi \to ee$ events will always be required to contain the LVL1 trigger muon in addition to the J/ψ.

$B^0 \to \pi^+\pi^-$ candidates are searched for at LVL2 by combining pairs of opposite-charge particles with $p_T > 4$ GeV, requiring the sum of p_T moduli to be above 10 GeV and the invariant mass of the pair to be in the range 4.5–6.5 GeV. The distance of both pions to the triggering muon should satisfy $\Delta R > 0.4$ to reject candidates with one or both pions belonging to the trigger *B*-jet. The option of lowering the minimum pion p_T to increase the event yield is being studied. With the

minimum pion p_T set to 1.5 GeV, the acceptance for signal events would triple. However, additional trigger requirements, such as a cut on the transverse impact parameter, would be needed to maintain an acceptable trigger rate.

For all the channels considered for the measurement of Δm_s, the LVL2 trigger is a D_s^- mass trigger. The baseline is to use the decay mode $D_s^- \rightarrow \phi^0 \pi^-$. This is done by considering combinations of oppositely charged tracks and applying kaon hypotheses to reconstruct the ϕ^0. The D_s^- is subsequently reconstructed from combinations of ϕ^0 with another track, applying a pion hypothesis. It would be possible to use the decay mode $D_s^- \rightarrow K^{*0} K^-$ as well, but since the K^{*0} is a much wider resonance than the ϕ^0, and pion–kaon separation is not available, the p_T thresholds for the particles would have to be raised to a point where the increase in statistics for the Δm_s measurement would be marginal.

After the LVL2 trigger, more refined selections can be made in the event filter, relying on improved track-reconstruction performance for making selections based, for example, on invariant-mass and vertexing cuts.

17.2 *CP*-violation studies

17.2.1 Overview

Within the Standard Model, *CP* violation in weak decays is introduced by the phase of the CKM quark-mixing matrix. The unitarity of the CKM matrix can be used to derive triangle relations between the matrix elements. The unitarity relation,

$$V_{ub}^* V_{ud} + V_{cb}^* V_{cd} + V_{tb}^* V_{td} = 0$$

provides the so-called unitarity triangle. The angle α is opposite to the side $V_{cb}^* V_{cd}$, β is opposite to the side $V_{ub}^* V_{ud}$ and γ is opposite to the side $V_{tb}^* V_{td}$. These angles can be measured, for example, in neutral B decays to final states f which can be reached by both B^0 and $\overline{B}^0$. Due to *CP* violation, the rates of B^0 and $\overline{B}^0$ decays are different, resulting for some decay modes in a measurable asymmetry A, defined as:

$$A(t) = \frac{N(\overline{B}^0 \rightarrow f)(t) - N(B^0 \rightarrow f)(t)}{N(\overline{B}^0 \rightarrow f)(t) + N(B^0 \rightarrow f)(t)} = a\cos(\Delta m t) + b\sin(\Delta m t), \qquad 17\text{-}1$$

where a is the direct *CP*-violation amplitude, b is the mixing-induced *CP*-violation amplitude and Δm is the mass difference of the $B^0 - \overline{B}^0$ system. B^0 and $\overline{B}^0$ refer to the B-flavours at production, which must be determined using tagging techniques. In the simplified case of pure mixing-induced *CP* violation, the asymmetry reduces to

$$A(t) = b\sin(\Delta m t) .$$

An important consideration of many *CP*-violation studies, and also for B^0-oscillation measurements, is the determination of the flavour of a B-hadron at production; this is referred to as flavour tagging and various methods are available as discussed below. Limitations in the tagging purity, as well as the presence of background, dilute the observed asymmetry, and this must be

taken into account in the analysis. Also, in proton–proton collisions, B and $\overline{B}$ hadrons are produced with different probabilities. This production asymmetry, which has been estimated to be of the order of 1% or less, has to be subtracted from the measured asymmetry.

Considering the simplified example of pure mixing-induced *CP* violation in the case of B_d^0 decays where the oscillation period is comparable with the lifetime, the time-integrated asymmetry can also be used for *CP*-asymmetry measurements ('event counting'). Starting from the expression $A(t) = b\sin(\Delta m t)$, the time-integrated asymmetry is $A = D_{int} b$, where $D_{int} = x/(1+x^2)$ is the dilution factor due to integrating over time from $t = 0$ and $x = \Delta m/\Gamma$. Note that, in contrast to experiments at e^+e^- machines where B-mesons are produce via Υ(4S) decays, the time-integrated asymmetry is non-zero. Taking into account the other dilution factors, the observable asymmetry is

$$A^{obs} = D_{tag} D_{back} (D_{int} b + A^P),$$

where D_{tag} is the dilution factor from tagging ($D_{tag} = 1 - 2\omega_{tag}$, where ω_{tag} is the wrong-tag fraction), and D_{back} is the dilution factor from background ($D_{back} = N_S/(N_S+N_B)$, where N_S and N_B are the numbers of signal and background events, respectively). A^P is the production asymmetry. Using the formula above, the statistical error on the *CP*-violation parameter b is:

$$\delta b \approx \frac{1}{D_{tag} \cdot \sqrt{D_{back}} \cdot D_{int} \cdot \sqrt{N_S}} \qquad 17\text{-}2$$

17.2.2 Measurement of asymmetry in $B_d^0 \to J/\psi K_S^0$

The measurement of the time-dependent *CP*-violating asymmetry in the decay $B_d^0 \to J/\psi K_S^0$ can provide a clean measurement of the angle β of the unitarity triangle. To a very good approximation, the Standard Model prediction for the asymmetry in this channel is given by:

$$A(t) = \sin 2\beta \sin(\Delta m_d t)$$

where Δm_d is the mass difference in the $B_d^0 - \overline{B_d^0}$ system. The predicted asymmetry is insensitive to the contribution from penguin diagrams. This makes the $B_d^0 \to J/\psi K_S^0$ decay the so-called gold-plated mode to measure the angle β.

The $B_d^0 \to J/\psi K_S^0$ decay, with $J/\psi \to \mu\mu$ or $J/\psi \to ee$, and $K_S^0 \to \pi^+\pi^-$, is also experimentally very clean, and data samples can be reconstructed with relatively low background. It is worth noting that, recently, the CDF Collaboration has measured $\sin 2\beta = 0.79^{+0.41}_{-0.44}$ (stat+syst), using a sample of about 400 events collected during the Run 1 Tevatron data-taking period [17-10]; the error is dominated by the statistical contribution. This demonstrates the feasibility of analysing this channel in the environment of a hadron collider. The current Standard Model best estimate of the unitarity triangle gives $\sin 2\beta = 0.725^{+0.055}_{-0.060}$ [17-11]. Several experiments are expected to make measurements of sin2β before LHC starts operation; for example BaBar expects to achieve a precision of about 5% [17-12]. However, as discussed below, ATLAS should be able to make a considerably more precise measurement of this parameter.

In the following, the analysis using various tagging methods for the $J/\psi \to \mu\mu$ and $J/\psi \to ee$ samples is discussed. Due to the LVL1 trigger requirement, the $J/\psi \to ee$ events must also contain a muon candidate with $p_T > 6$ GeV and $|\eta| < 2.4$, as discussed in Section 17.1.3. This muon, which usually comes from the decay of the second b-quark in the event, can be used to tag the

flavour of the B_d^0 at production. For $J/\psi \to \mu\mu$, the trigger muon may come either from the decay of the second *b*-quark in the event or from the J/ψ decay. In the former case, the muon may be used to tag the flavour of the B_d^0 at production, as for $J/\psi \to ee$. In the latter case, additional tagging methods can be used to enhance the statistics and provide valuable cross-checks of systematics. As discussed in Section 17.2.2.4 below, the additional methods of tagging that can be used are electron tag, *B*–π tag and jet-charge tag.

17.2.2.1 *J/ψ* reconstruction

The reconstruction of J/ψ decays was investigated using samples of $B_d^0 \to J/\psi K_s^0$ events, generated with PYTHIA in both J/ψ decay channels considered, and fully simulated with GEANT. The events were generated as explained in Section 17.1.2 and include the underlying event as simulated by PYTHIA; no additional pile-up events were added for this analysis. Studies have not yet been performed to evaluate the feasibility of continuing the analysis of this channel after the initial running at low luminosity, *i.e.* at luminosities above $10^{33}\,\mathrm{cm}^{-2}\mathrm{s}^{-1}$. Offline cuts on the transverse momenta of the leptons from the J/ψ decay are the same as those imposed by the LVL1 and LVL2 thresholds described in detail above. Track reconstruction in the entire Inner Detector was performed using the xKalman algorithm (see Section 3.1.2). For the $J/\psi \to ee$ case, a special electron fit option was used in xKalman: for identified electrons, the reconstruction program included, directly in the track-fitting procedure, a correction for possible energy losses due to bremsstrahlung.

Pairs of opposite-charge electrons or muons were fitted to a common vertex and their invariant mass calculated. Successful fits (χ^2 / d.o.f.<6) were retained and, for the muon case, an invariant-mass cut with a $[-3\sigma, +3\sigma]$ window around the nominal *J/ψ* mass was applied. For the electron case, the window was set to be asymmetric in order to take into account the bremsstrahlung energy losses that create a long tail at small invariant masses. This energy loss depends on the amount of material traversed by the electrons and is larger in the end-cap than in the barrel region of the Inner Detector. To take this into account, the mass window was set to $[-5\sigma, +3\sigma]$ ($[-7\sigma, +3\sigma]$) if the J/ψ was produced within the range $|\eta| < 0.7$ ($|\eta| > 0.7$). Finally, the transverse decay length of the reconstructed J/ψ was required to be greater than 250 μm.

For events passing the LVL1 trigger requirement (muon with $p_T > 6$ GeV in $|\eta| < 2.4$), the J/ψ reconstruction efficiency is about 50% in the electron channel and 80% in the muon channel (LVL2 trigger muon threshold at 3 GeV). These figures do not include the lepton trigger and identification efficiencies (see Section 17.2.2.3). The lower reconstruction efficiency in the electron channel is due to bremsstrahlung energy-loss effects causing the electrons to be lost in the reconstruction and causing the J/ψ to fail some of the cuts (mainly the mass-window cut). Further optimisation is needed, both in the track-reconstruction phase and in the selection cuts, to improve the efficiency for reconstructing J/ψ.

The invariant-mass distributions for the electron and muon case are shown in Figures 17-1 and 17-2, respectively. The distributions include only events in which the two reconstructed leptons have been successfully matched with the true generated leptons from J/ψ decay. The resolutions were estimated to be about 40 MeV (muons) and 60 MeV (electrons). For the electron case, the resolution was estimated by fitting only the symmetric core of the distribution.

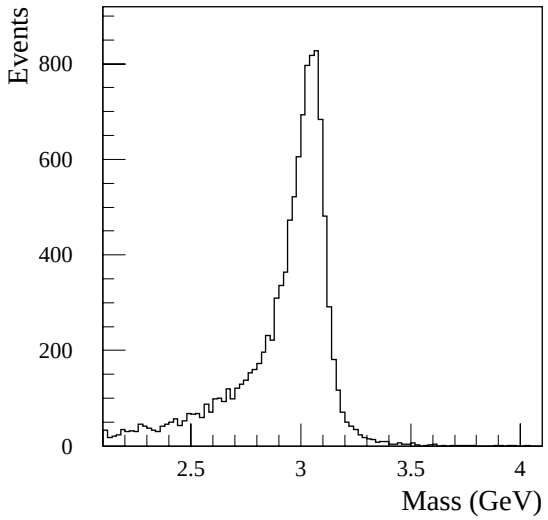

Figure 17-1 Invariant-mass distribution of $J/\psi \to ee$ (signal only).

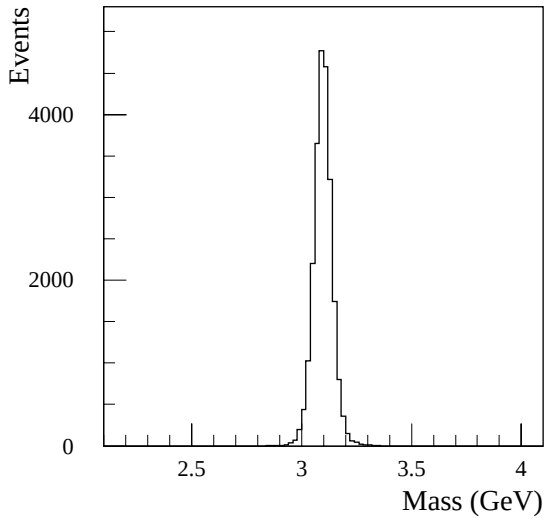

Figure 17-2 Invariant-mass distribution of $J/\psi \to \mu\mu$ (signal only) for events with the LVL2 trigger muon p_T threshold at 3 GeV.

The reconstructed resolution obtained for electrons from full simulation was parametrised as a function of $|\eta|$ and p_T in the fast simulation program ATLFAST. This provides a fast simulation description for background analyses. Since the distributions are non-Gaussian due to interactions in the Inner-Detector material, they were parametrised based on the location of a single hard bremsstrahlung, chosen at random from the appropriate distribution. The parametrisation gave the five fitted track parameters and the correlation matrix. The agreement between the full and the fast simulation is good as can be seen from Figure 17-3.

A similar fast-simulation parametrisation as a function of $|\eta|$ and p_T was made for muons. However, here, the distributions are very close to Gaussian, not having any significant tails in the absence of pattern-recognition problems.

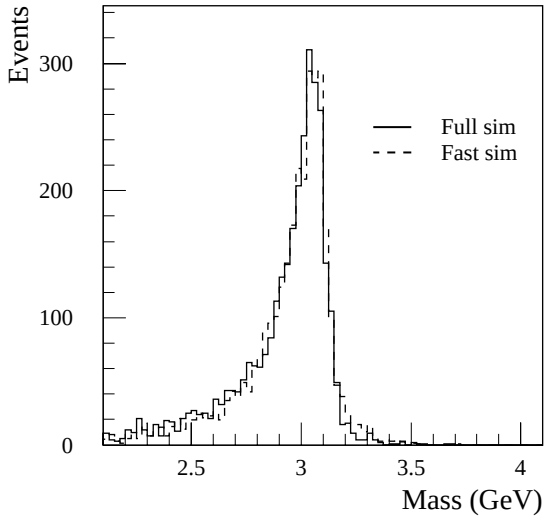

Figure 17-3 Comparison between full (solid line) and fast (dashed line) simulation for $J/\psi \to ee$.

17.2.2.2 K_S^0 reconstruction

The reconstruction of the decay $K_S^0 \to \pi^+\pi^-$ is described in detail in Section 3.6.2.1. The decay vertex was reconstructed using three-dimensional vertexing, and the pair was chosen as a K_S^0 candidate if a good vertex was found at a decay radius R between 1 cm and 37 cm and with $|z| < 210$ cm, and if the invariant mass of the pair was compatible with the K_S^0 mass.

For events in which a J/ψ has been successfully reconstructed, the total K_s^0 reconstruction efficiency is about 41%. This figure includes the acceptance for a K_s^0 decay inside the fiducial volume delimited by the R and z cuts listed above, the tracking efficiency and the efficiency of the selection cuts (cuts on fit probability, mass-window and transverse decay length from the primary vertex). The K_s^0 mass resolution is about 4.5 MeV for K_s^0 decays at low radii and increases to up to 7 MeV towards the external border of the fiducial decay volume.

In order to be able to perform a reliable estimation of the background to the $B_d^0 \to J/\psi K_s^0$ decay, using samples for which full GEANT simulation was not available, a fast simulation for charged pions, similar to the one for muons and electrons briefly described in the previous section, was developed. The parametrisation was established studying the resolutions of the five track parameters for pions in fully-simulated samples. The total sample was divided into bins of p_T, η and, in order to be able to describe also the pions from K_s^0, decay radius. In each bin, the track parameter resolutions were described as the sum of two Gaussians in order to take into account also the presence of tails. While an exponential description of the tails might have been more appropriate in some cases, the two-Gaussian description provides good results and allows one to take into account correlations in a more straightforward way. As discussed in [17-7], this method allows one to obtain a parametrisation of the full covariance matrix (including the correlation terms) as a function of p_T, η and R. This parametrisation was used to smear the five generated pion-track parameters in the fast-simulation program. The K_s^0 mass distribution obtained using this method is compared in Figure 17-4 to the one obtained with full simulation; reasonable agreement is observed between the two.

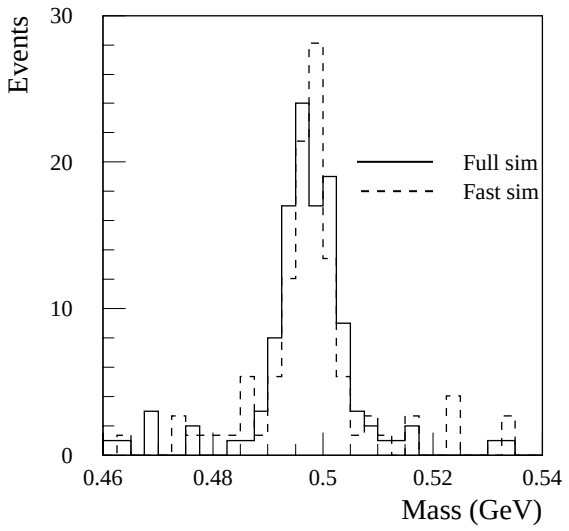

Figure 17-4 Comparison between full (solid line) and fast (dashed line) simulation for $K_s^0 \to \pi^+\pi^-$.

17.2.2.3 B_d^0 reconstruction

Leptons and pions coming from J/ψ and K_s^0 candidates which survived the selections described above were used in reconstructing $B_d^0 \to J/\psi K_s^0$ decays. The B_d^0 was reconstructed by performing a three-dimensional kinematic fit to the four tracks and applying vertex and mass constraints on both the ll and $\pi^+\pi^-$ systems. At the same time, the momentum of the K_s^0 (B_d^0) was required to point to the J/ψ (primary) vertex. The proper decay time of the B_d^0 was required to be greater than 0.5 ps and the transverse momentum was required to be greater than 5 GeV. A mass resolution of 19 (26) MeV and a transverse decay-length resolution of 64 μm (68 μm) were estimated for the reconstructed B_d^0 meson in events in which the J/ψ decayed to muons (electrons).

After the first three years of running at low luminosity, corresponding to an integrated luminosity of 30 fb^{-1}, it is estimated that ATLAS will reconstruct 14400 $J/\psi K_s^0$ decays in the $J/\psi \to ee$ channel and 473 550 (219 690) events in the μμ channel, assuming a LVL2 trigger threshold of 3 GeV (5 GeV) for the second muon. The relatively low number of $J/\psi \to ee$ events is due to the requirement of an additional muon which provides the LVL1 trigger and can be used for tag-

ging the flavour of the B_d^0 at production. Besides all the selection cuts described above, these numbers also include the estimated efficiencies of the detector to identify electrons and muons: ε = 85% for the LVL1 trigger muon, ε = 95% for other muons with p_T > 5 GeV, ε = 90% for muons with 3 GeV< p_T<5 GeV, and ε = 75% for all electrons.

17.2.2.4 Flavour tagging

To perform a measurement of the *CP*-violating asymmetry, it is necessary to know the flavour of the neutral *B* meson at production. Various methods have been developed for this purpose along the years, mainly by the LEP experiments and by CDF. Flavour tagging can be divided in two categories – Opposite-Side Tagging (OST) and Same-Side Tagging (SST) – depending on whether the algorithm deduces the flavour by looking at the products of the other *b*-quark in the event (the opposite side) or at the particles accompanying the *B*-meson under study (the same side). In this section, a brief description of the tagging algorithms developed so far for this analysis is given and the performance summarised. Each algorithm has been optimised by adjusting parameters to maximise the quality factor $Q = \varepsilon D_{\mathrm{tag}}^2$ that determines the statistical precision on the asymmetry measurement. Here, ε is the tagging efficiency defined as the fraction of reconstructed *B* candidates with a tag, and D_{tag} is the dilution factor due to mistags.

In the lepton-tagging technique, an additional lepton is searched for in the event, with the assumption that this tag lepton originates from a semi-leptonic decay of the other *b*-quark in the event. This method is known to have low efficiency (due to the low B_d^0 semi-leptonic branching ratio of about 10% and the kinematic cuts), but good purity. However, in the $J/\psi \to ee$ sample this method is fully efficient due to the presence of the trigger muon. In the $J/\psi \to \mu\mu$ sample, an additional lepton (muon or electron) with p_T > 5 GeV is searched for. In case the tag lepton was a muon (so that there are three muons in the event), the LVL1 trigger muon could be either one of the J/ψ legs or the tag muon. The total lepton-tagging efficiency in the $J/\psi \to \mu\mu$ sample is about 0.04 (electron or muon tag).

The mistag rate with lepton tagging was extensively studied in a large inclusive-muon sample and double-checked, with smaller statistics, in samples of $B_d^0 \to J/\psi K_s^0$ decays. The dependence of the mistag rate on the tag lepton transverse-momentum threshold is shown in Figures 17-5 and 17-6 for electrons and muons respectively. It can be seen that the wrong-tag fraction decreases with increasing tag p_T threshold. The mistag rate depends on p_T of the signal *B*-hadron as well as on the p_T of the tag lepton. With increasing p_T of the signal *B*-hadron, the wrong-tag fraction increases for a fixed tag p_T threshold. This is due to the fact that, as the p_T of the signal *B*-hadron increases, the p_T of the other *B* tends to increase as well, resulting in a higher probability for the leptons from cascade decays to pass the p_T threshold for the tag. This can be seen in Figure 17-7, which shows the wrong-tag fraction as a function of the signal *B*-hadron p_T, when the tag p_T was fixed to 6 GeV. For the hadronic channels $B_d^0 \to \pi^+\pi^-$ and $B_s^0 \to D_s^-\pi^+$ ($B_s^0 \to D_s^- a_1^+$), the average p_T of the signal *B* was about 20 GeV, and the wrong muon tag fraction was taken to be 0.22.

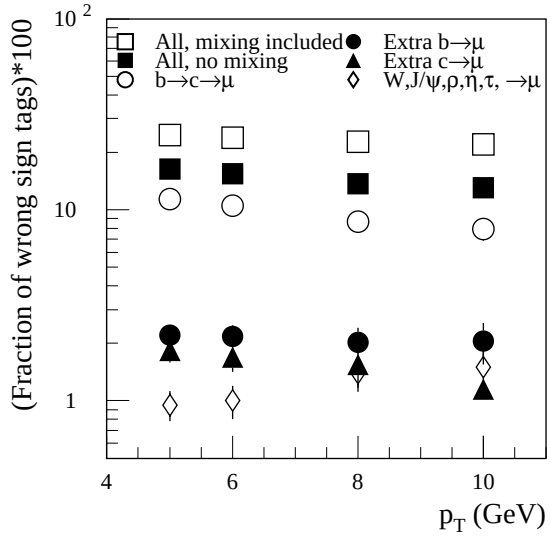

Figure 17-5 Muon wrong-tag fraction as a function of the tag p_T threshold. This plot is made for the case where the decay $J/\psi \to \mu\mu$ gives rise to a muon with p_T > 6 GeV. At tag p_T > 6 GeV, the average p_T of the signal-*B* is 26 GeV.

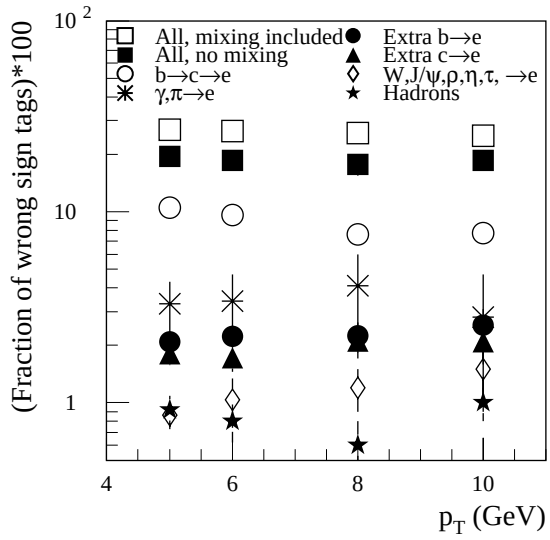

Figure 17-6 Electron wrong-tag fraction as a function of the tag p_T threshold. This plot is made for the case where the decay $J/\psi \to \mu\mu$ gives rise to a muon with p_T > 6 GeV. At tag p_T > 5 GeV, the average p_T of the signal-*B* is 25 GeV.

For muon tagging of the $J/\psi \to \mu\mu$ sample, a mistag rate of $\omega_{tag} = 0.24$ was applied in the analysis. Here the average p_T of the B_d^0 is about 25 GeV. For muon tagging of the $J/\psi \to ee$ sample, the wrong-tag fraction was lower, $\omega_{tag} = 0.21$, due to the lower p_T of the signal-*B* (17 GeV on average). Contributions to the mistag rate from hadrons misidentified as muons and from decays in flight of pions and kaons were found to be negligible. The mistag rates are also given in the summary in Table 17-1.

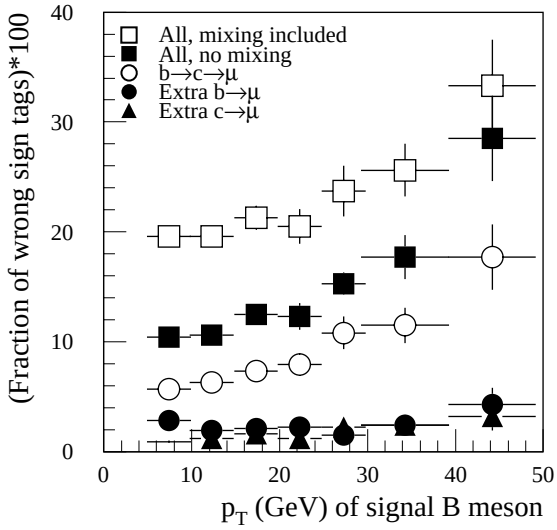

Figure 17-7 Muon wrong-tag fraction as a function of the signal *B*-hadron p_T. The tag muon was required to have p_T > 6 GeV.

For electron tagging of the $J/\psi \to \mu\mu$ sample, the fraction of wrong tags was 0.27 with a 5 GeV threshold. The contributions to the mistag rate from misidentified hadrons (about 1%) and from conversions (about 2%) were estimated using fully simulated Monte Carlo samples. The hadron rejection factor was about 1800, corresponding to a 75% electron efficiency. The electron was identified by using both the e.m. calorimeter and the TRT (see Section 7.3.1). The conversion-removal algorithm, similar to the one described in Section 7.5.1, has not yet been fully optimised for this analysis. The mistag rates are summarised in Table 17-1.

The B-π correlation tagging is an SST technique as it uses charged pions associated with the B_d^0 that has decayed to $J/\psi K_s^0$. The algorithm exploits the correlation between the flavour of the b-quark and the charge sign of a particle produced nearby in phase-space. Such charge–flavour correlations are expected to come both from particles produced in the fragmentation and from the decays of B^{**} resonances [17-13]. No attempt was made to separate the two contributions. In both cases, a positively-charged particle is correlated to a B_d^0 and a negatively-charged one to a $\overline{B_d^0}$. This particle will be referred to as a 'pion' in the following discussion, although it is not identified as such.

The algorithm selects charged-particle tracks contained in a cone $\Delta R < 0.7$ around the reconstructed B meson direction, with $|d_0|/\sigma_{d_0} < 3$ (where d_0 is the transverse impact parameter of the pion) and with 0.5 GeV < p_T < 4.0 GeV. If more than one particle survives this selection, the one with the highest p_L^{rel} (the momentum component along the reconstructed B direction) is selected. This set of cuts provides the highest quality factor, although other choices provided similar results within the statistical uncertainty. The results for the efficiency and the dilution factor for this algorithm are presented in Table 17-1.

As in the B-π algorithm, jet-charge tagging exploits the correlation between the charge of a jet (defined as a kinematically-weighted average of the charge of the particles in the jet) and the charge of the quark producing the jet. Although jet-charge tagging can be applied to both the B_d^0 jet and to the opposite jet, for the time-being it was applied only to the same-side jet. In the analysis, the signal is tagged as a B_d^0 ($\overline{B_d^0}$) if the jet-charge tag has $Q_{jet} > +c$ ($Q_{jet} < -c$), where c is a tunable cut.

The algorithm included in the jet all tracks with $p_T > 0.5$ GeV, $|d_0| < 1$ cm and $|\Delta z| < 5$ cm (where Δz is the difference between the z_0 of the track and the z-coordinate of the primary vertex), contained inside a cone $\Delta R < 0.8$ around the B direction. The four particles identified as the B_d^0 decay products were excluded. This set of cuts, together with the definition of the weights $w_i = p_T^k$, where $k = 1.25$ (1.0) for the $J/\psi \to ee$ ($J/\psi \to \mu\mu$) sample, and cut value $c = 0.26$ for both J/ψ decay channels, were chosen to maximise the quality factor Q. Different sets of cuts provided similar results within the statistical uncertainties. The results are summarised in Table 17-1.

Table 17-1 Efficiencies and dilution factors for the tagging algorithms considered in the analysis (n/a = not available). The notation μ6μ3 (μ6μ5) means that in the corresponding sample, the LVL2 trigger threshold for the second muon has been assumed to be 3 (5) GeV.

Tag	$B_d^0 \to J/\psi(ee)K_s^0$		$B_d^0 \to J/\psi(\mu 6 \mu 3)K_s^0$		$B_d^0 \to J/\psi(\mu 6 \mu 5)K_s^0$	
	ε_{tag}	D_{tag}	ε_{tag}	D_{tag}	ε_{tag}	D_{tag}
OST: electron tag	n / a	n / a	0.012	0.46	0.016	0.46
OST: muon tag	1.0	0.57	0.025	0.52	0.025	0.52
SST: B–π	0.80	0.14	0.82	0.16	0.84	0.17
SST: Jet-charge	0.71	0.12	0.64	0.17	0.66	0.18

It is worth noting that the performance shown in Table 17-1 for the various tagging methods is quite consistent with that achieved by CDF [17-10]. For example, for the SST methods, CDF obtains a dilution factor of 0.166 ± 0.022 for SVX tagged events or 0.174 ± 0.036 for non-SVX events, where SVX refers to the CDF Silicon Vertex Detector.

Note that there is scope to improve on the tagging performance by using an event-by-event likelihood analysis and including additional information such as $p_{\mathrm{T}}^{\mathrm{rel}}$ measurements, although this remains to be studied.

17.2.2.5 Event yields

The total number of events after tagging is summarised in Table 17-2 for each sample for an integrated luminosity of 30 fb^{-1}.

Table 17-2 Expected number of tagged events and relative background for each sample for an integrated luminosity of 30 fb^{-1}. The notation $\mu 6\mu 3$ ($\mu 6\mu 5$) means that in the corresponding sample, the LVL2 trigger threshold for the second muon has been assumed to be 3 (5) GeV. The *e*- and μ-tag samples are subclasses of the lepton-tagged sample, and the sample '*B*-π tagged events with no lepton tags' is a subclass of the sample '*B*-π tagged events'. The lepton tagged sample and the *B*-π tagged sample with no lepton tags are independent and can be combined in a straightforward way.

Event class	$B_d^0 \to J/\psi(ee)K_S^0$		$B_d^0 \to J/\psi(\mu 6\mu 3)K_S^0$		$B_d^0 \to J/\psi(\mu 6\mu 5)K_S^0$	
	Signal	Background	Signal	Background	Signal	Background
Lepton tagged events	14 400	900	17 700	1 600	8800	500
e tags	n / a	n / a	5 800	500	3 500	210
μ tags	14 400	900	11 900	1 100	5 300	310
B-π tagged events	11 600	900	390 700	15 300	184 100	5 000
B-π tagged events with no lepton tags	n / a	n / a	376 100	13 700	176 700	4 500

Since the lepton tag purity is much higher than the *B*-π tag purity, the lepton tag was used whenever it was available. The *B*-π tag was used only if there was no lepton tag. The highest statistical tagging power would be achieved by combing all available tagging information on an event-by-event basis. A study of the tag combination has not yet been performed. Jet-charge tags are not listed in this table. Jet-charge tags have proven, as expected, to be highly correlated with *B*-π tags, and since the *B*-π tag purity was higher that the jet-charge-tag purity, only *B*-π tags were used.

17.2.2.6 Background estimate

The background to the $B_d^0 \to J/\psi K_S^0$ decay was studied using large samples of J/ψ *X* and $\mu 6X$ events. The inclusive sample of J/ψ decays from *B*'s was produced with the same lepton-p_{T} thresholds as for the signal sample. This sample was used to give an estimate of the background coming from *B* decays containing a true J/ψ in the final state. Background contributions come from the combination of a true J/ψ with K_S^0 candidates from various sources: true K_S^0 from *B*-hadron decays, true K_S^0 from the fragmentation, and fake K_S^0.

The $\mu 6X$ sample contained events with muons from semileptonic B-hadron decays with a minimum muon transverse momentum of 6 GeV. This sample was used to estimate the background from fake J/ψ's (arising from lepton–lepton, lepton–hadron and hadron–hadron pairs) reconstructed in association with a true or a fake K_s^0.

The background samples were processed using the fast simulation program. However, good agreement was found with results obtained from smaller-statistics samples of fully-simulated background events. The total number of background events is presented in Table 17-2. Conservatively, a pessimistic 95% B-π tagging efficiency has been assumed for the background events. In all the samples, the biggest background contribution comes from true J/ψ background events. Background from fake J/ψ's was found to be about 5% of the total background. The background level under the $B_d^0 \to J/\psi K_s^0$ peak is rather small including all samples (see Figure 17-8).

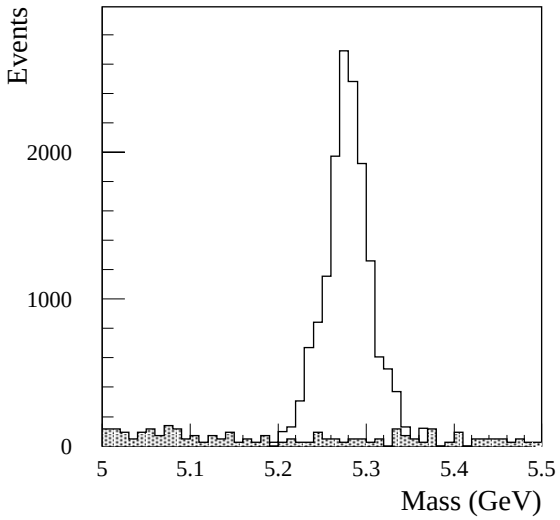

Figure 17-8 Invariant-mass distribution of the B_d^0 peak in the muon-tagged $J/\psi \to ee$ channel (open histogram) with superimposed the estimated background contribution (shaded histogram). Note that the selection includes a decay-time cut on the B_d^0.

The background from prompt J/ψ's has not yet been studied for this channel. This is a potential background source for the hadron-tagged samples, while the lepton-tagged samples with three leptons per event are very unlikely to be affected. However, the background from prompt J/ψ production was studied for the untagged decay $B_s \to J/\psi\phi$ (see Section 17.2.4.2), which is experimentally similar, and it was found to be negligible.

17.2.2.7 The statistical accuracy of the sin2β measurement

The accuracy of the $\sin 2\beta$ measurement was estimated with a fit to the time-dependent asymmetry distribution with a function of the form $A = D \sin 2\beta \sin(\Delta m_d t)$, where D is the overall dilution factor. For this analysis time dependence of the dilution due to background has been neglected. The time-dependent asymmetry was modelled including dilution factors from background and from tagging. An input value of $\sin 2\beta = 0.6$ was assumed for the only free parameter of the fit. The proper time of the B-decay was histogrammed using bins of width 0.83 ps (corresponding to about 250 μm in decay length). Due to the cut on the decay proper time used in the selection, the measurement was made for $t(B) > 0.5$ ps. The proper-time resolution, estimated using the fully-simulated signal sample, is 0.073 ps.

The results of the fit using lepton tagging and B–π tagging in the various samples considered are presented in Table 17-3, where the lepton-tagged events have been removed from the B-π tagged samples, leaving statistically independent samples. Since in the class $J/\psi(ee)$ all the events have a muon tag, no events are left in the B-π tagged sample. Note that the statistical precision from a number of different samples and tagging methods is comparable, allowing meaningful cross-checks to be made between them.

Table 17-3 Estimate of the error on sin2β using a time dependent analysis in each of the samples considered for lepton tagging and *B*–π tagging with an integrated luminosity of 30 fb^{-1}. Note that the J/ψ(μ6μ5) sample is a subset of the J/ψ(μ6μ3) one.

Tag	*J/ψ(ee)* sample	*J/ψ(*μ6μ3) sample	*J/ψ(*μ6μ5) sample
Lepton tags	0.018	0.023	0.030
B–π tag	n / a	0.015	0.019

As the $B_d^0 \to J/\psi(ee)K_s^0$ sample is statistically independent from the $B_d^0 \to J/\psi(\mu\mu)K_s^0$ ones, results from the two samples can be combined in a straightforward way. Using lepton tagging combined with *B*-π tagging, the estimated uncertainty on $\sin 2\beta$, with 30 fb^{-1} of data is $\delta(\sin 2\beta) = 0.010$ (stat) assuming a LVL2 trigger p_T threshold of 3 GeV for the second muon or $\delta(\sin 2\beta) = 0.012$ (stat) with a threshold of 5 GeV.

17.2.2.8 Systematic uncertainty

Previous studies have shown that the overall systematic error in the $\sin 2\beta$ measurement is small [17-14]. Contributions come from the production asymmetry of B_d^0 and $\overline{B_d^0}$ mesons, from asymmetries in the tagging efficiency and in the background, and from uncertainties in the determination of the various dilution factors. All these uncertainties need to be controlled, in order not to spoil the excellent statistical precision achievable on this measurement.

Many of the potential sources of systematic uncertainty can be controlled using the channels $B^+ \to J/\psi(\mu\mu)K^+$ and $B_d^0 \to J/\psi(\mu\mu)K^{*0}$ (where $K^{*0} \to K^+\pi^-$). For the first channel the results for charged *B*-mesons need to be extrapolated to the neutral case which may introduce some model dependence. For the second channel, the results are obtained directly for B_d^0 particles, allowing for the flavour oscillations. The reconstruction of these so-called control channels is discussed below before estimates of the systematic uncertainties are presented.

The availability of many tagging algorithms and the large statistics of tagged and untagged signal and control samples provide the flexibility to perform internal cross-checks of the analysis. The $B^+ \to J/\psi(\mu\mu)K^+$ and $B_d^0 \to J/\psi(\mu\mu)K^{*0}$ samples can be used to measure the wrong-tag fraction for the various tagging methods and also the charge asymmetry in the tagging efficiencies. For all these studies, it is important to reconstruct large statistics of control samples, so that the systematic errors will not appreciably degrade the statistical error on $\sin 2\beta$.

17.2.2.9 Reconstruction of $B^+ \to J/\psi(\mu\mu)K^+$

As discussed above, the decay channel $B^+ \to J/\psi(\mu\mu)K^+$ can be used to measure parameters that relate the observed asymmetry in $B_d^0 \to J/\psi K_s^0$ decays (and other channels) to the true *CP* asymmetry. The $B^+ \to J/\psi(\mu\mu)K^+$ decay (as well as the $B_d^0 \to J/\psi(\mu\mu)K^{*0}$ decay described below) was studied using a sample of events generated with PYTHIA and fully simulated inside the Inner Detector. Only J/ψ decays to muon pairs were considered. Muon identification efficiencies were included when calculating the expected number of signal events.

The trigger selection for this channel was the same as for the $B_d^0 \to J/\psi(\mu\mu)K_s^0$ decay channel. The J/ψ vertex was fitted and selection cuts were applied as described in Section 17.2.2.1. Once a J/ψ was successfully reconstructed, the event was searched for a track (the 'kaon') with transverse momentum greater than 1.5 GeV. The track was required to be inconsistent with coming from the primary vertex at the one standard deviation level ($|d|/\sigma_d > 1$). The two muons and the kaon were then fitted to a common vertex applying a mass constraint to the J/ψ and requiring the total momentum at the B vertex to point to the primary event vertex. The normalised χ^2 of the fit was required to be less than six. Finally, a cut $p_T(B) > 5$ GeV was applied and the mass was required to be within three standard deviations of the nominal B^+ mass.

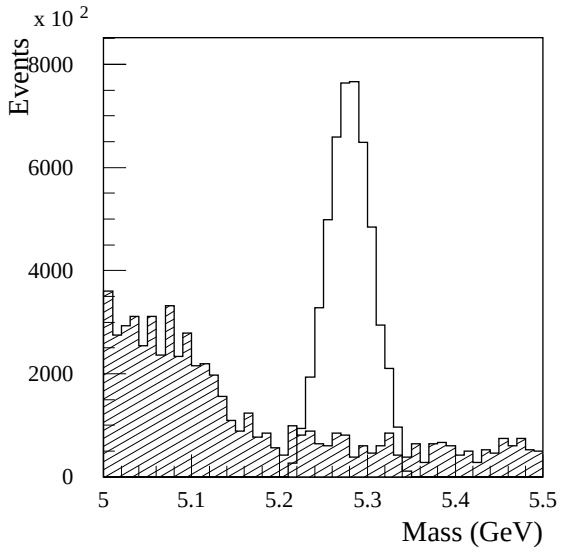

Figure 17-9 Invariant-mass distribution for the decay $B^+ \to J/\psi(\mu\mu)K^+$ (open histogram) with superimposed the estimated background contribution (shaded histogram).

The mass peak is shown in Figure 17-9; the mass resolution is about 26 MeV. The number of signal events expected for an integrated luminosity of 30 fb^{-1} is given in Table 17-4 for both LVL2 trigger options. Also given in this table are the numbers of untagged background events estimated using the inclusive $J/\psi X$ sample. The backgrounds from fake J/ψ and prompt J/ψ have not yet been included in this study. However, in the background estimate for the signal $B_d^0 \to J/\psi(\mu\mu)K_s^0$, the dominant background was found to originate from real J/ψ from B-decays. The selection cuts for this channel may need further optimisation to improve the signal-to-background ratio; tighter cuts should be feasible given the large statistics.

Table 17-4 Total number of events expected in the control samples (30 fb^{-1}).

Sample	Untagged signal	Untagged background	Lepton tagged signal	Lepton tagged background	B-π tagged signal	B-π tagged background
$B^+ \to J/\psi(\mu 6\mu 3)K^+$	5 078 000	929 000	198 000	13 800	4189 000	882 000
$B^+ \to J/\psi(\mu 6\mu 5)K^+$	2 471 000	509 000	122 000	8 500	2070 000	484 000
$B_d^0 \to J/\psi(\mu 6\mu 3)K^{*0}$	2 631 000	608 000	115 000	24 400	2170 000	578 000
$B_d^0 \to J/\psi(\mu 6\mu 5)K^{*0}$	1 292 000	311 000	63 600	12 200	1083 000	295 000

Also given in Table 17-4 are the numbers of tagged events and respective backgrounds, both for lepton tagging and B–π tagging. As in the $B_d^0 \to J/\psi(\mu\mu)K_s^0$ analysis, both muons and electrons with $p_T > 5$ GeV are used for tagging. A complete study of B–π tagging has not been performed for these channels, and tagging efficiencies on both signal and background equal to those estimated for the $B_d^0 \to J/\psi(\mu\mu)K_s^0$ case have been used. In Table 17-4, lepton tagged events have not been removed from the B–π tagged events. About 4% (5%) of the B–π tagged events in the $\mu 6\mu 3$ ($\mu 6\mu 5$) class have a lepton tag in addition to the B–π tag.

17.2.2.10 Reconstruction of $B_d^0 \to J/\psi(\mu\mu)K^{*0}$

Triggering of these channels and the J/ψ reconstruction were the same as for the $J/\psi(\mu\mu)K^+$ analysis. After the J/ψ was successfully reconstructed, all track pairs with $p_T > 0.5$ GeV were fitted to a common vertex. The normalised χ^2 of the fit was required to be less than 6 and the p_T of the reconstructed K^{*0} was required to be greater than 3 GeV. Candidates inside a three standard deviation mass window around the nominal K^{*0} mass were retained. In the fit, both pion and kaon mass assignments were tried. If both combinations passed all the K^{*0} selection cuts listed above, only the combination yielding the mass closest to the nominal K^{*0} mass was retained.

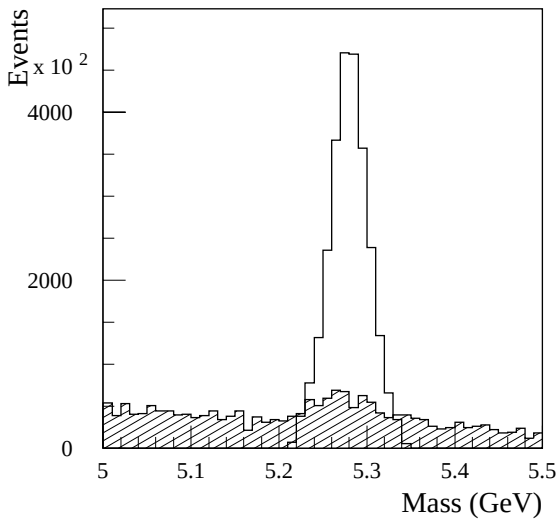

Figure 17-10 Invariant-mass distribution of the decay $B_d^0 \to J/\psi(\mu\mu)K^{*0}$ (open histogram) with superimposed the estimated background contribution (shaded histogram).

The two muons and the two hadron tracks were then fitted to a common vertex. Due to the large K^{*0} width, a mass constraint was applied only to the J/ψ vertex. The final cuts on the B vertex were similar to those described for the $J/\psi(\mu\mu)K^+$ analysis (χ^2/dof < 6, three standard deviation mass window and $p_T(B) > 5$ GeV).

The mass peak is shown in Figure 17-10; the mass resolution is about 23 MeV. The number of expected signal events for an integrated luminosity of 30 fb^{-1} is given in Table 17-4. The background shown in the figure and in the table includes the contribution from the reflection of the signal, where the π and K masses are wrongly assigned in the K^{*0} fit, as well as the contribution from other $B \to J/\psi X$ final states. Note that the peak in the background distribution near the B_d^0 mass is due to the K^{*0} reflection.

The numbers of tagged events (lepton tagging and B–π tagging) and the respective numbers of background events are also given in Table 17-4. The signal and background B–π tagging efficiencies have been deduced from the results obtained in the $B_d^0 \to J/\psi(\mu\mu)K_S^0$, as a complete study of the algorithm for this sample has not been performed yet.

17.2.2.11 Uncertainty on the production asymmetry

The production asymmetry, A^P, is not expected to exceed about 1% and it can be measured by using the decay channels discussed above which are expected to have negligible *CP* violation. It can be measured in the untagged control samples by counting the numbers of reconstructed B and $\bar{B}$ mesons, taking account of the flavour oscillations in the case of B_d^0. The statistical uncertainty on this measurement will be around $\delta A^P = 0.05\%$ (0.07%) from the $B^+ \to J/\psi(\mu\mu)K^+$ sample and about 0.07% (0.10%) from the $B_d^0 \to J/\psi(\mu\mu)K^{0*}$ sample, for a LVL2 trigger muon threshold of 3 GeV (5 GeV). It is assumed that any *CP*-violation effects in the two control samples can be neglected. Note that the large numbers of events available in these channels would be sufficient to study the p_T dependence of any observed production asymmetry.

Systematic effects due to small differences in the reconstruction efficiencies for K^+ and K^- remain to be evaluated. A cross-check of corrections for such effects may be made by using the flavour oscillations in the decays $B_d^0 \to J/\psi(\mu\mu)K^{*0}$, for example.

17.2.2.12 Uncertainties from tagging

Systematic effects on the *CP*-violation asymmetry measurement related to tagging can be studied using the $B^+ \to J/\psi(\mu\mu)K^+$ and $B_d^0 \to J/\psi(\mu\mu)K^{*0}$ events for lepton (electron and muons) tagging, and $B_d^0 \to J/\psi(\mu\mu)K^{*0}$ for *B*–π tagging.

In all tagging methods, a fraction of the produced *B* mesons are mistagged, as discussed in Section 17.2.2.4. The wrong-tag fraction can be measured by comparing the numbers of positive-charge and negative-charge tags associated with the decays $B^+ \to J/\psi(\mu\mu)K^+$ and $B_d^0 \to J/\psi(\mu\mu)K^{*0}$, allowing for the oscillations in the case of B_d^0. The wrong-tag fraction can be measured separately for the tagging of *B* and $\bar{B}$ mesons, and the average value can be computed. By using the numbers of tagged signal and background events listed in Table 17-4, the statistical uncertainty on the measurement of the dilution due to tagging is estimated to be $\delta(D_{\rm tag})/D_{\rm tag} = 0.0038$ (0.0048) for lepton tagging using the $B^+ \to J/\psi(\mu\mu)K^+$ sample with a LVL2 trigger $p_{\rm T}$ threshold of 3 GeV (5 GeV) for the second muon. For *B*–π tagging the result is $\delta(D_{\rm tag})/D_{\rm tag} = 0.0028$ (0.0037) for a 3 GeV (5 GeV) trigger threshold. Slightly larger uncertainties are obtained using the $B_d^0 \to J/\psi(\mu\mu)K^{*0}$ sample.

17.2.2.13 Uncertainties from background

Another contribution to the systematic error on sin2β comes from the uncertainty on the backgrounds to the signal and the control samples. Assuming conservatively a 5% uncertainty on the normalisation of the signal background, this propagates to give an uncertainty on the dilution from background of about $\delta(D_{\rm back})/D_{\rm back} = 0.0065$ (0.0055) for the 3 GeV (5 GeV) trigger threshold. The systematic uncertainty is smaller for the latter sample, because the signal-to-background ratio is better with a 5 GeV cut on the second muon. Here it is assumed that there is no *CP*-violation in the background. As in the case of the $B_d^0 \to \pi^+\pi^-$ analysis discussed in Section 17.2.3, it should be possible to measure the background using sidebands.

17.2.2.14 Summary of the sin2β measurement precision

Combining the various sources of uncertainty discussed above, one obtains an overall precision for the sin2β measurement as follows. The statistical precision of the sin2β measurement is $\delta(\sin 2\beta)$ (stat.) = 0.010 (0.012) for a LVL2 muon-trigger threshold of 3 GeV (5 GeV). The total systematic uncertainty is $\delta(\sin 2\beta)$ (syst.) = 0.005, independent of the LVL2 muon-trigger threshold. This level of precision is considerably better than at e^+e^- *B*-factories that will run before the start-up of ATLAS. For example BaBar expects to achieve a precision of about 0.05 [17-12].

17.2.3 Measurement of asymmetry in $B_d^0 \to \pi^+\pi^-$

The channel $B_d^0 \to \pi^+\pi^-$ is more complicated than the $B_d^0 \to J/\psi K_S^0$ one, both from the theoretical and the experimental point of view.

From the theoretical point of view, $B_d^0 \to \pi^+\pi^-$ is more complicated because of the interplay between *CP*-violation induced via tree-level and penguin diagrams, giving an observed time-dependent asymmetry that depends on a total of three parameters. The asymmetry *A(t)* for $B_d^0 \to \pi^+\pi^-$ is given by Equation 17-1. The two coefficients *a* and *b* that can be determined experimentally are related to the angle α in the unitarity triangle (where $\alpha = \pi - \beta - \gamma$ is assumed) by

$$a = 2\frac{A_P}{A_T}\sin\delta\sin\alpha \qquad 17\text{-}3$$

$$b = -\sin(2\alpha) - 2\frac{A_P}{A_T}\cos\delta\cos(2\alpha)\sin\alpha, \qquad 17\text{-}4$$

where A_T and A_P are the tree and penguin amplitudes, and δ is the phase difference between them. In this decay mode, the direct *CP*-violation component *a* may be sizeable.

The parameters *a* and *b* can be extracted from a fit to the observed asymmetry as a function of proper decay time. Since there are three unknowns, α, δ and A_P/A_T, and since δ is not believed to be calculable A_P/A_T must be given by theory. The evaluation of this quantity is currently the subject of intensive theoretical studies which will soon be aided by new measurements, for example from the BaBar collaboration [17-12]. Fleischer and Mannel [17-15] estimate that, with the help of measurements of the $B^+ \to \pi^+K^0$ and $B^+ \to \pi^+\pi^0$ branching ratios, the theoretical uncertainty on the penguin contribution would yield an uncertainty on α of less than 3º. The current best Standard Model fit of the unitarity triangle yields an estimate $\sin2\alpha = -0.26^{+0.29}_{-0.28}$ [17-11]. A small value of $\sin2\alpha$ could mean no observable *CP* asymmetry in this channel, but a tight bound on $\sin2\alpha$ would nevertheless be a valuable constraint on the unitarity triangle.

Experimentally, the $B_d^0 \to \pi^+\pi^-$ signal must be extracted from the huge combinatorial background; this can be achieved using a combination of cuts, including vertexing. In the case of ATLAS, a more difficult physics background is other two- and three-body decays, which cannot be removed given the poor *K*/π separation. A simple event-counting method would rely too much on the background description, so an overall fit, using all available information, is necessary. It is likely that some of the background channels will themselves exhibit *CP*-violation effects, requiring a sophisticated analysis that fits the contribution to the observed asymmetry from the different channels.

17.2.3.1 Reconstruction

To select B_d^0 candidates, the presence of a pair of oppositely-charged particles each with $p_T > 4$ GeV was required. The pair should form a vertex with a χ^2 of the fit corresponding to a probability of more than 5%, and the invariant mass of the pair must be in the range 4.6–6.0 GeV [17-16]. The B_d^0 flight direction was required to be aligned in the transverse plane with the direction from the beam-line to the decay vertex. Tracks were not considered if they were consistent with originating from a low-mass displaced vertex; a track is eliminated if it forms with any other track a vertex where the two tracks had $p_T > 1$ GeV, separation $\Delta R < 0.5$, invariant mass less than 2 GeV, the vertex of the pair had a χ^2 probability of more than 1%, and the vertex was separated from the beam-line by more than ten standard deviations. This requirement also removed efficiently *B* decays with three or more prongs. The resolutions for the mass and decay time are $\sigma_m = 70$ MeV and $\sigma_t = 0.065$ ps respectively.

17.2.3.2 Backgrounds

The list of signal and background branching ratios and yields is given in Table 17-5. As the final results were obtained from an overall fit of the mass histograms, the yields in the mass histogram and in a $\pm 1\sigma_m$ mass window around the B_d^0 mass are listed separately. The $B_d^0 \to K^+\pi^-$ branching ratio is a recent, still imprecise, first measurement from CLEO [17-17]. The $B_d^0 \to \pi^+\pi^-$ branching ratio was inferred from the CLEO upper limit. The other branching ratios were inferred from the first two with a simple SU(3) symmetry assumption, except for the Λ_b decays which were set to their experimental upper limits [17-18]. It should be noted that these branching ratios are much less favourable than the estimated ones used in the ATLAS Technical Proposal [17-14]. Charmless decays to three-body final states other than $B \to \pi^+\pi^-\pi$ and $B \to \rho\pi^-$ involving charged kaons were neglected. The most abundant background is the decay $B_d^0 \to K^+\pi^-$, because of the absence of π/K separation, and because the mass resolution (σ_m = 70 MeV) is worse than the separation between the peaks (~40 MeV).

Table 17-5 Branching ratios and yields in the $\pi^+\pi^-$ sample for an integrated luminosity of 30 fb^{-1}. The *B* Comb. component corresponds to cases not explicitly listed when the pion candidates come from the same *B* hadron, while the Comb. component is the combinatorial background from all other sources (see text).

Channel	*BR*'s ($\times 10^{-5}$)	Yield 4.6–6.0 GeV	Yield $\pm 1\sigma_m$
$B_d^0 \to \pi^+\pi^-$	0.7	9500	6500
$B_d^0 \to K^+\pi^-$	1.5	19 800	12 100
$B \to \rho\pi^-$	2.5	8100	200
$B \to \pi^+\pi^-\pi$	5.0	2100	0
$B_s^0 \to \pi^+K^-$	0.7	2500	1400
$B_s^0 \to K^+K^-$	1.5	5200	3400
$\Lambda_b \to p\pi^-$	8.0	15 900	1100
$\Lambda_b \to pK^-$	8.0	16 700	2500
B Comb.	-	36 400	200
Comb.	-	19 500	2600

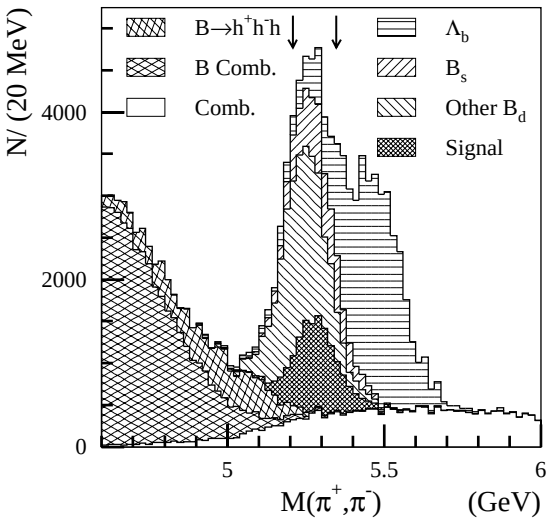

Figure 17-11 $\pi^+\pi^-$ mass spectrum. The arrows indicate a $\pm 1\sigma$ window.

The *B* combinatorial background is important below 5 GeV but does not contribute to the peak. It involves a variety of decays with three or four particles in the final state, such as $B_d^0 \to D^+\pi^-$ followed by $D^+ \to K^0\pi^+$, or $B_d^0 \to \pi^+\pi^-\pi\pi$. Usually, in these cases, the B_d^0 candidate does not fulfil the pointing requirement, unless the additional particles have low momentum. The truly combinatorial background is the random coincidence of high-impact-parameter tracks. The use of full simulation and reconstruction was mandatory to parametrise the tracking resolution, including exponential tails in addition to the parametrisation described in Section 17.2.2.2. A high-statistics sample was then simulated with fast simulation to demonstrate the required greater than 10^7 rejection factor on the LVL1 trigger output. About 50% of the combinatorial background involves a track from additional primary *D* mesons, 25% involves tracks from different *B* hadrons and the remainder involves a

track from a *B* hadron and a primary track. The shape of the combinatorial background is due to a kinematic effect – tracks with $p_T > 4$ GeV from different jets were combined. Figure 17-11 shows the final mass spectrum.

17.2.3.3 Results from event counting

Using Equation 17-2, results were first obtained using a simple event-counting method. The number of signal events found in the one-standard-deviation mass window around the nominal B_d^0 mass was 6500, and the background dilution was $D_{\text{back}} = 0.22$. Initial-state tagging was performed with the triggering muon, yielding a tagging dilution of $D_{\text{tag}} = 0.56$ (see Section 17.2.2.4). The time-integrated method yielded a dilution of $D_{\text{int}} = 0.59$. The statistical sensitivity to $\sin 2\alpha$ was then, in the absence of penguin decays, $\delta_{stat}(\sin 2\alpha) = 0.080$. Systematic uncertainties arising from the lepton tagging are expected to be of order 0.01, as in the $B_d^0 \rightarrow J/\psi K_s^0$ channel.

By the year 2005, the branching ratios of the two-body decay channels will have been measured at the *B* factories and at the Tevatron. A 5% relative uncertainty on these branching ratios will give a relative uncertainty on the asymmetry of less than 5% considering only the uncertainty on dilution from the background. However, it is possible that these backgrounds will exhibit some *CP* asymmetry themselves in which case the event-counting method will yield some linear combination of the signal and background *CP* asymmetries.

17.2.3.4 Results from time-dependent fit, allowing for *CP* violation in the background and using hadron identification

To be able to cope with the possible background *CP* asymmetry, and to use fully the time information and the one-standard-deviation π/K separation (see Section 3.4.4), an unbinned maximum-likelihood fit was performed (see [17-16] for more details) for events with mass above 5 GeV. For each event, the likelihood is the sum of the likelihoods of each decay hypothesis (as listed in Table 17-5 plus the charge-conjugated modes, three-body final states being neglected). The likelihood of a given decay hypothesis is computed using the corresponding event fraction, the proper-time and its uncertainty, and, for the corresponding particle-type assignment, the invariant mass of the pair and the measured specific ionisation, as well as the flavour at production and decay time. The flavour information was used to distinguish decays of the Λ_b (which does not oscillate) and the B_s^0 (which oscillates rapidly, with a period of about 0.4 ps for $\Delta m_s = 15\ \text{ps}^{-1}$) from those of the B_d^0 (which oscillates slowly with a period of about 14 ps).

The *CP* asymmetry parameters for all of the decays modes were free parameters of the fit. The time-dependent asymmetry for the non-flavour specific states (namely $B_d^0 \rightarrow \pi^+\pi^-$ and $B_s^0 \rightarrow K^+K^-$) are of the form given in Equation 17-1. *CP* asymmetry for decays to flavour-specific states is time independent and can originate only from direct *CP* violation, since no interference can occur through mixing. Other free parameters were the numbers of events for each decay channel. The total number of events was constrained to the observed one using the Poisson likelihood. The number of events for each channel (except for the combinatorial background) was constrained by the branching ratios given in Table 17-5, with a 5% uncertainty corresponding to the expected uncertainty on these branching ratios in the year 2005. The validity of the fitting method was checked by performing Monte-Carlo experiments with event statistics corresponding to 30 fb^{-1}, with randomised input *CP* asymmetry for signal and all backgrounds. The differ-

ence between the fitted asymmetry and the input asymmetry divided by the fit uncertainty was a normal Gaussian. The fit uncertainties on the *CP* parameters were almost independent of the input *CP* asymmetries, and were symmetric to a very good approximation.

If only the *b* coefficient for the decay $B_d^0 \to \pi^+\pi^-$ was fitted (which equals to sin 2α in the absence of penguin diagrams), fixing the other parameters at their true values, the uncertainty was $\delta b(B_d^0 \to \pi^+\pi^-) = 0.059$. This represents a 25% gain compared to the simple event counting method. If penguins were allowed (*i.e.* the *a* coefficient for $B_d^0 \to \pi^+\pi^-$ was also allowed to vary), the precision on *b* degraded to 0.070. Fitting simultaneously all the background asymmetries degraded the precision on *b* to 0.083. Note that a good accuracy of about 0.02 can also be obtained on the asymmetry in some of the background channels such as $B_d^0 \to K^+\pi^-$, which could be interesting in itself (the asymmetry in $B_d^0 \to K^+\pi^-$ could help in constraining the angle γ [17-19]).

If the numbers of events of each of the decay channels were also included in the fit, constraining the branching ratios with fractional errors of 5%, the final statistical uncertainty obtained was $\delta b(B_d^0 \to \pi^+\pi^-) = 0.085$, showing that there is little dependence on the input branching ratios. In fact, if no input branching ratio information was used, the uncertainty degraded only to 0.090, and the number of events of the various channels can be obtained from the data (provided the list of decays in Table 17-5 is complete).

The uncertainty on the *CP* parameters with and without specific ionisation information is shown on Table 17-6. If specific ionisation were not used, the sensitivity would be $\delta b(B_d^0 \to \pi^+\pi^-) = 0.117$, *i.e.* 35% worse, mainly because of the increased correlation of *b* with the *CP* asymmetry in the backgrounds $B_d^0 \to K^+\pi^-$ and $B_s^0 \to \pi^+K^-$. Furthermore, in this case, the fit did not converge unless the branching ratio information was included. The robustness of the fit was tested by degrading the assumed mass resolution, the proper-time resolution or specific ionisation resolution by 10% (in reality, these resolutions would be measured from reference samples with better accuracy). In all cases, this induced a shift of less than 0.01 in $b(B_d^0 \to \pi^+\pi^-)$.

Table 17-6 Sensitivity to *CP* asymmetries using the 5% constraint on the branching ratios, with and without using specific-ionisation (*dE/dx*) information.

Parameter	Sensitivity (with *dE/dx*)	Sensitivity (no *dE/dx*)
$a(B_d^0 \to \pi^+\pi^-)$	0.065	0.078
$b(B_d^0 \to \pi^+\pi^-)$	0.085	0.117
$a(B_d^0 \to K^+\pi^-)$	0.020	0.027
$a(B_s^0 \to \pi^+K^-)$	0.150	0.251
$a(B_s^0 \to K^+K^-)$	0.097	0.111
$b(B_s^0 \to K^+K^-)$	0.097	0.111
$a(\Lambda_b \to p\pi^-)$	0.022	0.032
$a(\Lambda_b \to pK^-)$	0.023	0.036
a(Comb.)	0.014	0.014

The precision on $b(B_d^0 \to \pi^+\pi^-)$ quoted above does not depend on the actual values of α, A_P/A_T and δ, but the resulting sensitivities on α and δ do. Figure 17-12 shows the precision on α for various input values of α and δ, and various values of the uncertainty on A_P/A_T, when the fit was performed using the specific-ionisation information. A precision of better than 5° was obtained for α in most cases, except when α was close to 45° or 135°, which corresponds to $|\sin 2\alpha| \sim 1$ which is strongly disfavoured by the Standard Model fit [17-11].

Due to the form of Equation 17-3 and Equation 17-4, a four-fold ambiguity in the result is unavoidable. For example, for input values $\alpha = 90°$, $\delta = 30°$ and $A_P/A_T = 0.2$, the solutions $(\alpha,\delta) = (90°, 30°)$, $(109°, 148°)$, $(270°, 210°)$ and $(289°, 330°)$ have the same χ^2-minimum. Additional secondary χ^2 minima sometimes cannot be excluded from the χ^2 difference – in the above example, solutions $(167°, 79°)$ and $(347°, 259°)$ have $\chi^2 - \chi^2_{\min} \sim 3$. Only an overall CKM unitarity-triangle fit can resolve these ambiguities.

Depending on the exact values of α and δ, and provided that A_P/A_T can be theoretically calculated to within 10%, the analysis of the decay $B^0_d \to \pi^+\pi^-$ could provide a constraint on α with a precision approaching 2° after three years of low-luminosity running, with the help of the specific-ionisation measurement in the TRT.

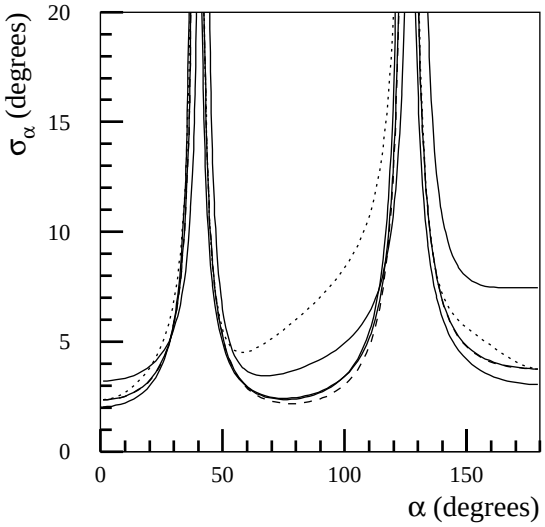

Figure 17-12 Precision for measuring α as a function of α after three years of low-luminosity data-taking. The three solid lines were obtained (from bottom to top) with phase values $\delta = 0°$,30° and 60°, and with $A_P/A_T = 0.2\pm0.02$. The dashed lined was obtained with $\delta = 30°$ and no uncertainty on A_P/A_T and the dotted line with 50% uncertainty on A_P/A_T. Note that the precision in the [-180º–0º] range is symmetric to the one shown.

17.2.4 Analysis of the decay $B^0_s \to J/\psi\,\phi$

17.2.4.1 Introduction

The channel $B^0_s \to J/\psi\phi$ can be used for various studies. Only a very small *CP* asymmetry is predicted in the Standard Model as discussed below, and the observation of a sizeable effect would be a clear sign of new physics. Measurement in ATLAS of the *CP* asymmetry at the level predicted by the Standard Model for this channel is marginal. However, a number of other parameters can be determined within the Standard Model, for example the width difference $\Delta\Gamma_s$. Although these other measurements do not strictly belong in this section, they are covered here since many aspects of the different analyses are coupled.

In the Standard Model, the interference term between the amplitudes for the direct weak decay $B^0_s \to J/\psi\phi$ and the same decay via B^0_s mixing is proportional to

$$e^{-i\xi} = (V^*_{ts}V_{tb}\,V^*_{cs}V_{cb})/(V_{ts}V^*_{tb}V_{cs}V^*_{cb}).$$

This measures the weak-interaction-induced phase that is expected to give rise to a rather small *CP*-violation asymmetry. The phase ξ is related to the angle γ of the unitarity triangle ($\xi = 2\lambda\sin\gamma|V_{ub}|/|V_{cb}|$, where λ is the sine of the Cabibbo angle), but the small expected value of ξ (0.024 – 0.054, see [17-20]) makes the extraction of γ via a measurement of ξ difficult. Larger than expected *CP* violation in the decay $B^0_s \to J/\psi\phi$ would indicate that processes beyond the Standard Model are involved. Tagged samples of $B^0_s \to J/\psi\phi$ decays are needed for the measurement of ξ.

The decay $B_s^0 \to J/\psi\phi$ is also very useful for measuring several, as yet unmeasured, parameters in the B_s^0-meson system. The different masses of the *CP*-even ($B_s{}^L$) and *CP*-odd ($B_s{}^H$) mass eigenstates give rise to mixing between B_s^0 and $\bar{B}_s^0$ mesons. The difference of widths, $\Delta\Gamma_s = \Gamma_H - \Gamma_L$, could be as much as 20% of the average B_s^0 width $\Gamma_s = (\Gamma_H + \Gamma_L)/2$ [17-21]. The angular distribution of the $B_s^0 \to J/\psi\phi$ decay products can be expressed in terms of the amplitudes $A_\parallel$ and A_0 for decays to *CP*-even, and $A_\perp$ for decays to *CP*-odd $J/\psi\phi$ configurations. The expression for the angular distribution contains time-dependent terms proportional to $e^{-\Gamma_H t}$ or to $e^{-\Gamma_L t}$, allowing $\Delta\Gamma_s$ to be determined experimentally. The phase differences between the amplitudes $A_\parallel$, A_0 and $A_\perp$, caused by strong final-state interactions, are parametrised by δ_1 and δ_2, and are measured through their effect on the interference between the amplitudes. Measurements of these parameters require no tagging of the B_s^0 flavour at production.

The B_s^0 decay proper time and the angular distributions of the secondary particles in the decay channel $B_s^0 \to J/\psi\phi$ thus carry information about eight independent parameters of physics interest:

- $\Delta\Gamma_s = \Gamma_H - \Gamma_L$;
- $\Gamma_s = (\Gamma_H + \Gamma_L)/2$;
- two independent *CP* amplitudes $A_\parallel$ and $A_\perp$ (A_0 is constrained by a normalisation condition);
- the strong phase differences δ_2, δ_1;
- the weak phase difference ξ;
- the B_s^0 mixing parameter $x_s = \Delta m_s/\Gamma_s$.

Measurements exist at present only for the B_s^0 lifetime. A method is proposed, based on earlier theoretical works [17-22], to measure some of these parameters, and estimate the expected precision.

The discussion of the $B_s^0 \to J/\psi\phi$ channel is arranged as follows. Firstly the experimental aspects of reconstructing $B_s^0 \to J/\psi\phi$ decays are addressed in Section 17.2.4.2. Then, Section 17.2.4.3 describes how the flavour at production can be tagged for this channel; tagging is used for the extraction of the weak phase difference, ξ, associated with *CP*-violation (Section 17.2.4.5). In Section 17.2.4.4, the maximum-likelihood method that is used to determine the various parameters from the measured angular distributions is described. This is followed in Section 17.2.4.5 by a discussion of how the parameters are determined in two steps, first using the full sample without tagging to determine Γ_s, $\Delta\Gamma_s$, $A_\parallel$, $A_\perp$ and δ_2-δ_1, and then using the subset of tagged events to determined the additional parameter ξ. The conclusions for this channel are presented in Section 17.2.4.6.

17.2.4.2 Reconstruction of $B_s^0 \to J/\psi\,\phi$

The decay $B_s^0 \to J/\psi(\mu\mu)\phi(KK)$ was used for this investigation. Simulated events were generated with PYTHIA and fully simulated with GEANT. The expression $\mu 6\mu 3$ implies the presence of one muon with p_T of at least 6 GeV and one muon with p_T of at least 3 GeV. All of the particles were required to have $|\eta| < 2.5$, and the p_T of each kaon from the ϕ decay was required to be greater than 0.5 GeV. The selection procedure followed quite closely that for the $B_d^0 \to J/\psi K_s^0$ study, and, from the point of view of the experimental techniques, the channels are similar in many ways.

The reconstruction of the J/ψ proceeded as described for $B_d^0 \to J/\psi K_s^0$. Successful fits were retained if the invariant mass was within three standard deviations of the nominal J/ψ mass ($\sigma = 39$ MeV). In the ϕ reconstruction, pairs of oppositely-charged $p_T > 0.5$ GeV particles were fitted to a common vertex and their invariant mass was calculated assuming kaon hypotheses. Successful fits were retained within the mass interval [1.0092–1.0296] GeV. The particles were also required to be collimated within 15 degrees in φ and 10 degrees in θ.

The muons and kaons coming from the J/ψ and ϕ candidates were assumed to come from a $B_s^0 \to J/\psi\phi$ decay and a three-dimensional kinematic fit was performed. The four particles were required to be consistent with coming from a common vertex (probability larger than 0.02), and the momentum of the B_s was required to point to the primary vertex. Cuts on the p_T of the B_s^0 (greater than 10 GeV) and on the proper time (longer than 0.5 ps) were also applied. The resolution on the reconstructed B_s^0 mass was 27 MeV. The residual distribution of the proper lifetime of the reconstructed B_s^0 was well described by a double Gaussian function (Figure 17-13). In the modelling of the angular distributions, described below, a simplified parametrisation of the proper-time resolution was used with a single-Gaussian of width 0.063 ps (see Figure 17-14).

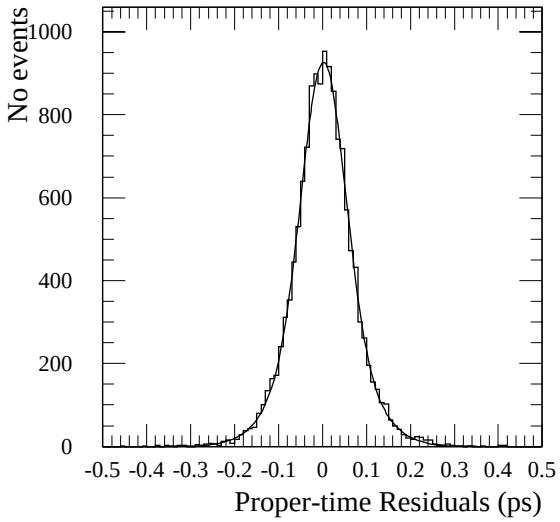

Figure 17-13 Residual distribution of the proper lifetime of the reconstructed B_s^0, fitted with a double Gaussian of widths 0.05 ps and 0.09 ps.

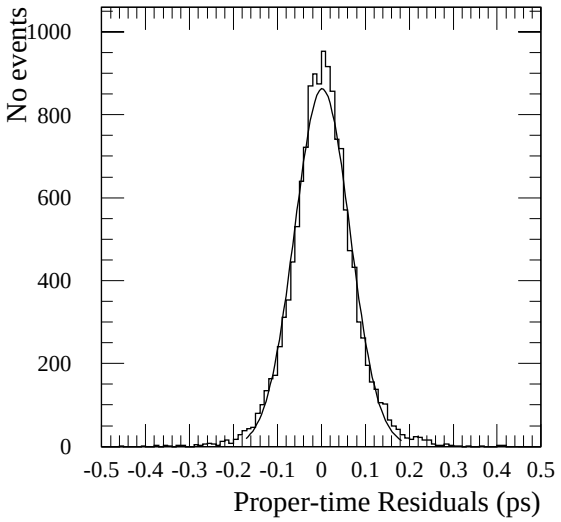

Figure 17-14 Residual distributions of the proper lifetime of the reconstructed B_s^0, fitted with a single Gaussian of width 0.063 ps.

The backgrounds from other processes were estimated using the following Monte Carlo samples: an inclusive sample of $c\bar{c}$ events containing a J/ψ produced by a direct colour-octet model implemented in PYTHIA [17-23]; an inclusive sample of $b\bar{b}$ events giving rise to a J/ψ; and a sample of $B_d^0 \to J/\psi K^{*0}$ decays. The number of events selected for each sample is given in Table 17-7. Essentially all the background came from events containing a b-quark, with the reconstructed J/ψ being genuine and the ϕ being fake. The dominant channel giving rise to such backgrounds is $B_d^0 \to J/\psi K^{*0}$. Typically, the fake ϕ contains one genuine and one misassigned charged kaon. The use of specific ionisation could help in controlling the K^{*0} reflection, but this is still to be studied.

The background studies were mainly done with the fast-simulation program. A smaller sample of inclusive $b\bar{b} \to J/\psi X$ events was, however, studied with full simulation and reconstruction, and the results obtained were found to be consistent with the fast-simulation study.

Table 17-7 Signal statistics and background composition after the acceptance cuts in $|\eta|$ and p_T (first two columns), and after the reconstruction of simulated events (last column). Note that the $B_d \to J/\psi\, K^{*0}$ background is included in the inclusive $b\bar{b} \to J/\psi X$ samples, and should not be double counted.

Process	Cross-section [μb]	N events for 30 fb^{-1}	Reconstruction efficiency	N rec. events for 30 fb^{-1}
signal $B_s^0 \to J/\psi\phi$	2.7 x 10^{-5}	810 000	0.39	318 000
$pp \to J/\psi(\mu 6 \mu 3)X$	1 x 10^{-2}	3 x 10^{8}	<3x10^{-5}	<9400
$b\bar{b} \to J/\psi(\mu 6 \mu 3)X$	4 x 10^{-3}	12 x 10^{7}	4x10^{-4}	47 000
$B_d^0 \to J/\psi(\mu 6 \mu 3)K^{0*}$	2.5 x 10^{-4}	7.5 x 10^{6}	3x10^{-3}	21 000

17.2.4.3 Tagging

Much of the analysis described below can be performed without tagging the flavour at production of the B_s^0 that decayed to $J/\psi\phi$. However, the measurement of the weak phase, described at the end of Section 17.2.4.5, requires tagging. Here some issues of tagging that are specific to the $B_s^0 \to J/\psi\phi$ analysis are addressed.

Events with an additional lepton can provide a subsample of tagged events. However, the efficiency of lepton tagging is low due to the relatively small semileptonic branching ratios of B-mesons and the effects of the p_T and η cuts. The tagging efficiency can be increased by using the jet charge to determine the flavour of the B at production. Note that the mass of the resonance B^{**} is expected to be such that the decay to $B_s^0 K$ is not kinematically possible [17-24], and therefore, the jet-charge tag can exploit only the fragmentation correlation in case of B_s^0 mesons.

The jet charge Q_{jet} is defined by:

$$Q_{jet} = \frac{\sum_i q_i p^{\kappa}{}_i}{\sum_i \left| p^{\kappa}{}_i \right|}$$

where q_i is the charge of the i^{th} particle, and p_i is a momentum measure. According to fragmentation models, the particles are ordered in the momentum component parallel to the original quark direction. On the other hand, maximising the momentum component transverse to the beam-line would guarantee that no very hard forward particles are wrongly assigned to the jet. Various options were considered, and the best results were obtained by using the momentum component parallel to the reconstructed B-meson direction, which is used in the following. The parameter κ controls the relative influence of the soft and hard tracks in the jet charge. Using Monte Carlo models, the optimum performance was obtained with a value of κ near to 0.5, though in principle additional information could be extracted by considering a range of κ values.

Only particles which satisfied the general acceptance requirements of $p_T > 0.5$ GeV and $|\eta| < 2.5$ were considered. Particles were required to be in a cone with $\Delta R<0.8$ of the reconstructed B-meson momentum vector, and particles from the $B_s^0 \to J/\psi\phi$ decay were excluded. Particles with impact parameters $|d_0| > 1$ cm were also excluded, as they probably originate from decays rath-

er than the fragmentation process. After these selections, there were cases where there were no particles remaining to form the jet charge, and also cases where the charge was based only on one particle.

The algorithm was optimised by minimising the estimate of the statistical error on the *CP*-violating weak phase measurement by adjusting the square of the dilution factor D_{tag} and the tag efficiency ε. This resulted in a lower efficiency (62%) and a higher purity (D_{tag} = 0.23) than for jet-charge tagging in the $B_d^0 \to J/\psi K_S^0$ analysis. In principle, the algorithm could be further optimised by excluding cases where the estimated jet charge is near to zero where the chances of incorrect assignment are high. Preliminary studies indicate that the performance is enhanced with the exclusion of cases with $|Q_{jet}| < 0.3$. This will be optimised further using higher statistics.

17.2.4.4 Modelling of $B_s^0 \to J/\psi\,\phi$ decays and the likelihood function

The precision of the experimental determination of the parameters describing the $B_s^0 \to J/\psi\phi$ decay was estimated using a maximum-likelihood fit to Monte Carlo simulated data. The decay $B_s^0 \to J/\psi\phi$ was modelled according to a probability density function:

$$F^{\pm}(t,\Omega) = \frac{1}{4\pi^2} \times \frac{9}{8} \times \sum_{i=1}^{8} f_i^{\pm}(t) \times F_i(\Omega) \qquad 17\text{-}5$$

where the superscript +(-) indicates B_s^0 ($\bar{B}_s^0$), the functions f_i are bilinear combinations of time-dependent decay amplitudes, and $\Omega = (\theta_1,\theta_2,\varphi)$, where θ_1,θ_2 and φ are angles describing the direction of the secondary particles in the decay $B_s^0 \to J/\psi(\mu\mu)\,\phi(KK)$ as defined in Figure 17-15. The functions F_i are trigonometric functions of the decay angles. The functions f_i and F_i are defined in [17-25]. In the simulation, the values of the eight unknown independent parameters (two amplitude values $A_{||}$ and $A_{\perp}$, two strong phase differences δ_2 and δ_1, the mixing parameter x_s, the weak phase ξ and the two decay rates Γ_H and Γ_L) were chosen based on the latest theoretical and experimental results ([17-21], [17-22] and [17-26]).

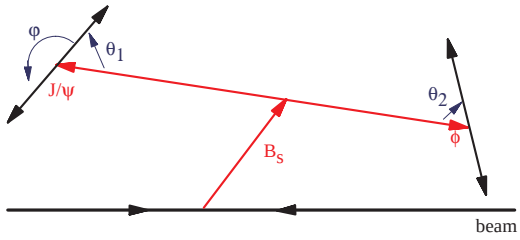

Figure 17-15 Definition of the three angles: θ_1 is the angle of the muon momentum in the J/ψ rest frame with the *z*-axis parallel to the J/ψ momentum in the B_s^0 rest frame; θ_2 is defined in a similar way for the φ decay; φ is the angle between the J/ψ and the φ decay planes.

The simulation took into account the proper-time resolution approximated by a single Gaussian function as obtained from the full detector simulation and reconstruction. The acceptance as a function of proper time and the three angles was included. The background was also simulated, and was taken to be flat in the decay angles. The time dependence of the background was assumed to have a form $e^{-\Gamma t}$ where Γ corresponds to the average neutral *B*-hadron lifetime. The level of background, *b*, will be determined from the invariant-mass distribution, and was fixed in the fit. The likelihood function had the form:

$$L = \prod_{i=1}^{N} \frac{\int_0^{\infty} \left(\varepsilon_1 F^+(t_i, \Omega_i) + \varepsilon_2 F^-(t_i, \Omega_i) + b e^{-\Gamma t_i} \right) \times e^{-(t_i - t')^2 / 2\delta t^2} dt'}{\int_{t_{min}}^{\infty} \left(\int_0^{\infty} \left(\varepsilon_1 F^+(t, \Omega) + \varepsilon_2 F^-(t, \Omega) + b e^{(-\Gamma t)} \right) \times e^{-(t - t')^2 / 2\delta t^2} dt' \right) dt}$$

where for untagged events $\varepsilon_1 = \varepsilon_2 = 0.5$; for events with a B_s^0 tagged as a particle $\varepsilon_1 = 1\text{-}\omega$ and $\varepsilon_2 = \omega$, where ω is the wrong-tag fraction; for a B_s^0 tagged as an antiparticle $\varepsilon_1 = \omega$ and $\varepsilon_2 = 1\text{-}\omega$. The index i is running over the events. Finally, t_{min} is the minimum proper lifetime allowed in the event selection.

17.2.4.5 Parameter determination and estimation of precision

The most complete analysis would include both tagged and untagged events in a single maximum-likelihood fit. It became clear, however, that the expected experimental precision was not sufficient to allow the simultaneous determination of all eight unknown parameters. Instead, the analysis was divided into two steps. In the first step, the full event statistics were used. In the second step only the events with a tag were analysed. This allowed several useful approximations to be made.

The full event statistics, including both tagged and untagged events, were modelled according to Equation 17-5. Five parameters, $\Delta\Gamma_s$, Γ_s, $A_\parallel$, $A_\perp$ and δ_2-δ_1, were determined in the fit assuming $\varepsilon_1 = \varepsilon_2 = 0.5$, which leads to the cancellation of the oscillatory terms in the likelihood function. With this assumption, the three other parameters ξ, x_s and $\delta_2+\delta_1$ have a negligible influence on the likelihood function, and so were fixed in the fit.

The rate difference $\Delta\Gamma_s = \Gamma_H - \Gamma_L$ could be determined by this method with a relative statistical error of less than 12% with 30 fb^{-1}, corresponding to 300 000 signal events (see Figure 17-16). The result depends strongly on the value of $\Delta\Gamma_s/\Gamma_s$, while the decay-time resolution is not critical here (see Figure 17-17). The relative statistical errors on the other free parameters are summarised in Table 17-8. The statistical errors are typically a few percent, except for the strong phase difference $\delta_2 - \delta_1$, for which the probability density function is insensitive if $(\delta_2 - \delta_1) \sim \pi$, as suggested by theoretical models (see Dighe, Dunietz and Fleischer in [17-22], and references therein).

Table 17-8 Summary of the analysis of the full sample with 30 fb^{-1}.

Number of signal events	300 000
Number of background events	45 000
$\delta t/t$	4.4%
Input parameters	$\Delta\Gamma_s/\Gamma_s = 0.15$, $x_s = 20$, $\xi = 0.039$, $\delta_2+\delta_1 = -\pi$
$\delta(\Delta\Gamma_s)/\Delta\Gamma_s$	12%(stat.)+7%(syst.)
$\delta(\Gamma_s)/\Gamma_s$	0.7%(stat.)+0.3%(syst.)
$\delta(A_\parallel)/A_\parallel$	0.7%(stat.)+0.3%(syst.)
$\delta(A_\perp)/A_\perp$	3%(stat.)+1%(syst.)

Several sources of systematic errors were considered. The mean lifetime in the background sample must be known, and will be determined from sidebands in the reconstructed mass distribution. If this mean lifetime was overestimated by 3% in the likelihood function, the measured value of $\Delta\Gamma_s$ was shifted downwards by 0.04, giving a 7% systematic error. The likelihood fit also used the measured proper decay time and its error for each event. The error depends on the position uncertainty on the secondary

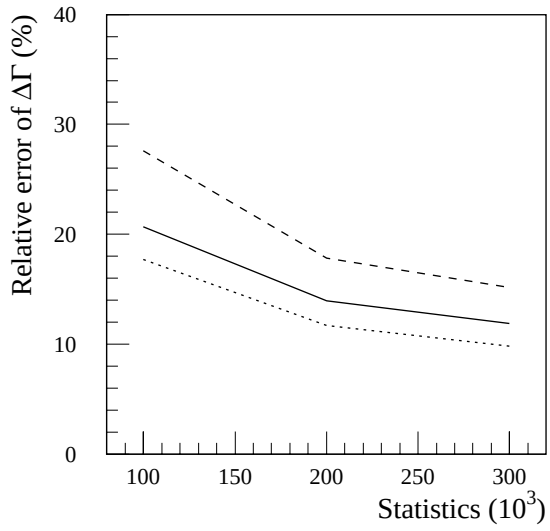

Figure 17-16 The relative error of $\Delta\Gamma_s$ as a function of signal statistics for three levels of background: 15% (full line), 30% (dashed line) and no background (dotted line). $\Delta\Gamma_s$ was determined by a maximum-likelihood fit. The four other parameters of the fit were Γ_s, $A_{\|}$, $A_{\perp}$ and δ_2-δ_1.

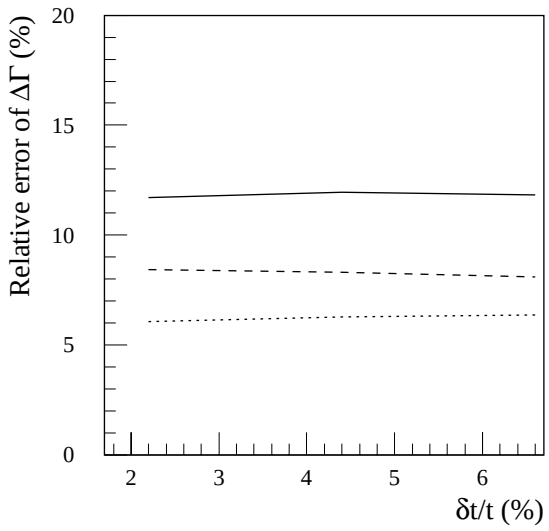

Figure 17-17 The relative error of $\Delta\Gamma_s$ as a function of the relative precision of the proper-lifetime measurement for three values of the ratio $\Delta\Gamma_s/\Gamma_s$. The full line corresponds to $\Delta\Gamma_s/\Gamma_s$ = 15%, the dashed line to $\Delta\Gamma_s/\Gamma_s$ = 20%, and the dotted line to $\Delta\Gamma_s/\Gamma_s$ = 25%. The statistics here is 300 000 signal events, and the background is 15% of the signal.

vertex and on the momentum error, and a mis-estimation of either can introduce a systematic error on the $\Delta\Gamma_s$. This effect was tested by assuming a proper decay-time uncertainty in the likelihood fit that was 5% larger than the uncertainty used in the simulation; this conservative estimate resulted in a negligible systematic error.

The angular distribution of the background may have a complicated shape. Decay channels that are flat in decay angle (*e.g.* the decay to non-resonant states $B \to J/\psi K\pi$) will gain apparent structure due to incorrect mass assignments. Background channels with polarisation (such as $B_d^0 \to J/\psi K^{*0}$) will have an intrinsic angular structure and will also be deformed by incorrect mass assignments. However, the actual background shape can be estimated from the side bands. Also, if the background composition is well determined, the background shape can be calculated from the measured distributions of the background channels. No estimate is included as yet for the systematic effects of the non-flat background distributions.

The second part of the analysis was done for tagged events only, using the jet-charge-tag method described in Section 17.2.4.3 (there is scope to improve the measurement by using other tagging methods in addition). In order to give an estimate of the performance in a simple case, seven of the eight parameters were fixed, leaving only the weak phase ξ free. This was based on the assumption that the values of the other parameters can be determined in other measurements (using untagged $B_s^0 \to J/\psi\phi$, and $B_d^0 \to J/\psi K^{*0}$, and $B_s^0 \to D_s\pi$ events). For this ideal case, where all other parameters were measured with negligible errors, the weak phase can be obtained with a statistical precision $\delta(\xi) \sim 0.03$, assuming the Standard Model expected values: $\xi = 0.039$, $x_s = 20$ and $\Delta\Gamma_s/\Gamma_s = 0.15$. The errors obtained for different values of the mixing parameter and proper decay-time resolutions are shown in Figure 17-18. The results for the tagged analysis are summarised in Table 17-9.

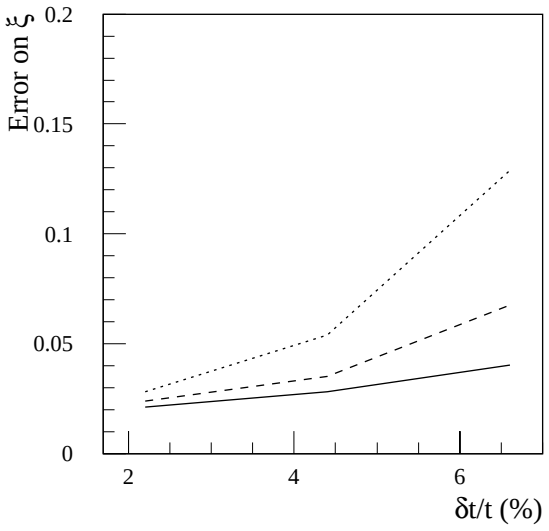

Figure 17-18 The error on the weak phase ξ as a function of the relative precision of proper-lifetime measurement for three values of the B_s^0 mixing parameter x_s. The full line corresponds to $x_s = 20$, the dashed line to $x_s = 30$ and dotted line to $x_s = 40$. The weak phase ξ was determined by a maximum-likelihood fit, while all other seven parameters were fixed.

Table 17-9 Summary of the tagged-sample analysis with 30 fb^{-1} data.

Number of signal events	180 000
Number of background events	27 000
Proper-time resolution	4.4%
Input parameters	$\Delta\Gamma_s/\Gamma_s = 0.15$, $x_s = 20$, $\tau_{Bs} = 1.61$ ps, $\delta_2 = 0$, $\delta_1 = -\pi$ $\lvert A_\parallel \rvert / \lvert A_0 \rvert = 0.8$; $\lvert A_\perp \rvert / \lvert A_0 \rvert = 0.37$ $\xi = 0.039, \tau_B = 1.58$ ps.
$\delta(\xi)$	0.03 (stat.)

The results presented above are derived in the context of the Standard Model. However, it is possible to express the *CP* asymmetry purely in terms of the helicity amplitudes, Γ_s, $\Delta\Gamma_s$, x_s and the phase ξ. The precision of the asymmetry measurement can be studied, independent of the model, as a function of any triplet of $\Delta\Gamma_s$, x_s and ξ values, using the already-measured value of Γ_s. Table 17-10 shows results for some examples of input parameters. The first row in the Table shows the case of the Standard Model, with the input parameters based on an overall fit to existing experimental data. The second and third rows show two examples for non-standard models [17-27], [17-28]. As expected, there is some degradation of the precision on the measurement of ξ with increasing x_s, due to the difficulty in resolving the rapid oscillations. On the other hand, the precision of the measurement of ξ is not strongly dependent on the value of ξ. For example, keeping $x_s = 20$, $\Delta\Gamma_s/\Gamma_s = 0.15$ and using an input value $\xi = 0.16$ (instead of 0.04 in the Standard Model), leaves the precision unchanged at $\delta(\xi) = 0.03$. Thus, the analysis gives high sensitivity to any new physics that significantly enhances the *CP* asymmetry in this channel over a wide range of x_s values.

Table 17-10 Precision on measurement of *CP*-violation parameter, ξ, as a function of $\Delta\Gamma_s/\Gamma_s$, x_s and the true value of ξ.

x_s	$\Delta\Gamma_s/\Gamma_s$	Input value of ξ	δ(ξ)
20	0.15	0.04 (SM)	0.03
33	0.15	0.08 ([17-27])	0.05
39	0.15	0.17 ([17-28])	0.07

17.2.4.6 Conclusions

The main results of the $B_s^0 \to J/\psi\phi$ study are summarised in Tables 17-8 and 17-9. ATLAS can measure $\Delta\Gamma_s$ with a relative error $\delta(\Delta\Gamma_s)/\Delta\Gamma_s$ = 12% (stat.)+7% (syst.). The fit allows the simultaneous determination of other parameters (the average B_s^0 width Γ_s and the amplitudes $A_\parallel$ and $A_\perp$ for the decays to *CP*-even and *CP*-odd $J/\psi\phi$ configurations). Making use of events tagged using the jet-charge technique, the *CP*-asymmetry parameter ξ can be measured with high precision (δ(ξ) = 0.03 for x_s = 20).

17.2.5 Analysis of the decay $B_d^0 \to D^0K^{*0}$

The use of the decay amplitudes of several neutral B_d^0 decays in determining the angle $\gamma = \arg(-V_{ud}V^*_{ub}/V_{cd}V^*_{cb})$ was investigated. The following relations hold between six decay modes of the B_d^0 to neutrals:

$$A(B_d{}^0 \to \bar{D}^0 K^{*0}) = A(\bar{B}_d{}^0 \to D^0 \bar{K}^{*0}),$$

$$A(B_d{}^0 \to D^0 K^{*0}) = A(\bar{B}_d{}^0 \to \bar{D}^0 \bar{K}^{*0}),$$

$$A(B_d{}^0 \to D^0{}_{CP} K^{*0}) \neq A(\bar{B}_d{}^0 \to D^0{}_{CP} \bar{K}^{*0}),$$

when D^0 and K^{*0} decay into $K\pi$, and $D^0{}_{CP}$ indicates a decay to *CP* eigenstates ($\pi\pi$, KK). Two triangles can be constructed, which differ in the length of one side only [17-29]. The angle 2γ is formed as shown in Figure 17-19. Thus, by measuring the decay rates in the different channels, the angle γ could be determined.

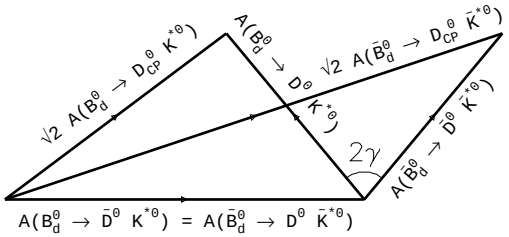

Figure 17-19 The two triangles formed of decay amplitudes of six possible decays of the form $B^0{}_d \to D^0K^{*0}$.

The assumed branching ratios used in the study were agreed between the LHC experiments (see [17-30]); some of the expected branching ratios are very low, in particular that for $B_d^0 \to D^0K^{*0}$, which is of the order of 10^{-6}. After the requirement that the events contained a trigger muon with $p_T > 6$ GeV and that the four final-state particles were within the detector acceptance, approximately 60 events were retained per year in the rarest decay mode. Furthermore, the LVL2 trigger for this decay, based on the D^0 and K^{*0} invariant masses, would have to operate with high p_T thresholds for the hadrons in or-

der to limit the rate from the combinatorial background. It can be concluded that the measurement of all the six decay modes by ATLAS alone would not be feasible assuming Standard Model branching ratios.

17.2.6 Conclusions on *CP* violation

The angle β of the unitarity triangle is expected to be measured with a precision of

$$\delta(\sin 2\beta) = 0.012 \text{ (stat.)}$$

with an integrated luminosity of 30 fb^{-1}, collected at low-luminosity data-taking. The precision can be improved further to about 0.010, if triggering on muons with p_T>3 GeV can be achieved at LVL2. Systematic uncertainties arising from the production asymmetry, flavour tagging and background are expected to be controlled to better than 1% by using the non-*CP*-violating decays $B^+ \to J/\psi(\mu\mu)K^+$ and $B_d^0 \to J/\psi(\mu\mu)K^{*0}$ (where $K^{0*} \to K^+\pi^-$). Furthermore, the availability of many tagging algorithms and the large statistics of tagged and untagged signal and background samples provide the flexibility to perform internal cross-checks of the analysis.

Since the ATLAS Technical Proposal, significant progress has been made in the analysis of the decay $B_d^0 \to \pi^+\pi^-$ to overcome problems associated with the large background. An effort has been made to use the specific ionisation in the TRT to separate pions, kaons and protons on a statistical basis. A sophisticated fitting method has been developed to use maximally the event-by-event information: each event was assigned a probability to belong to any of the decay classes (signal and backgrounds), based on the probability distribution functions on proper time and its uncertainty, the invariant mass, the specific ionisation of the two particles and the flavour at production and at the decay time. Possible *CP* asymmetries in the background were taken into account. With an integrated luminosity of 30 fb^{-1}, the fit gave a statistical precision on the mixing-induced *CP*-violation amplitude *b* of:

$$\delta b(B_d^0 \to \pi^+\pi^-) = 0.085 \text{ (stat.)}.$$

The branching ratios of the signal and background channels were constrained to estimated values within 5% uncertainty, since the branching ratios are expected to be measured before ATLAS can proceed to the *CP*-violation measurement of this channel. However, if the branching fractions were left completely free in the fit, the precision would degrade only to 0.090. On the other hand, if no *dE/dx* information were used, the precision would degrade to 0.117. The sensitivity to the direct *CP*-violation amplitude *a* was 0.065. If there were no penguin graphs contributing to this decay, the *b* coefficient would be equal to $\sin 2\alpha$, which could be measured with a precision of 0.059.

The sensitivity to the angle α of the unitarity triangle depends on the value of α, on the ratio of the penguin and tree-level amplitudes, and on the strong phase δ. Nevertheless, over most of the range, the precision on α approaches 2° after three years of low luminosity running.

The third angle of the unitarity triangle, γ, is difficult to measure. Using tagged $B_s^0 \to J/\psi\phi$ decays, the weak phase $\xi = 2\lambda\sin\gamma|V_{ub}|/|V_{cb}|$ can be measured with a statistical precision of 3% (x_s = 20) using the 180 000 reconstructed events expected for an integrated luminosity of 30 fb^{-1}. Nevertheless, there is no sensitivity to the angle γ in the Standard Model. The use of the six decays $B_d^0 \to D^0K^{*0}$ does not seem feasible for γ measurement either. The unitarity triangle will, however, already be overconstrained by the measurements of the two angles α and β, and the B_s^0-mixing measurement (see following section), which measures a side of the unitarity trian-

gle. The current Standard Model best estimate for the angle γ yields $\gamma = (59.5\,^{+8.5}_{-7.5})^{o}$ [17-11]. Furthermore, it has been proposed that the ratio of the branching fractions of charged and neutral B mesons into $K\pi$ final states would constrain $\sin^2\gamma$, but there are diverging views on the theoretical validity of the proposal (see [17-11] and references therein).

The $B_s^0 \to J/\psi\phi$ decays are also useful for various other measurements of the B_s^0-meson system, and an angular-analysis technique was developed. Since tagging is not needed, the statistics are fairly large – 300 000 events for an integrated luminosity of 30 fb^{-1}. The width difference of the B_s^0-meson eigenstates, $\Delta\Gamma_s$, is expected to be measured with a relative statistical precision of 12%, and Γ_s can be measured with a relative statistical precision of 0.7%. In addition, the decay amplitudes to *CP*-even and *CP*-odd final states can be measured with a relative precision of 0.7% and 3%, respectively.

17.3 Measurements of B_s^0 oscillations

17.3.1 Introduction

The observed B_s^0 and $\bar{B}_s^0$ states are linear combinations of two mass eigenstates, denoted here as H and L. Due to the non-conservation of flavour in charged weak-current interactions, transitions between B_s^0 and $\bar{B}_s^0$ states occur with a frequency proportional to $\Delta m_s = m_H - m_L$.

Experimentally, these $B_s^0 - \bar{B}_s^0$ oscillations have not yet been observed directly. In the Standard Model, their frequency is predicted in [17-11] to be between 12.0 ps^{-1} and 17.6 ps^{-1} with 68% CL, and lower than 20 ps^{-1} at 95% CL, significantly larger than the corresponding value Δm_d in the $B_d^0 - \bar{B}_d^0$ system. From measurements done by the ALEPH, DELPHI and OPAL experiments at LEP, by SLD at SLC, and by CDF at the Tevatron, a combined lower bound of $\Delta m_s > 12.4$ ps^{-1} at 95% CL has been established [17-31]. In the $B_d^0 - \bar{B}_d^0$ system, the oscillations have been directly observed and a rather precise value $\Delta m_d = 0.464 \pm 0.018$ ps^{-1} [17-32] has been measured.

The values for Δm_d and Δm_s predicted in the Standard Model by computing the corresponding box diagrams, with the top-quark contribution assumed to be dominant, are proportional to $|V_{td}|^2$ and $|V_{ts}|^2$ respectively. The direct determination of V_{td} and V_{ts} from Δm_d and Δm_s is, however, hampered by hadronic uncertainties. These uncertainties partially cancel in the ratio:

$$\frac{\Delta m_s}{\Delta m_d} = \frac{M_{B_s}}{M_{B_d}} \frac{\hat{B}_{B_s} f_{B_s}^2}{\hat{B}_{B_d} f_{B_d}^2} \left|\frac{V_{ts}}{V_{td}}\right|^2 ,$$

where M_B are the B-meson masses, $\hat{B}_B$ are the bag parameters, and f_B are the B-meson form factors. Using the experimentally-measured masses and a value for the ratio $\xi = (\sqrt{\hat{B}_{B_s}} f_{B_s})/(\sqrt{\hat{B}_{B_d}} f_{B_d})$ which can be computed in lattice QCD, a better constraint for $|V_{ts}/V_{td}|$ can be obtained, which can then be converted into a constraint of $|V_{td}|$, the worst-measured side of the unitarity triangle.

The probability density to observe an initial B_s^0 meson decaying at time t after its creation as a $\bar{B}_s^0$ meson is given by:

$$P_{B^0\bar{B}^0}(t) = \frac{\Gamma_s^2 - \left(\frac{\Delta\Gamma_s}{2}\right)^2}{2\Gamma_s} e^{-\Gamma_s t}\left(\cosh\frac{\Delta\Gamma_s t}{2} + \mu_0 \cos\Delta m_s t\right),$$

where $\mu_0 = -1$, $\Delta\Gamma_s = \Gamma_H - \Gamma_L$ and $\Gamma_s = (\Gamma_H + \Gamma_L)/2$. For an initial B_s^0 meson, the probability density $P_{B^0B^0}(t)$ to decay as a B_s^0 meson at time t is given by the above expression with $\mu_0 = +1$. The small effects of *CP* violation are neglected in the above relation. Unlike $\Delta\Gamma_d$ which can be safely neglected, the width difference in the $B_s^0 - \bar{B}_s^0$ system $\Delta\Gamma_s$ could be as much as 20% of the total width Γ_s [17-21].

Experimentally, Δm_s can be determined by measuring the asymmetry:

$$A(t) = \frac{P_{B^0B^0}(t) - P_{B^0\bar{B}^0}(t)}{P_{B^0B^0}(t) + P_{B^0\bar{B}^0}(t)} \sim \frac{\cos\Delta m_s t}{\cosh\frac{\Delta\Gamma_s t}{2}}.$$

B_s^0 ($\bar{B}_s^0$) is tagged at the production point by the muon used for the LVL1 trigger; at the decay vertex, the meson's state is given by the charge-sign of one of the decay products. From the fit of the measured asymmetry, the oscillation period can be determined.

17.3.2 Event reconstruction

The signal channels considered for the measurement of $B_s^0 - \bar{B}_s^0$ oscillations were $B_s^0 \to D_s^- \pi^+$ and $B_s^0 \to D_s^- a_1^+$, with $D_s^- \to \phi\pi^-$ followed by $\phi \to KK$ (called ϕ mode in the following). For both B_s decay channels, the decay mode $D_s^- \to K^{*0}K^-$ with $K^{*0} \to K^+\pi^-$ (called K^{*0} mode in the following) may also be considered in order to increase the signal statistics. The K^{*0} mode analysis for $B_s^0 \to D_s^- a_1^+$ decay channel is discussed in this report. However, since this mode is not yet included in the LVL2 trigger, the maximum value of Δm_s which can be measured by ATLAS was computed without the K^{*0} mode, and the effect of including this decay mode is shown separately. Using a 3 GeV cut on the p_T of the three tracks from $D_s^- \to K^{*0}K^-$ and other cuts similar to those for the ϕ-mode trigger, an increase of around 235 Hz would be expected in the LVL2 trigger rate from adding the K^{*0} mode.

The simulated events were generated using PYTHIA 5.7 in the framework of ATGEN-B (ATLAS program for *B*-event generation), and then passed through the ATLAS simulation program DICE (Inner Detector only). Details about the general physics parameters used in ATGEN-B may be found in Section 17.1.2. In the simulation, the *b*-quark was forced to decay semileptonically giving a muon with $p_T > 6.0$ GeV and $|\eta| < 2.5$. The $\bar{b}$ was forced to produce the required *B*-decay channel. All the final-state particles from the *B* decay were required to have $p_T > 0.5$ GeV and $|\eta| < 2.5$. The simulated events were reconstructed using the xKalman package from ATRECON.

17.3.2.1 Reconstruction of the D_s^- decay vertex in the $D_s^- \to \phi\pi^-$ decay mode

The reconstruction of the D_s^- vertex in the $D_s^- \to \phi\pi^-$ decay mode proceeded via two steps (here and in the following charge-conjugate states are implicitly included). The ϕ decay vertex was first reconstructed by considering all combinations of pairs of oppositely-charged tracks with $p_T > 1.5$ GeV for both tracks. Kinematic cuts on the angles between the two tracks

$\Delta\theta_{KK} < 10°$ and $\Delta\varphi_{KK} < 10°$ were also imposed. The two-track vertex was then fitted assigning the kaon mass to both tracks. Combinations passing a fit-probability cut of 1% with the invariant mass within $3\sigma_{\phi}$ of the nominal ϕ mass were selected as ϕ candidates. To all accepted ϕ candidates, a third negative track with $p_T > 1.5$ GeV from the remaining ones was added. The pion mass was assigned to the third track and a three-track vertex was refitted. Combinations of three tracks which had a fit probability greater than 1% and an invariant mass within $3\sigma_{D_s}$ of the nominal D_s^- mass were selected as D_s^- candidates. Figure 17-20 and Figure 17-21 show the reconstructed invariant-mass distributions for ϕ and D_s^-, respectively, in the channel $B_s^0 \to D_s^-(\phi\pi^-)a_1^+$. Similar distributions were obtained in the decay channel $B_s^0 \to D_s^-(\phi\pi^-)\pi^+$.

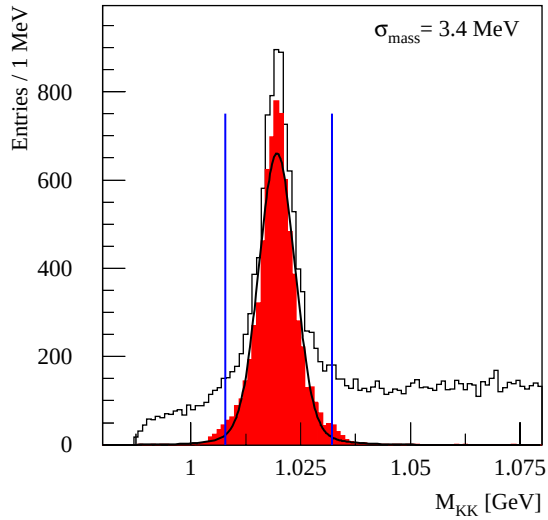

Figure 17-20 Reconstructed ϕ invariant-mass distribution in the channel $B_s^0 \to D_s^-(\phi\pi^-)a_1^+$. In the dark histogram, the reconstructed ϕ matches a generated ϕ. The distributions only include the contribution from Monte Carlo events for the indicated signal channel.

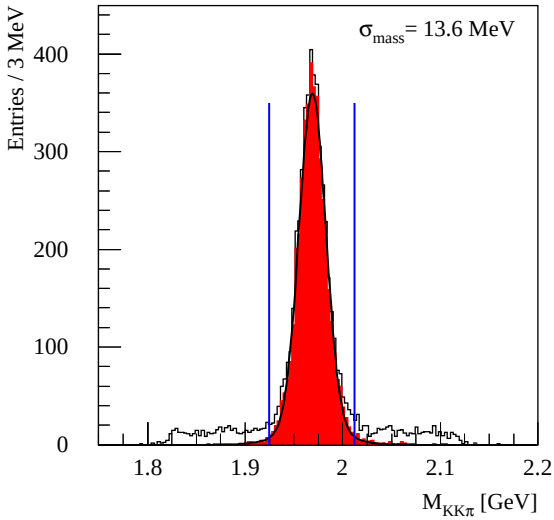

Figure 17-21 Reconstructed D_s^- invariant-mass distribution in the channel $B_s^0 \to D_s^-(\phi\pi^-)a_1^+$. In the dark histogram, the reconstructed D_s^- matches a generated D_s^-. The distributions only include the contribution from Monte Carlo events for the indicated signal channel.

17.3.2.2 Reconstruction of the D_s^- decay vertex in the $D_s^- \to K^{*0}K^-$ decay mode

The reconstruction of the D_s^- decay vertex in the decay mode $D_s^- \to K^{*0}K^-$ was performed using similar techniques to those used in the $D_s^- \to \phi\pi^-$ case. First, K^{*0} candidates were reconstructed from combinations of pairs of oppositely-charged tracks, with $p_T > 3.0$ GeV for each track, and $\Delta\theta_{K\pi} < 10°$ and $\Delta\varphi_{K\pi} < 20°$ assuming that the positive-charge track was a kaon and the negative-charge one was a pion. The two tracks were required to originate from the same vertex (vertex fit probability greater than 1%) and have an invariant mass within one Γ_{BW} of the nominal K^{0*} mass.

Additional negative-charge tracks with $p_T > 3.0$ GeV were combined with K^{*0} candidates, applying the kaon hypothesis for the additional tracks. The three tracks were then fitted as originating from a common vertex; no mass constraint was required for the tracks from K^{*0}, due to the large K^{*0} natural width. Combinations with a fit probability greater than 1% and with an invariant mass within $3\sigma_{D_s}$ of the nominal D_s^- mass were selected as D_s^- candidates.

The invariant-mass distributions of the reconstructed K^{*0} and D_s^- candidates are shown in Figure 17-22 and Figure 17-23, respectively.

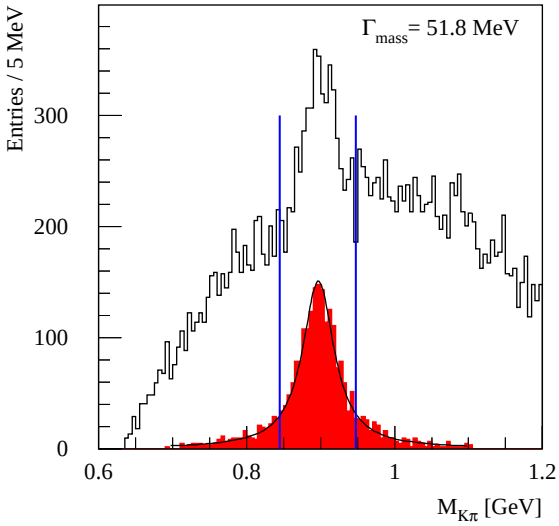

Figure 17-22 Reconstructed K^{*0} invariant-mass distribution in the $B_s^0 \to D_s^-(K^{*0}K^-)a_1^+$ channel. In the dark histogram, the reconstructed K^{*0} matches a generated K^{*0}. The distributions only include the contribution from Monte Carlo events for the indicated signal channel.

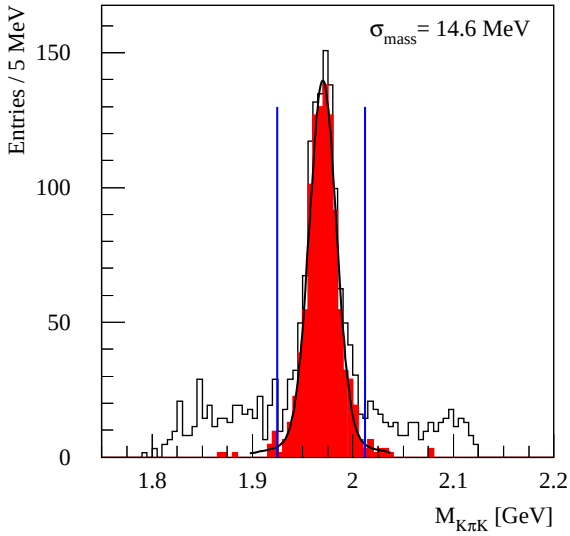

Figure 17-23 Reconstructed D_s^- invariant-mass distribution in the $B_s^0 \to D_s^-(K^{*0}K^-)a_1^+$ channel. In the dark histogram, the reconstructed D_s^- matches a generated D_s^-. The distributions only include the contribution from Monte Carlo events for the indicated signal channel.

17.3.2.3 Reconstruction of the a_1^+ decay vertex

For each reconstructed D_s^- meson, a search was made for a_1^+ candidates in three-particle combinations of the remaining charged tracks. In a first step, ρ^0 mesons were reconstructed from all combinations of two tracks with opposite charges and with $p_T > 0.5$ GeV for both tracks, each particle in the combination being assumed to be a pion. Kinematic cuts $\Delta\theta_{\pi\pi} < 15°$ and $\Delta\varphi_{\pi\pi} < 35°$ were used to reduce the combinatorial background. The two selected tracks were then fitted as originating from the same vertex; from the combinations passing a fit probability cut of 1%, those with an invariant mass within 1.5 Γ_{BW} of the nominal ρ^0 mass were selected as ρ^0 candidates.

Next, a positive track with $p_T > 0.5$ GeV from the remaining charged tracks was added to the ρ^0 candidate, assuming the pion hypothesis for the extra track. The three tracks were then fitted as originating from a common vertex, without any mass constraints. Combinations with a fit probability greater than 1% and with an invariant mass within 300 MeV of the nominal a_1^+ mass were selected as a_1^+ candidates.

The invariant-mass distributions of the reconstructed ρ^0 and a_1^+ candidates are shown in Figure 17-24 and Figure 17-25, respectively.

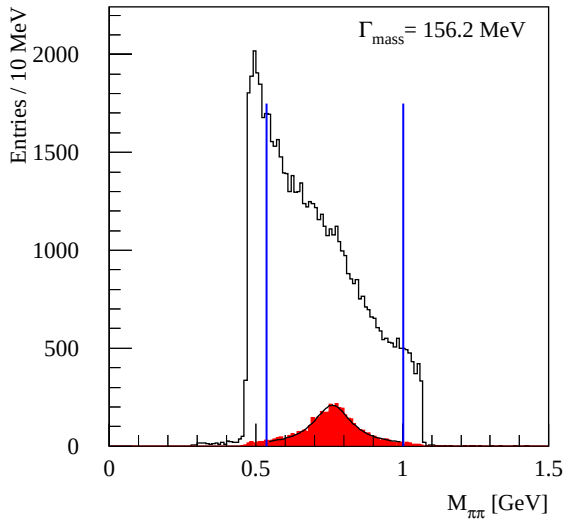

Figure 17-24 Reconstructed ρ^0 invariant-mass distribution in the channel $B_s^0 \to D_s^-(\phi\pi^-)a_1^+(\rho^0\pi^+)$. In the dark histogram, the reconstructed ρ^0 matches a generated ρ^0. The distributions only include the contribution from Monte Carlo events for the indicated signal channel.

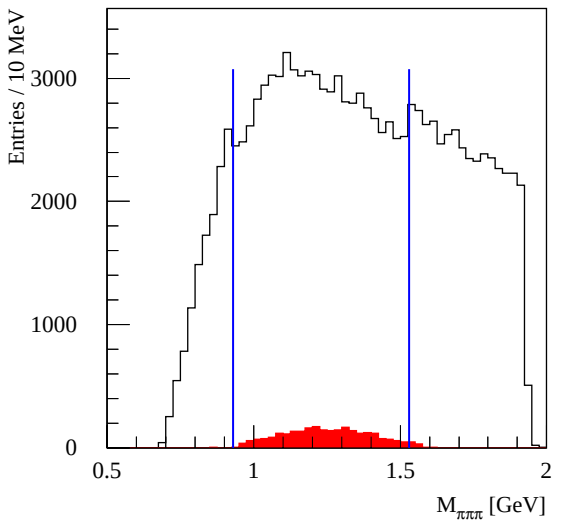

Figure 17-25 Reconstructed a_1^+ invariant-mass distribution in the channel $B_s^0 \to D_s(\phi\pi^-)a_1^+(\rho^0\pi^+)$. In the dark histogram, the reconstructed a_1^+ matches a generated a_1^+. The distributions only include the contribution from Monte Carlo events for the indicated signal channel.

17.3.2.4 Reconstruction of the B_s^0 decay vertex

For the $B_s^0 \to D_s^-\pi^+$ channel, the B_s^0 decay vertex was reconstructed by considering all D_s^- candidates and adding a fourth track from the remaining tracks in the event. This track was required to have opposite charge with respect to the pion track from the D_s^- and $p_T > 1.0$ GeV. The four-track decay vertex was refitted including ϕ and D_s^- mass constraints, and requiring that the total momentum of the B_s^0 vertex pointed to the primary vertex and the momentum of D_s^- vertex pointed to the B_s^0 vertex.

For the $B_s^0 \to D_s^- a_1^+$ channel, the B_s^0 candidates were reconstructed combining the D_s^- candidates with the a_1^+ candidates. A six-track vertex fit was then performed with mass constraints for the tracks from ϕ and D_s^-; due to the large a_1^+ natural width, the three tracks from the a_1^+ were not constrained to a_1^+ mass. Similarly, for the K^{*0} mode, the tracks from K^{*0} were not constrained to the K^{*0} mass. As in the $B_s^0 \to D_s^-\pi^+$ channel, the total momentum of the B_s^0 vertex was required to point to the primary vertex and the momentum of D_s^- vertex was required to point to the B_s^0 vertex.

In order to be selected as B_s^0 candidates, the four-track and six-track combinations were required to give a probability greater than 1% for the vertex fit. The signed separation between the reconstructed B_s^0 vertex and the primary vertex, and between the D_s^- and B_s^0 vertex were required to be positive (the momentum should not point backward to the parent vertex). To improve the purity of the sample, further cuts were imposed: the accepted B_s^0 candidates were required to have a proper decay time greater than 0.4 ps, an impact parameter smaller than 55 μm and $p_T > 10$ GeV.

17.3.3 Background analysis

Background to the channels being considered for the measurement of Δm_s can come from two sources: from other four- or six-body B-hadron decay channels, and from combinatorial background (random combinations with some or all particles not originating from a B decay).

For $B_s^0 \to D_s^- \pi^+$, the following four-body decay channels were considered as potential sources of background: $B_d^0 \to D_s^- \pi^+$, $B_d^0 \to D^- \pi^+$ (with $D^-, D_s^- \to \phi\pi^-$ and $\phi \to KK$) and $\Lambda_b^0 \to \Lambda_c^+ \pi^-$ followed by $\Lambda_c^+ \to pK^-\pi^+$. The similar six-body decay channels considered as potential sources of background for $B_s^0 \to D_s^- a_1^+$ were: $B_d^0 \to D_s^- a_1^+$, $B_d^0 \to D^- a_1^+$ (with $D^-, D_s^- \to \phi\pi^-$, $\phi \to KK$ for the ϕ mode and $D^-, D_s^- \to K^{*0}K^-$, $K^{*0} \to K^+\pi^-$ for the K^{*0} mode) and $\Lambda_b^0 \to \Lambda_c^+ \pi^-$ followed by $\Lambda_c^+ \to pK^-\pi^+\pi^+\pi^-$. The simulated four- and six-body background events were passed through the detailed detector-simulation program, reconstructed and analysed using the same programs, the same conditions and the same cuts as the signal events.

In order to study the combinatorial background, a very large sample of simulated inclusive-muon events is needed. The results presented here are based on a sample of 1.1 million $b\bar{b} \to \mu X$ events, with $p_T > 6$ GeV and $|\eta| < 2.4$ for the muon corresponding the trigger conditions. Even with this large sample, the background estimate is based on very low statistics.

The $b\bar{b} \to \mu X$ sample was analysed in the framework of the fast-simulation program ATLFAST++ (see Section 2.5), applying the same algorithms and the same cuts that were used for the fully-simulated samples. A careful check was made of the performance of the fast-simulation program by running it on signal and six-body background samples, and comparing the results with those from the detailed simulation. Good agreement was obtained for the number of reconstructed events and the widths of the mass peaks for the reconstructed particles.

17.3.4 Evaluation of signal and background statistics

The reconstructed B_s^0 invariant-mass distributions in the decay channels $B_s^0 \to D_s^-(\phi\pi^-)\pi^+$, $B_s^0 \to D_s^-(\phi\pi^-)a_1^+(\rho^0\pi^+)$ and $B_s^0 \to D_s^-(K^{*0}K^-)a_1^+(\rho^0\pi^+)$ are shown in Figure 17-26, Figure 17-27 and Figure 17-28, respectively, for an integrated luminosity of 10 fb^{-1}.

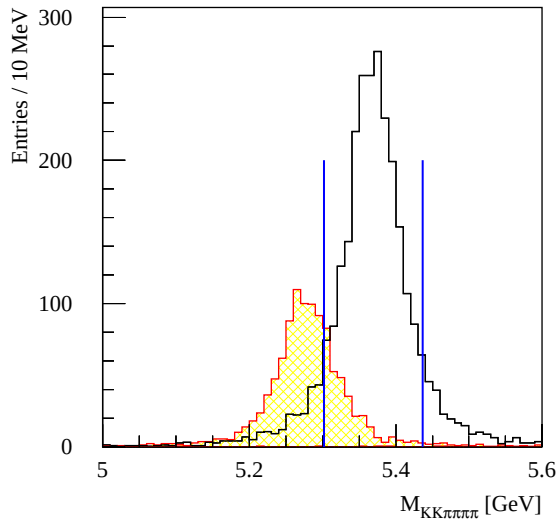

Figure 17-26 Reconstructed B_s^0 invariant-mass distribution for $B_s^0 \to D_s^-(\phi\pi^-)\pi^+$ decays. The open histogram shows the signal, the hatched histogram shows the background from $B_d^0 \to D_s^-(\phi\pi^-)\pi^+$ decays and the dark histogram shows the fake reconstructed B_s^0 decays from the signal sample. The combinatorial background is not shown here.

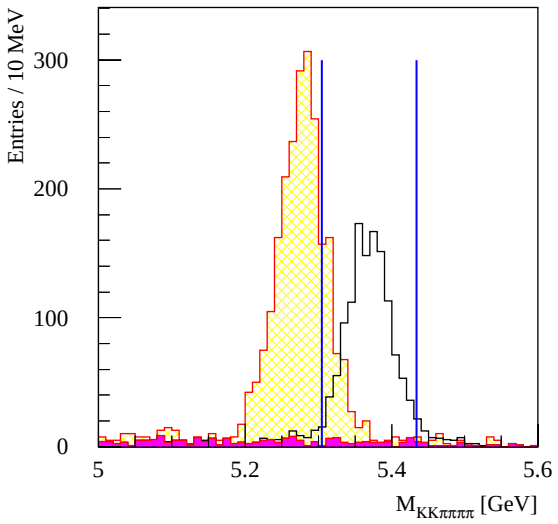

Figure 17-27 Reconstructed B_s^0 invariant-mass distribution for $B_s^0 \to D_s^-(\phi\pi^-)a_1^+(\rho^0\pi^+)$ decays. The open histogram shows the signal, the hatched histogram shows the background from $B_d^0 \to D_s^-(\phi\pi^-)a_1^+(\rho^0\pi^+)$ decays and the dark histogram shows the fake reconstructed B_s^0 decays from the signal sample. The combinatorial background is not shown here.

For $B_s^0 \to D_s^-(\phi\pi^-)a_1^+$ and $B_s^0 \to D_s^-(K^{*0}K^-)a_1^+$ the results are from fully-simulated samples; for $B_s^0 \to D_s^-(\phi\pi^-)\pi^+$ they are from a fast-simulation analysis. The reconstructed mass distributions for the four- and six-body background channels are also shown in the figures. The combinatorial background, for which only very limited statistics are available, is not shown in these figures; its distribution is expected to be flat in the relevant mass range. The mass resolutions of the reconstructed B_s^0 mesons were obtained by fitting single-Gaussian distributions. The results are 33.5 MeV for $B_s^0 \to D_s^-(\phi\pi^-)\pi^+$, 32.2 MeV for $B_s^0 \to D_s^-(\phi\pi^-)a_1^+(\rho^0\pi^+)$ and 30.5 MeV for $B_s^0 \to D_s^-(K^{*0}K^-)a_1^+(\rho^0\pi^+)$.

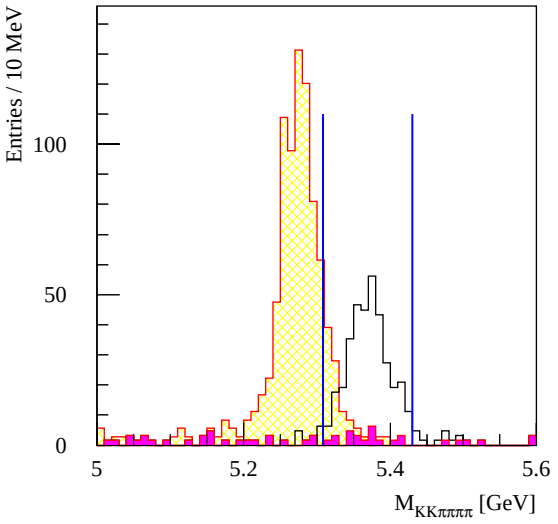

Figure 17-28 Reconstructed B_s^0 invariant-mass distribution for $B_s^0 \to D_s^-(K^{*0}K^-)a_1^+(\rho^0\pi^+)$ decays. The open histogram shows the signal, the hatched histogram shows the background from $B_d^0 \to D_s^-(K^{*0}K^-)a_1^+(\rho^0\pi^+)$ decays and the dark histogram shows the fake reconstructed B_s^0 decays from the signal sample. The combinatorial background is not shown here.

The numbers of events expected for the various signal and background channels that have been analysed are given in Table 17-11 for an integrated luminosity of 30 fb^{-1}. The cross-sections and

Table 17-11 Signal and background samples analysed for the study of $B_s^0 - \bar{B}_s^0$ oscillations. The numbers presented for the combinatorial background are for the sum of the $B_s^0 \to D_s^-(\phi\pi^-)\pi^+$ and $B_s^0 \to D_s^-(\phi\pi^-)a_1^+$ analysis channels.

Process	Cross-section [μb]	Events for 30 fb^{-1}	Simulated events	Rec. events	Rec. events for 30 fb^{-1}
$B_s^0 \to D_s^-(\phi\pi^-)\pi^+$	1.281x10^{-5}	384 180	47 775	5 018	6 750
$B_s^0 \to D_s^-(\phi\pi^-)a_1^+$	1.281x10^{-5}	384 180	18 784	1 506	3 620
$B_s^0 \to D_s^-(K^{*0}K^-)a_1^+$	1.589x10^{-5}	476 970	9 988	208	1 000
$B_d^0 \to D_s^-(\phi\pi^-)\pi^+$	4.519x10^{-6}	135 570	24 698	694	710
$B_d^0 \to D_s^-(\phi\pi^-)a_1^+$	2.098x10^{-5}	629 460	9 699	186	1 390
$B_d^0 \to D_s^-(K^{*0}K^-)a_1^+$	2.605x10^{-5}	781 500	9 988	41	345
$B_d^0 \to D^-(\phi\pi^-)a_1^+$	8.204x10^{-6}	246 135	9 949	1	3
$B_d^0 \to D^-(K^{*0}K^-)a_1^+$	7.651x10^{-6}	229 530	9 989	6	15
$\Lambda_b^0 \to \Lambda_c^+(pK\pi\pi\pi)\pi^-$	1.968x10^{-6}	59 040	10 994	0	0
Comb. background sum (ϕ mode only)			1.1x10^6	see text	14 500

the numbers of events for 30 fb^{-1} are calculated after the following cuts: one *b*-quark is required to decay semileptonically giving a muon with $p_T > 6.0$ GeV and $|\eta| < 2.5$; the other *b*-quark is required to give rise to the given *B*-hadron decay channel. In addition, in the simulated samples the final-state particles from the given *B*-hadron decay channel are required to have $p_T > 0.5$ GeV and $|\eta| < 2.5$.

The events reconstructed from the samples for the exclusive decay modes were counted in a $\pm 2\sigma_{B_s}$ window around the nominal B_s^0 mass. Using the fraction of events reconstructed in the simulated sample and the number of events expected for an integrated luminosity of 30 fb^{-1}, the expected number of reconstructed events was estimated. The numbers or reconstructed events given in the table have been corrected for the additional cuts imposed on the simulated sample using the cross-section given by PYTHIA, for muon efficiency (on average 0.85) and for LVL2 trigger efficiency (0.85).

A total of 10370 reconstructed events is expected for the ϕ mode of the $B_s^0 \to D_s^-\pi^+$ and $B_s^0 \to D_s^- a_1^+$ decay channels for an integrated luminosity of 30 fb^{-1}. An increase of around 30% in the number of events could be obtained by including the K^{*0} mode for both B_s decay channels.

The only significant backgrounds come from the $B_d^0 \to D_s^- a_1^+$ and $B_d^0 \to D_s^-\pi^+$ channels, and from the combinatorial background. Note that the number of reconstructed events from the two B_d^0 decay channels is conservative since the branching-ratio values used are upper limits. As expected, due to the combination of the D^- mass shift ($M_{D^-} - M_{D_s^-} = 90$ MeV) and B_d^0 mass shift ($M_{B_s} - M_{B_d} \approx 100$ MeV), very few $B_d^0 \to D^- a_1^+$ events are reconstructed in a $\pm 2\sigma_{B_s}$ window

around B_s^0 nominal mass. Due to the different decay topology, the $\Lambda_b^0 \to \Lambda_c^+ \pi^-$ channel does not give any contribution to the background. No contribution to the background for $B_s^0 \to D_s^- \pi^+$ is expected from $B_d^0 \to D^- \pi^+$ and $\Lambda_b^0 \to \Lambda_c^+ \pi^-$ decays.

The statistics available for estimating the combinatorial background are very limited, despite the large size (1.1 million events) of the $\mu 6X$ sample. Each simulated event was therefore passed 20 times through the fast-simulation program, different random smearing of the track parameters being applied each time. The number of background events was counted in an enlarged mass window ($[M_{B_s} - 150$ MeV, $M_{B_s} + 150$ MeV$]$). On average, 0.4 events per pass were reconstructed in the mass window summing the $B_s^0 \to D_s^- \pi^+$ and $B_s^0 \to D_s^- a_1^+$ channels for the ϕ mode. Normalising to the number of $\mu 6X$ events expected for an integrated luminosity of 30 fb^{-1}, applying correction factors for the reconstruction and trigger efficiencies, and scaling for the size of the mass window, the combinatorial background was estimated to be 14 500 events in a $\pm 2\sigma_{B_s}$ window around the B_s^0 mass, and the range of variation was estimated to be between 9600 and 20 900 event at 90% CL. Correlations between the results from the 20 passes were taken into account. The corresponding background for the K^{*0} mode of the $B_s^0 \to D_s^- a_1^+$ is 5600 events.

17.3.5 Determination of the proper-time resolution

The proper time of the reconstructed B_s^0 candidates was computed from the reconstructed transverse decay length, d_{xy}, and from the B_s^0 transverse momentum, p_T:

$$t = \frac{d_{xy} M_{B_s^0}}{c p_T} \equiv d_{xy} g$$

where $g = M_{B_s^0}/(c p_T)$.

The transverse decay length is the distance between the interaction point and the b-hadron decay vertex, projected onto the transverse plane. Figure 17-29 shows, for the example of the $B_s^0 \to D_s^-(\phi\pi^-) a_1^+(\rho^0\pi^+)$ decay mode, the difference $d_{xy} - d_{xy}^0$ fitted with two Gaussian functions, where d_{xy}^0 is the true transverse decay length. For each event, the decay-length uncertainty, $\sigma_{d_{xy}}$, was estimated from the covariance matrices of the tracks associated with the vertices. The pull of the transverse decay length, $(d_{xy} - d_{xy}^0)/\sigma_{d_{xy}}$, was found to have a Gaussian shape with a width of $S_{d_{xy}} = 0.958 \pm 0.020$.

The distribution for $(g - g_0)/g_0$, shown in Figure 17-30, also has a Gaussian shape, with a width of $S_g = (0.631 \pm 0.013)\%$. Here $g_0 = t_0/d_{xy}^0$, with t_0 being the true proper time. The proper-time resolution function $\mathrm{Res}(t, t_0)$ was parametrised, in close analogy with [17-33], with a Gaussian function:

$$\mathrm{Res}(t, t_0) = \frac{1}{\sqrt{2\pi}\sigma(t_0)} \exp\left[-\frac{1}{2}\left(\frac{t - t_0}{\sigma(t_0)}\right)^2\right],$$

with the width $\sigma(t_0)$ computed event-by-event as:

$$\sigma(t_0) = \sqrt{(g S_{d_{xy}} \sigma_{d_{xy}})^2 + (t_0 S_g)^2}.$$

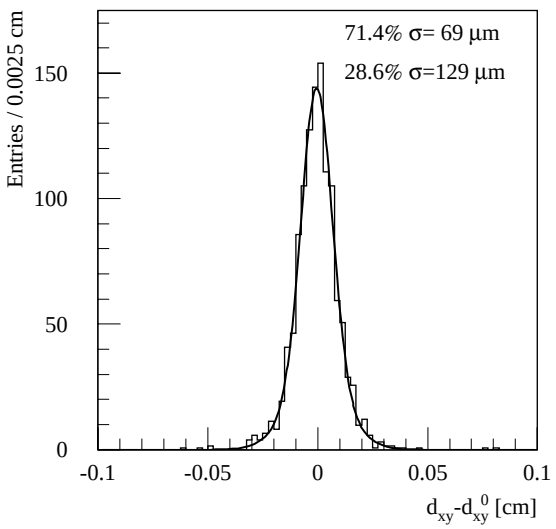

Figure 17-29 Decay-radius resolution for the decay channel $B_s^0 \to D_s^-(\phi\pi^-)a_1^+(\rho^0\pi^+)$

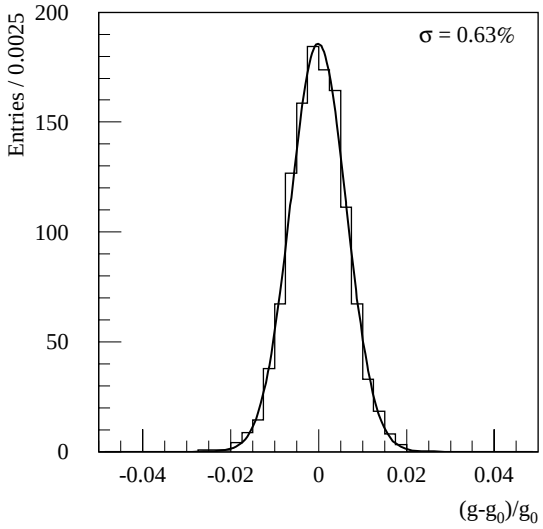

Figure 17-30 Fractional resolution on g-factor for the decay channel $B_s^0 \to D_s^-(\phi\pi^-)a_1^+(\rho^0\pi^+)$

Figure 17-31 shows, for the example of the $B_s^0 \to D_s^-(\phi\pi^-)a_1^+(\rho^0\pi^+)$ decay mode, the proper-time resolution together with the parametrisation obtained from the $\mathrm{Res}(t, t_0)$ function given above. The parametrisation reproduces well the tails seen in the distribution for reconstructed events. The $t - t_0$ distribution has an rms of 0.071 ps. To illustrate the deviations from the Gaussian shape, when the distribution was fitted with two Gaussian functions, the widths obtained were 0.050 ps for the narrow Gaussian function (60.5%) and 0.093 ps for the broader one (39.5%). Similar distributions were obtained for the other two analysed channels.

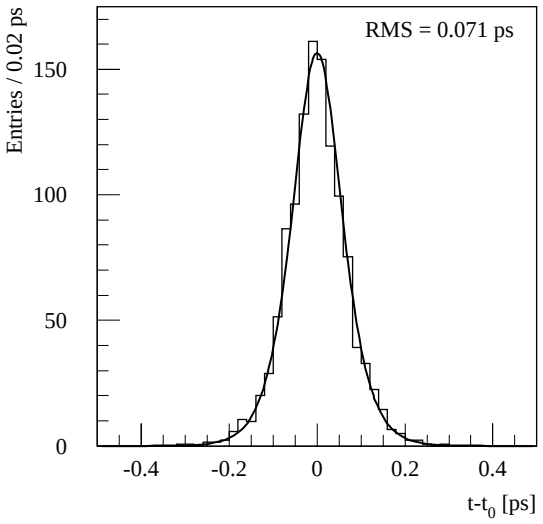

Figure 17-31 Proper-time resolution for the decay channel $B_s^0 \to D_s^-(\phi\pi^-)a_1^+(\rho^0\pi^+)$. The curve displays the resolution as obtained from the $\mathrm{Res}(t, t_0)$ function given in the text.

17.3.6 Extraction of Δm_s reach

The maximum value of Δm_s measurable in ATLAS was estimated using a simplified Monte Carlo model. The input parameters of this model were: the number of signal events, N_{sig}, the number of background events from B_d^0 decays, N_{B_d}, and the number of events for the combinatorial background, N_{comb}; the characteristics of the events involved in the computation of the proper-time resolution (see below); the wrong-tag fraction. The wrong-tag fraction was assumed to be the same for both B_s^0 and B_d^0 mesons: $\omega_{\mathrm{tag}} = 0.22$ (see Section 17.2.2.4). The proper-time resolution obtained with detailed simulation for the $B_s^0 \to D_s^-(\phi\pi^-)a_1^+(\rho^0\pi^+)$ decay channel was assumed for all signal events.

Monte Carlo experiments with $N_{\rm sig}$ signal events oscillating with a given frequency Δm_s, together with N_{B_d} B_d^0 background events oscillating with frequency Δm_d and $N_{\rm comb}$ combinatorial events (no oscillations), were generated in the following way. For each event with an oscillating b hadron, the true proper time t_0 was generated according to an exponential distribution using the slope obtained from a fit of the true proper time of the simulated sample. The uncertainty on the measurement of the transverse decay length, $\sigma_{d_{xy}}$, and the true value of the g-factor, g_0, were generated at random according to the distributions obtained from the simulated samples (the distributions were fitted with the sum of three and two Gaussian functions for $\sigma_{d_{xy}}$ and g_0, respectively). From the computed true decay length, $d_{xy}^0 = t_0/g_0$, the corresponding reconstructed decay length was generated as $d_{xy} = d_{xy}^0 + S_{d_{xy}}\sigma_{d_{xy}}\Omega$, with Ω being a random number distributed according to the normal distribution. The reconstructed g-factor was generated as $g = g_0 + g_0 S_g \Omega'$, with Ω' a random number distributed according to the normal distribution function. From the transverse decay length and g-factor, the reconstructed proper time was then computed as $t = g d_{xy}$. The probability for the event to be mixed or unmixed was determined from the t_0 and Δm_s values (Δm_d value if the event was a B_d^0 event). For a fraction of the events, selected at random, the state was changed between mixed and unmixed, according to the wrong-tag fraction, $\omega_{\rm tag}$. For the combinatorial background, the reconstructed proper time was generated assuming that it has the same distribution as the one for B_s^0 mesons. Half of the combinatorial events were added to the mixed events and half to the unmixed events.

The asymmetry

$$A(t) = \frac{\frac{dn(++)}{dt} - \frac{dn(+-)}{dt}}{\frac{dn(++)}{dt} + \frac{dn(+-)}{dt}} \sim D \frac{\cos\Delta m_s t}{\cosh\frac{\Delta\Gamma_s t}{2}}$$

was computed for the 'generated events' for $t > 0.4$ ps, in agreement with the experimental cut on the reconstructed proper time. Here *n(++)* is the number of events with the tagging muon and the reconstructed D_s having the same sign ($B_{s_0}^0$ meson did not oscillate), and *n(+–)* is the number of events in which they have unlike sign (B_s^0 meson oscillated). The asymmetry distribution $A(t)$ was then analysed with a method based on the amplitude fit proposed in [17-34]. According to this method, $A(t)$ was fitted with the function $A_{\rm fit}\cos(\Delta m_s t)/\cosh(\Delta\Gamma_s t/2)$ where Δm_s and $\Delta\Gamma_s$ were constant values and $A_{\rm fit}$ was the only free parameter. The fit was repeated for different values of Δm_s and an $A_{\rm fit}(\Delta m_s)$ distribution was obtained ($\Delta\Gamma_s$ was a constant parameter). The value of Δm_s which gave the maximum $A_{\rm fit}$ was considered as the Δm_s measured in that experiment.

The experiment was performed for different true Δm_s values. For each true Δm_s value, the experiment was repeated 1000 times. The fitted amplitude distribution was averaged over these 1000 experiments as a function of the Δm_s value in the asymmetry fit function $A_{\rm fit}(\Delta m_s)$; the average distribution was then fitted with a Gaussian function and the width σ of the distribution was determined. An experiment was called 'successful' if the measured Δm_s value was within $\pm 1.96\sigma$ of the true Δm_s value, corresponding to a 95% probability that the measured Δm_s value would fall within $\pm 1.96\sigma$ of the true value given Gaussian errors. The maximum value of Δm_s for which 95% of the generated experiments were successful was taken as the maximum value of Δm_s which is expected to be measurable. For each experiment, the difference between the reconstructed Δm_s and the true Δm_s was computed; this distribution was fitted with a Gaussian function and its width was taken as the accuracy of the Δm_s measurement.

With an integrated luminosity of 30 fb^{-1}, the maximum value of Δm_s that is expected to be measurable is 38.5 ps^{-1}.The expected accuracy of the Δm_s measurement is 0.04 ps^{-1} for Δm_s = 12 ps^{-1}, 0.05 ps^{-1} for Δm_s = 20 ps^{-1}, 0.10 ps^{-1} for Δm_s = 30 ps^{-1}, and 0.16 ps^{-1} for Δm_s = 38.5 ps^{-1}. The time-dependent asymmetry for a single 'experiment' with an integrated luminosity of 30 fb^{-1} is shown in Figure 17-32, when Δm_s = 38.5 ps^{-1}.

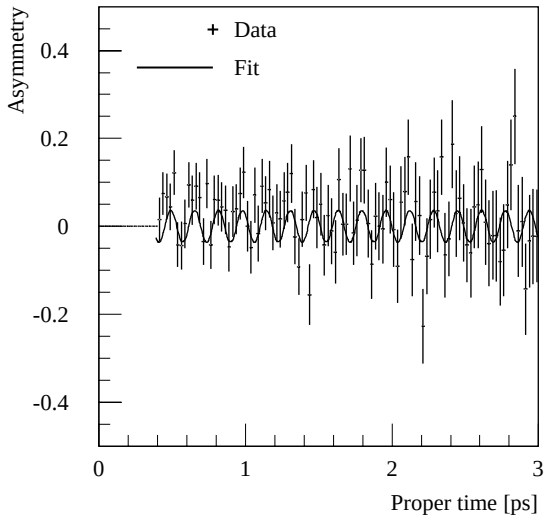

Figure 17-32 The time-dependent asymmetry for Δm_s = 38.5 ps^{-1} in a single 'experiment' for an integrated luminosity of 30 fb^{-1}. The crosses correspond to 'simulated data' and the line to the fit with a cosine function.

17.3.7 Dependence of Δm_s reach on experimental quantities

The previous analysis was repeated for different values of the integrated luminosity 5 fb^{-1}, 10 fb^{-1}, 20 fb^{-1} and 30 fb^{-1}. The proper-time resolution was also varied, by changing the widths $S_{d_{xy}}$ and S_g by the same factor. The values of the scaling factors used were 0.75 and 1.5. For these values, the proper-time resolution, fitted with two Gaussian functions with the same normalisation ratio as for the nominal values, had the widths 0.033 ps (0.074 ps) and 0.064 ps (0.138 ps), respectively, to be compared with the nominal 0.050 ps (0.093 ps); the value in parenthesis is the width of the second, broader Gaussian function. All combinations given by these proper-time resolution values and integrated luminosity values were tried. The dependence of the Δm_s reach on the integrated luminosity is shown in Figure 17-33 for different values of the proper-time resolution, and assuming that $\Delta\Gamma = 0$.

The dependence of the maximum value of Δm_s which can be measured on the fraction of signal events in the sample of reconstructed events is shown in Figure 17-34 for the nominal proper-time resolution. The values in the plot were obtained assuming that the number of signal events remains constant at the values given in Table 17-11 and that the numbers of combinatorial background events and of background events coming from B_d^0 change with the same factor. The dependence on the background is not very strong for the assumed conditions; however, this dependence could change if the combinatorial background has some asymmetry or if it has a different proper time dependence. If the combinatorial background was taken to be 20 900 events, which was estimated to be the 90% CL upper limit for the combinatorial background, while the numbers of signal events and background events from other sources were as in Table 17-11, the maximum value of Δm_s that is expected to be measurable would be 36.0 ps^{-1} with an integrated luminosity of 30 fb^{-1}.

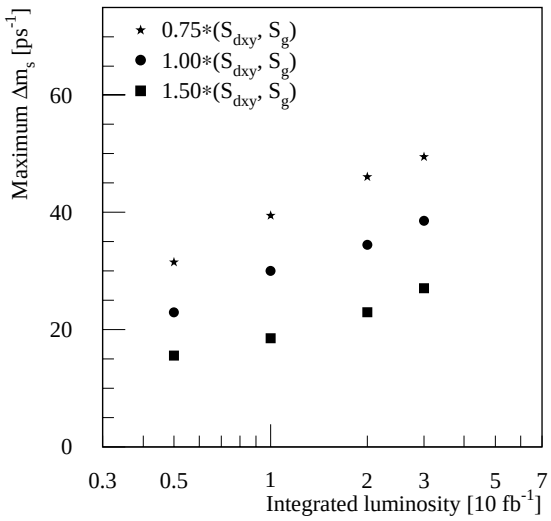

Figure 17-33 Sensitivity range of ATLAS for the Δm_s measurement as a function of the integrated luminosity for various proper-time resolutions.

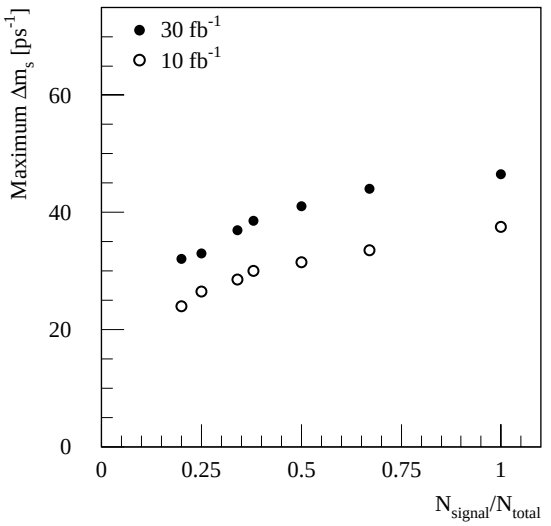

Figure 17-34 Sensitivity range of ATLAS for the Δm_s measurement as a function of the signal content of the sample, for nominal proper-time resolution and integrated luminosities of 10 fb^{-1} and 30 fb^{-1}.

For values of $\Delta\Gamma/\Gamma_s \leq 0.2$ no significant change in the sensitivity range was observed. If the K^{*0} mode was also considered, the Δm_s limit did not improve, mainly due to the decrease in the signal-to-background ratio resulting from the conservative estimate of the combinatorial background to be added to the sample.

17.3.8 Conclusions

The maximum value of Δm_s which we expect to be able to measure with 30 fb^{-1} data, with the performance of the detector presented in the previous sections and with the assumed cross-sections of the involved processes, is 38.5 ps^{-1}. The expected accuracy of the Δm_s measurement is 0.16 ps^{-1} for Δm_s = 38.5 ps^{-1}, and better for lower values of Δm_s. The dependence of the Δm_s sensitivity range on various parameters shows that we should be able to measure Δm_s over the whole range predicted in the Standard Model.

17.4 Rare decays $B \to \mu\mu(X)$

17.4.1 Introduction

Certain rare decays, for which the decay products themselves provide a distinctive signature that can be used in the LVL1 trigger, can be studied very effectively in ATLAS making use of the high rate of *B*-hadron production. These so-called 'self-triggering' modes include decays of the type $B_{d,s} \to \mu\mu(X)$. Such decays involve flavour-changing neutral currents (FCNC) and are

strongly suppressed in the Standard Model, with predicted branching ratios typically in the range 10^{-5}–10^{-10}. New physics might result in significant enhancements compared to the Standard Model predictions.

The potential to study rare decays of the type $B_{d,s} \to \mu\mu(X)$ is discussed in the following. For the purely muonic decays, ATLAS will be sensitive to branching ratios of order 10^{-9} and should be able to measure the branching ratio for $B_s \to \mu\mu$ assuming the Standard Model prediction. Large-statistics samples will be collected for decays of the type $b \to (s, d)ll$ that give final states such as $B_d^0 \to K^{*0}\mu\mu$, $B_d^0 \to \rho^0\mu\mu$ and $B_s^0 \to \phi^0\mu\mu$. This will allow precise measurements to be made of the decay dynamics, as well as of the branching ratios, giving significant constraints on new physics.

These rare decay modes are forbidden at the tree level in the Standard Model, so the decays involve loop diagrams. In non-standard models of electroweak interactions, FCNC processes can be allowed at the tree level and thus, the branching ratios of these rare decays would not be so suppressed. In addition, in the presence of new physics, additional particles may be present in the loops again enhancing the decay probability. Due to the very low Standard Model predictions for the branching fractions for purely muonic decays, a significant enhancement in measured branching fractions would clearly demonstrate the effects of new physics. The measurement of the lepton forward–backward asymmetry in semimuonic B decays is another promising tool to probe the new physics beyond the Standard Model.

In the context of Standard Model, the principal interest lies in the measurement of the branching fractions of the $B \to \mu\mu(X)$ channels. The measurement of the branching fractions of the decays $B_d^0 \to \rho^0\mu\mu$ and $B_d^0 \to K^{*0}\mu\mu$ allows the CKM matrix-element ratio $|V_{td}|/|V_{ts}|$ to be determined. The square of this ratio is useful also for the estimation of the ratio of the mass differences $\Delta m_s/\Delta m_d$ in the $B_d^0 - \bar{B}_d^0$ and $B_s^0 - \bar{B}_s^0$ systems (see [17-35]), complementary to direct measurements of the oscillation periods.

17.4.2 Theoretical approach

In the theoretical approach used here, the effective Hamiltonian which governs the $b \to q$ transition has the following structure [17-36]:

$$H_{eff} = \frac{G_F}{\sqrt{2}} V_{tb} V_{tq}^* \sum_i C_i(\mu) O_i(\mu)$$

where $q = d, s$, G_F is the universal Fermi constant, $C_i(\mu)$ are the Wilson coefficients which contain the information on the short-distance dynamics of the theory, and $O_i(\mu)$ are the basis operators. The parameter μ in the equation is a typical scale which separates the long and short-distance (LD and SD) physics. For B decays it is convenient to choose this scale $\mu \sim m_b$. The contributions of the LD effects are contained in the $B \to M$ transition form factors that enter in the calculation of the Wilson coefficients, where B is the B-meson and M is any other meson. These form factors are the main source of uncertainties in the theoretical predictions for exclusive decays (see, *e.g.* [17-37] and references therein).

Table 17-12 presents theoretical predictions for the branching ratios of $B \to K^*\gamma$ and $B \to K^*\mu\mu$. The columns ‘QM’ and ‘Lat’ present the results obtained with the two sets of transition form factors taken from [17-37]. The column ‘Ali’ refers to the results in [17-38]. In order to estimate

the uncertainties in the CKM matrix elements V_{td} and V_{ts}, the uncertainty on the form factors is required. One can see from the table that the results obtained with the different theoretical approaches agree within the errors and are consistent with the experimental data.

Table 17-12 Non-resonant branching fractions of radiative and rare *B*-decays.

Decay mode	QM $BR \times \lvert V_{ts}/0.038\rvert^2$	Lat $BR \times \lvert V_{ts}/0.041\rvert^2$	Ali $BR \times \lvert V_{ts}/0.033\rvert^2$	Experimental *BR*
$B \to K^*\gamma$	4.2×10^{-5}	4.2×10^{-5}	$(4.9 \pm 2.0) \times 10^{-5}$	$(4.0 \pm 1.9) \times 10^{-5}$ [17-32]
$B \to K^*ee$	1.50×10^{-6}	1.45×10^{-6}	$(2.3 \pm 0.9) \times 10^{-6}$	$< 2.9 \times 10^{-4}$ [17-32]
$B \to K^*\mu\mu$	1.15×10^{-6}	1.10×10^{-6}	$(1.5 \pm 0.6) \times 10^{-6}$	$< 2.3 \times 10^{-5}$ [17-32]

For studies of SD effects, information about the Wilson coefficient $C_{7\gamma}$ is important. The experimental measurement of the lepton forward–backward asymmetry in semileptonic *B*-decays caused by FCNC transitions will provide information on this coefficient. To illustrate the possible sensitivity to new physics, one can compare the Minimal Supersymmetric Standard Model (MSSM) with the Standard Model. In each case, a range of allowed values of $C_{7\gamma}$ is provided by CLEO results on rare radiative decays [17-39]. The quantity $R_{7\gamma} = C_{7\gamma}^{MSSM}(M_W)/C_{7\gamma}^{SM}(M_W)$ lies in one of the following intervals

$$-4.2 < R_{7\gamma} < -2.4 \qquad 0.4 < R_{7\gamma} < 1.2$$

The shape of the differential forward–backward asymmetry distribution turns out to be qualitatively different for positive and negative values of $R_{7\gamma}$ [17-40]. The lepton forward–backward asymmetry remains sensitive to the value of the Wilson coefficient after the experimental cuts, and thus it will be possible for ATLAS to test the Standard Model in the exclusive $B \to Ml^+l^-$ decays.

17.4.3 Simulation of rare *B*-decay events

17.4.3.1 Simulation of $B_{d,s} \to \mu\mu$

Purely muonic *B*-decays are predicted to have very low branching fractions within the Standard Model (10^{-9}–10^{-10}), whereas they may have significantly higher ones in non-standard models. The following Standard Model branching ratios were assumed for the present study [17-41]: $Br(B_d \to \mu\mu) = 1.5 \times 10^{-10}$, $Br(B_s \to \mu\mu) = 3.5 \times 10^{-9}$. Simulations were made with the PYTHIA event generator. The Inner-Detector response was simulated fully and the particles were reconstructed in the Inner Detector. The muon reconstruction efficiency was assumed to be 85% for the LVL1 trigger muon, and 95% for the other muon. About 1500 signal events were simulated in

Table 17-13 Efficiencies of selection cuts for $B_{d,s} \to \mu\mu$

Cut	Efficiency
Decay length of B^0 > 0.7 mm, χ^2/dof < 3	0.70
Angle between p_T of B^0 and line joining primary and B^0 decay vertices $\alpha < 1^o$	0.94
Isolation: $n_{ch}(p_T > 0.8$ GeV) = 0 in a cone $\theta < 20^o$	0.40

each channel, with $p_T(\mu) > 6$ GeV and $|\eta(\mu)| < 2.5$ for each muon. About 9000 background events were simulated and reconstructed with the same criteria. The sensitivity of signal events to cuts is shown in Table 17-13.

After applying all the cuts, the numbers of events expected for 30 fb^{-1} at low luminosity are shown in Table 17-14. The $B_s \to \mu\mu$ channel can be observed, assuming the branching fraction predicted by the Standard Model. The significance of the signal, however, is only 2.8σ.

Table 17-14 Number of expected events after three years of LHC running at low luminosity (30 fb^{-1})

Channel	Signal	Background
$B_d^0 \to \mu\mu$	4	93
$B_s^0 \to \mu\mu$	27	93

The feasibility to reconstruct the purely muonic decays $B_{d,s}^0 \to \mu\mu$ at high luminosity was also estimated. This estimation was based on the assumption that the pixel *B* layer will be operational at high luminosity, and that no degradation of the impact-parameter and p_T resolutions will occur. For each channel, 1000 signal events with corresponding pile-up were fully simulated and reconstructed in the Inner Detector. The background was studied at the particle level using the parametrisation for p_T and impact parameter resolutions from ATLFAST. A sample of 10 000 background events with pile-up was used for this study. The numbers of events for both channels and the corresponding backgrounds expected for 100 fb^{-1} are given in Table 17-15.

Table 17-15 Number of expected events after one year of LHC running at high luminosity (100 fb^{-1}).

Channel	Signal	Background
$B_d^0 \to \mu\mu$	14	660
$B_s^0 \to \mu\mu$	92	660

Combining the low- and high-luminosity samples, a 4.3σ significance can be obtained for the channel $B_s^0 \to \mu\mu$. The 95% CL upper limit for the branching fraction for $B_d^0 \to \mu\mu$ obtained with the combined sample would be $3\text{x}10^{-10}$. It should be noted, however, that the *B* mass resolution of 69 MeV is not good enough to separate B_s and B_d on an event-by-event basis, but their relative fractions would have to be fitted from the joint mass distribution. The study of rare muonic *B* decays at high luminosity will significantly improve the results which can be obtained at low luminosity, especially if data collection is continued for several years.

17.4.3.2 Simulation of $B_d^0 \to K^{*0}\mu\mu$, $B_d^0 \to \rho^0\mu\mu$ and $B_s^0 \to \phi^0\mu\mu$

Studies have been performed for the rare-decay channels $B_d^0 \to K^{*0}\mu\mu$, $B_d^0 \to \rho^0\mu\mu$, and $B_s^0 \to \phi^0\mu\mu$. In the future, the potential for studying $B_s^0 \to K^{*0}\mu\mu$ and $B_d^0 \to \omega\mu\mu$ decays will also be evaluated. The following predicted values for the branching ratios were assumed: $Br\ (B_s^0 \to \phi^0\mu\mu) = 1\times10^{-6}$, $Br(B_d^0 \to K^{*0}\mu\mu) = 1.5\times10^{-6}$ and $Br(B_d^0 \to \rho^0\mu\mu) = 1\times10^{-7}$. Events were simulated fully and then reconstructed in the Inner Detector. For each channel, 1500 signal events were analysed with the following experimental cuts: both muons were required to have $p_T(\mu) > 6$ GeV and $|\eta(\mu)| < 2.5$, and both hadrons were required to have $p_T(h) > 1$ GeV and $|\eta(h)| < 2.5$. The same reconstruction and trigger efficiencies for the muons were assumed as above. The reconstruction efficiency for hadrons was found to be 90% averaged over the full pseudorapidity region for $p_T > 1$ GeV.

The uncertainty in the theoretical predictions for the transition form-factors influences strongly the dimuon q^2-distributions (where q^2 is the invariant-mass squared of the muon pair) and the branching ratios. Different analytical expressions for the matrix element for $B_d^0 \to K^{*0}\mu\mu$ were

implemented in PYTHIA and the results were compared. It was found that the individual-muon p_T distributions remain essentially unaffected by the choice of form factors. An important conclusion from this study was that, although the q^2-dependence of form factors affects q^2-dependence of the events, it does not influence the efficiency of triggering and reconstructing the signal events, or the rejection of the background [17-42].

The mass resolutions obtained by the Gaussian fit with the full reconstruction were: $\sigma(\phi^0)$ = 3 MeV, $\sigma(B_s^0 \to \phi^0\mu\mu)$ = 52 MeV, $\sigma(K^{*0})$ = 30 MeV, $\sigma(B_d^0 \to K^{*0}\mu\mu)$ = 50 MeV, and $\sigma(B_d^0 \to \rho^0\mu\mu)$ = 55 MeV. In case of the ρ^0 resonance, requiring the mass to be in the interval [0.60,0.94] MeV corresponded to 82% efficiency. In order to exclude the reflection of K^* to ρ^0, hadron pairs forming an invariant mass within two standard deviations around the nominal K^* mass using the K/π mass assignments were excluded. For the remaining pairs, both hadrons were assumed to be pions and the effective mass of the pair was required to be within the ρ^0 mass window. The possible reflections from $B_s^0 \to \phi^0\mu\mu$ to $B_d^0 \to \rho^0\mu\mu$ and $B_d^0 \to K^{*0}\mu\mu$ were found to be negligible.

For background studies, the following reactions were simulated by PYTHIA: B_d^0-meson decays $B_d^0 \to J/\psi K_S^0$, $B_d^0 \to \rho^0\mu\mu$ and $B_d^0 \to \omega^0\mu\mu$, B_s^0-meson decays $B_s^0 \to K^{*0}\mu\mu$ and $B_s^0 \to \phi^0\mu\mu$, semimuonic decays of one of the *b*-quarks, and semimuonic decays of both *b*-quarks. It was found that the last reaction gave the main contribution to the background. Therefore, 13000 events of this type were simulated and analysed similarly to the signal events.

The mass distributions for the $B_{d,s}^0$ signals are shown, together with those for the backgrounds, in Figure 17-35, Figure 17-36 and Figure 17-37. The sensitivity of signal events to the applied cuts is shown in Table 17-16. The application of all cuts leaves about 9% of the simulated signal events. The expected numbers of signal and background events after three years of LHC running at low luminosity are presented in Table 17-17.

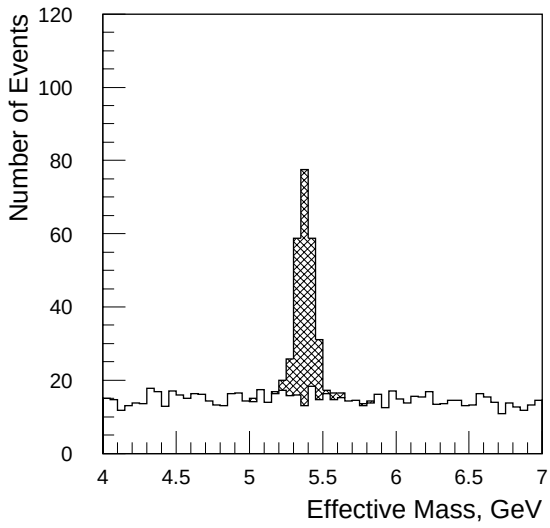

Figure 17-35 Reconstructed signal (cross-hatched) and background for $B_s^0 \to \phi^0\mu\mu$ with 30 fb^{-1}.

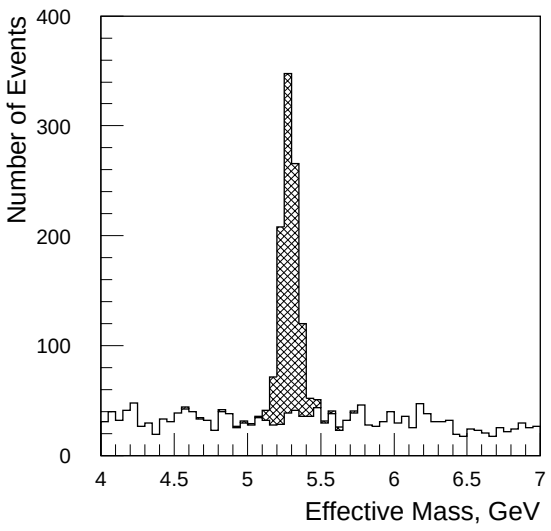

Figure 17-36 Reconstructed signal (cross-hatched) and background for $B_d^0 \to K^{*0}\mu\mu$ with 30 fb^{-1}.

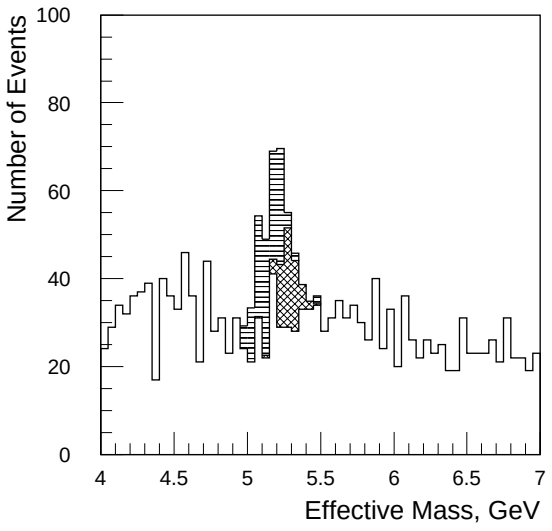

Figure 17-37 Reconstructed signal (cross-hatched) and background for $B_d^0 \to \rho^0\mu\mu$ with 30 fb^{-1}. The horizontally hatched histogram shows the reflection from $B_d^0 \to K^{*0}\mu\mu$.

Table 17-16 Efficiencies of selection cuts for $B_d^0 \to K^{*0}\mu\mu$, $B_d^0 \to \rho^0\mu\mu$ and $B_s^0 \to \phi^0\mu\mu$.

Cut	$B_d^0 \to K^{*0}\mu\mu$	$B_d^0 \to \rho^0\mu\mu$	$B_s^0 \to \phi^0\mu\mu$
$m(hh) = m\ (K^{*0}, \varphi^0) \pm 2\sigma$ OR $m(\pi\pi) \in [0.60, 0.94]$ MeV	0.81	0.82	0.82
Decay length of $B^0_d > 0.8$ mm, χ^2/ d.o.f <10, angle between p_T of B^0_d and line joining primary and B^0_d decay vertices $\alpha < 1^o$	0.45	0.40	0.43
$m(\mu\mu) \notin J/\psi$, $m(\mu\mu) \notin \psi'$ $	0.85	0.86	0.85
$n_{ch}(p_T>0.8$ GeV) = 0 in a cone $\theta< 5^o$	0.65	0.67	0.65
p_T of $K^{*0} > 5$ GeV	0.71		
$m(hh\mu\mu) = m(B_d^0)^{+\sigma}_{-2\sigma}$	0.74	0.75	0.75

Table 17-17 Number of events expected after 30 fb^{-1} of low-luminosity running.

Channel	*Br*	Signal	Background
$B_d^0 \to \rho^0\mu\mu$	10^{-7}	220	950
$B_d^0 \to K^{*0}\mu\mu$	1.5×10^{-6}	2000	290
$B_s^0 \to \phi^0\mu\mu$	10^{-6}	410	140

From the ratio of the branching fractions for the two decay modes $B_d^0 \to K^{*0}\mu\mu$ and $B_d^0 \to \rho^0\mu\mu$, the ratio $|V_{td}|/|V_{ts}|$ can be determined, since the decay rates are proportional to the respective CKM matrix elements:

$$\frac{N(B_d^0 \to \rho^0\mu\mu)}{N(B_d^0 \to K^{0*}\mu\mu)} = \kappa_d \frac{|V_{td}|^2}{|V_{ts}|^2},$$

where κ_d is the ratio of form factors squared.

The theoretical uncertainty of the form factor for the decay $B_d^0 \to \rho^0\mu\mu$ is large due to the *u*-loop matrix-element contribution to the $b \to dll$ process. It was shown in [17-43], that the $|V_{td}|/|V_{ts}|$ ratio can be determined experimentally with a small theoretical uncertainty arising from hadronic form factors in the dimuon kinematic mass region 16.5 GeV^2 < q^2 < 19.25 GeV^2. The fraction of signal events in this kinematic region was estimated using the GI form factor parametrisation [17-42] and found to be 24% of the total number of events. With these events, the ratio $|V_{td}|/|V_{ts}|$ can be measured with a statistical accuracy of 14% for 30 fb^{-1} of low-luminosity data; the theoretical systematic uncertainty is about 7% [17-43].

Note that the reflection from $B_d^0 \to K^{*0}\mu\mu$ to $B_d^0 \to \rho^0\mu\mu$ is sizeable (see Figure 17-37) due to the large difference in the branching ratios assumed for the two channels. After assigning the wrong mass hypotheses to the K^{*0} decay products, the decay $B_d^0 \to K^{*0}\mu\mu$, reconstructed as $B_d^0 \to \rho^0\mu\mu$, gives a mass peak below, but close to, the $B^0{}_d$ mass. In contrast, the combinatorial background is approximately flat. Taking into account that the branching ratio for $B_d^0 \to K^{*0}\mu\mu$ can be measured with high accuracy, it is assumed that the $B_d^0 \to \rho^0\mu\mu$ signal can be extracted from an overall fit.

17.4.4 The measurement of the forward–backward asymmetry

The forward–backward (*FB*) charge asymmetry $A_{FB}(\hat{s})$ in the decays $B_d^0 \to M\mu\mu$ is defined by the following equation:

$$A_{FB}(\hat{s}) = \frac{\int_0^1 \left(\frac{d^2\Gamma}{ds\,d\cos\theta}\right) d\cos\theta - \int_{-1}^0 \left(\frac{d^2\Gamma}{ds\,d\cos\theta}\right) d\cos\theta}{\int_0^1 \left(\frac{d^2\Gamma}{ds\,d\cos\theta}\right) d\cos\theta + \int_{-1}^0 \left(\frac{d^2\Gamma}{ds\,d\cos\theta}\right) d\cos\theta}$$

where θ is the angle between the lepton l^+ and the *B*-meson direction in the rest frame of the lepton pair, and $\hat{s} = q^2/M_B^2$. In Figure 17-38 the theoretical curves for $A_{FB}(\hat{s})$ in the Standard Model and MSSM for $B_d^0 \to K^{*0}\mu\mu$ [17-37] are presented. These curves include the resonant contributions for J/ψ and ψ'.

The general trend of the behaviour of A_{FB} for Standard Model is that the asymmetry is positive at low q^2, has a zero at $\hat{s} \approx 0.14$, and then becomes negative, irrespective of the details of the form-factor behaviour (except for the resonant region – for a detailed analysis of the behaviour of *FB* asymmetry in this region, see [17-40]). The maximum of $A_{FB}(\hat{s})$ occurs at $\hat{s} = 0.05$. For the

MSSM, the shape of A_{FB} is sensitive to the value of $C_{7\gamma}$, or equivalently to the value of $R_{7\gamma}$. For $R_{7\gamma} > 0$ the shape is similar to that in the Standard Model, but for $R_{7\gamma} < 0$ the asymmetry is negative at low q^2.

In the simulation, the resonant region $0.33 < \hat{s} < 0.55$ was excluded from the analysis. To estimate the experimental resolution of A_{FB} measurements in $B_d^0 \to K^{*0}\mu\mu$ decays, the total numbers of signal and background events after three years of low-luminosity running were used (see Table 17-17). The numbers of signal and background events for each $\hat{s}$-region were estimated assuming that the signal $d\Gamma/d\hat{s}$ distribution is similar to the one presented in [17-44], and that the background distribution is flat. The sensitivity to the asymmetry was then the calculated, and results are presented in Table 17-18 where it can be seen that three regions are useful for measurements. If negative values of A_{FB} are experimentally observed in the first $\hat{s}$-region, this will demonstrate a clear signal of non-standard physics. The measurements in the second and third $\hat{s}$-regions, which practically do not depend on the models, will show possible systematic uncertainties in the experimental data.

In Figure 17-38, the average values of A_{FB} and the expected errors on A_{FB} for three $\hat{s}$-regions are shown. One can see that the expected measurement accuracy is sufficient to separate the Standard Model and the MSSM in the case $R_{7\gamma} < 0$ using measurements in the first $\hat{s}$-region.

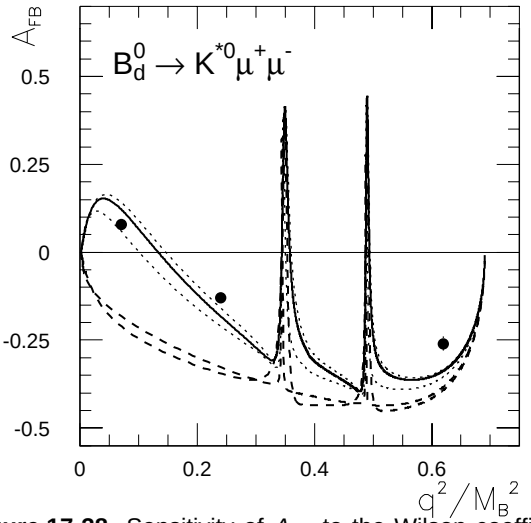

Figure 17-38 Sensitivity of A_{FB} to the Wilson coefficient $C_{7\gamma}$. The three points are the simulation results. The solid line shows the Standard Model prediction, the dotted lines show the range predicted by the MSSM for $R_{7\gamma} > 0$ and the dashed lines show the range predicted by the MSSM for $R_{7\gamma} < 0$.

Table 17-18 Expected sensitivity for asymmetry measurements after three years at low luminosity (30 fb^{-1}) and theoretical predictions of the asymmetry. Here $\hat{s}_{min} = 4m_l^2/M_B^2$, where m_l is the lepton mass and $\hat{s}_{max} = (M_B - M_K^*)^2/M_B^2$.

Quantity	$\hat{s}_{min} \div 0.14$	$0.14 \div 0.33$	$0.55 \div \hat{s}_{max}$
δA_{FB}(stat.)	5%	4.5%	6.5%
SM A_{FB}	10%	-14%	-29%
MSSM A_{FB}	$(-17 \div 0.5)$ %	$(-35 \div -13)$ %	$(-33 \div -29)$ %

17.4.5 Conclusions

ATLAS will be able to study rare semi-muonic and muonic *B*-decays. It will be possible to measure branching ratios of the decay channels $B_s^0 \to \phi^0 \mu\mu$, $B_d^0 \to K^{*0} \mu\mu$ and $B_d^0 \to \rho^0 \mu\mu$. From the ratio of branching fractions for the two latter channels, it will be possible to determine the ratio $|V_{td}|/|V_{ts}|$ with a 14% statistical accuracy within the Standard Model. Measurements of the forward–backward charge asymmetry in the decay $B_d^0 \to K^{*0} \mu\mu$ will also be feasible and may reveal new physics effects, for example in some parameter-space regions of the MSSM.

Combining three years of low-luminosity and one year of high-luminosity data taking, the decay $B_s \to \mu\mu$ would be observed and a stringent upper limit for the decay $B_d \to \mu\mu$ would be set, assuming Standard Model branching ratios. Given that these decays are highly suppressed in the Standard Model, there are hopes that any non-standard physics effects would significantly enhance the branching ratios, in which case the signals would be easier to detect.

17.5 Precision measurements of *B* hadrons

Precision measurements of *B*-hadrons are important to validate the Standard Model and to search for new physics. As discussed above, ATLAS can make a significant contribution to the study of *CP*-violation in *B*-meson decays. It will also be able to measure the oscillation parameter of the B_s meson for values of Δm_s well beyond the range predicted in the Standard Model, and the corresponding mass difference $\Delta\Gamma_s$. In addition, measurements of very rare decays to final states with muon pairs will be possible, testing and constraining parameters of the Standard Model, and possibly revealing new physics. In this Section some additional physics topics are presented that can be addressed by ATLAS.

Many precision measurements will be made in other experiments before 2005 when ATLAS is expected to take its first data. For example, the BaBar, Belle and CLEO experiments at e^+e^- machines will address in detail the decays of the B^0 and B^+ mesons, while experiments at hadron machines will also study B_s and B_c mesons and *B*-baryons. Nevertheless, given the large statistics available in a variety of exclusive final states (see Table 17-19), ATLAS may be able to improve the precision of mass, lifetime and other measurements in some cases. For example, ATLAS is expected to measure the B_s lifetime with a statistical accuracy of 0.7% after three years at low luminosity with the $B_s^0 \to J/\psi\phi$ channel.

In the following two examples of precision studies are discussed: the analysis of the B_c meson, and measurements of Λ_b polarisation.

17.5.1 Measurements with the B_c meson

The B_c meson exhibits some unique features regarding both its production and decay properties, due to its explicit double-heavy-flavour content. In addition, in hadronic spectroscopy the properties of B_c can be used in interpolating between charmonium and bottomonium resonances, and QCD-inspired potential models can be scrutinised with different combinations of charm and bottom constituent masses. Since m_c/m_b is small, the B_c system enables testing the heavy-quark symmetries and understanding better the next-to-leading terms in the heavy-quark effective theory, and its application to heavy–light *B* mesons.

The expected large production rates should bring the possibility of detecting the non-leptonic decay mode $B_c \to J/\psi\pi$, or the semileptonic one $B_c \to J/\psi\mu\nu$, through charmonium decaying into a muon pair [17-45]. With the foreseen statistics, the former channel would allow a very precise determination of the B_c mass. The latter one could be useful to extract the CKM matrix element V_{cb} [17-46], provided that the B_c production cross-section can be determined elsewhere. Furthermore, the B_c lifetime measurement is a very clean test of the interplay between strong and weak interactions inside hadrons, as both quarks can undergo a weak decay inside the same particle, in contrast to usual singly-heavy *D* or *B* mesons. Doubly-heavy baryons [17-47] are potentially detectable at the LHC, completing the interesting panorama of heavy–heavy systems.

Table 17-19 Number of reconstructed events with ATLAS with an integrated luminosity of 30 fb^{-1}.

Decay mode	Branching fraction	*N* of events
$B_d^0 \to \pi\pi$	0.7×10^{-5}, estimated from limit in [17-17]	6 500
$B_d^0 \to J/\psi K_s^0$	4.45×10^{-4} [17-32]	630 000
$B_s^0 \to D_s\pi$	3.0×10^{-3}, same as for $B_d^0 \to D\pi$ in [17-32]	6 800
$B_s^0 \to J/\psi\phi$	9.3×10^{-4} [17-32]	300 000
$B_s^0 \to D_s a_1$	6.0×10^{-3}, same as for $B_d^0 \to D a_1$ in [17-32]	3600
$B_d^0 \to D_s a_1$	$< 2.6\times10^{-3}$ [17-32]	5 900
$\Lambda_b \to J/\psi\Lambda^0$	3.7×10^{-4} [17-49]	75 000
$B_c \to J/\psi\pi$	0.2×10^{-2} estimate based on [17-47] and [17-48].	12 000
$B_c \to J/\psi\mu\nu$	2×10^{-2} estimate based on[17-47] and [17-48].	300 000 (inclusive reconstruction)

17.5.2 Λ_b polarisation measurement

17.5.2.1 Introduction

Polarisation measurements of *B*-hadrons could clarify the problems of different polarisation models [17-50] that failed to reproduce the existing data on strange-hyperon production [17-51]. In particular, information about the quark-mass dependence of polarisation effects could be obtained. Hadrons with non-zero spin can be polarised perpendicularly to their production plane. For symmetry reasons, in *pp* collisions this polarisation vanishes as the Feynman variable x_F approaches zero, so that the expected observed polarisation in ATLAS is smaller than in experiments covering more forward regions (for example LHCb). Thus, a polarisation measurement in ATLAS will require very high precision.

17.5.2.2 Method of polarisation measurement

A polarisation measurement can be obtained with Λ_b baryons via the angular distributions of the cascade decay $\Lambda_b \to J/\psi\Lambda^0$, $J/\psi \to \mu\mu$, $\Lambda^0 \to p\pi$. The decay is described by the Λ_b polarisation, P_b, four helicity amplitudes and the known asymmetry parameter for the $\Lambda^0 \to p\pi$ decay, $\alpha(\Lambda^0) = 0.646$. The $J/\psi \to \mu\mu$ decay depends only on one amplitude which is absorbed into the normalisation.

The angular distribution function, ω, can be written in terms of five measurable angles that are defined in Figure 17-39:

$$\omega(\theta, \theta_1, \theta_2, \varphi_1, \varphi_2) = \frac{1}{4\pi^2} \sum_{i=1}^{19} \alpha_i f_i \times F_i(\theta, \theta_1, \theta_2, \varphi_1, \varphi_2) ,$$

where the α_i are bilinear combinations of the four helicity amplitudes, the f_i are combinations of P_b and $\alpha(\Lambda^0)$, and the F_i are functions of the five angles θ, θ_1, θ_2, φ_1 and φ_2. The expressions for α_i, f_i and F_i can be found in [17-52]. From the measured angular distributions, 19 independent moments $\langle F_i \rangle$ can be obtained. Since the system of equations is over-constrained, the polarisation, P_b, can be determined.

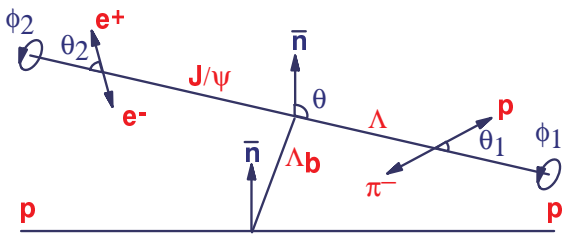

Figure 17-39 The definition of the five angles. θ is the polar angle of the Λ^0 momentum $\bar{p}_\Lambda$ in the Λ_b rest frame relative to the normal $\bar{n}$ to the production plane. θ_1 and φ_1 are the angles of the proton in Λ^0 rest frame, with the *z*-axis being parallel with p_Λ and the *y*-axis being parallel to $\bar{n} \times \bar{p}_\Lambda$. θ_2 and φ_2 are defined for the J/ψ decay in a similar way.

17.5.2.3 Event selection, background and estimation of precision

The events were simulated within the Inner Detector only. Efficiency factors were applied for muon reconstruction and identification. The LVL2 trigger will select $J/\psi \to \mu\mu$ decays with p_T larger than 6 GeV for one muon and 3 GeV for the other muon. The muon tracks in the Inner Detector were fitted requiring that they originate from a common point. A simultaneous J/ψ mass and vertex constrained fit was performed. The transverse flight distance from the primary vertex to the Λ_b decay point was required to be larger than 250 μm and, for the Λ^0 candidate, a transverse flight distance in the range 1 – 42 cm was required. A second fit then constrained the J/ψ mass and Λ^0 momentum to point to the dimuon vertex. The J/ψ–Λ^0 invariant-mass spectrum had a Gaussian core with σ = 22 MeV. The proper decay-time of the Λ_b candidate was required to be larger than 0.5 ps. Within the mass region of three standard deviations around the Λ_b mass, the background was ~2% and it was dominated by J/ψ's from B-hadrons combined with Λ^0's coming from the fragmentation. The Λ_b reconstruction properties and background composition are summarised in Table 17-20. After three years of low-luminosity data-taking, the number of reconstructed $\Lambda_b \to J/\psi\Lambda^0$ events will be ~75 000. The branching ratio for $\Lambda_b \to J/\psi\Lambda^0$ was taken to be 3.7×10^{-4}, as measured by CDF [17-49].

Table 17-20 Summary of the Λ_b analysis with an integrated luminosity of 30 fb^{-1}.

Number of reconstructed $\Lambda_b \to J/\psi\,\Lambda^0$ decays.	**75 000**
Number of background events, dominated by $J/\psi+\Lambda^0$, where the J/ψ is from a *B*-decay and the Λ^0 is from fragmentation.	1 500
Reconstruction efficiency of $J/\psi \to \mu\mu$ for decays with $p_T(\mu_1) > 6$ GeV and $p_T(\mu_2) > 3$ GeV. Efficiency includes the trigger and the combined muon identification, including calorimetry.	0.78
Reconstruction efficiency of $\Lambda^0 \to p\pi$ with $p_T(p) > 0.5$ GeV and $p_T(\pi) > 0.5$ GeV. Reconstructed Λ^0 candidate must have decay radius $1 < r < 42$ cm and invariant mass within $\pm 3\sigma$ from the Λ_b mass.	0.56
Efficiency of final cuts on Λ_b proper lifetime $\tau > 0.5$ ps, invariant mass within $\pm 3\sigma$ from the Λ_b mass.	0.48
J/ψ mass resolution, $\sigma_{J/\psi}$	39 MeV
Λ^0 mass resolution, $\sigma_{\Lambda 0}$	2.5 MeV
Λ_b mass resolution, $\sigma_{\Lambda b}$	22 MeV
Resolution on Λ_b proper decay-time τ, σ_t	0.073 ps
Statistical error on Λ_b polarisation P_b, σ_{Pb}	0.016

The estimated statistical precision of the polarisation measurement using the above method of moments was $\sigma(P_b)$~0.016. Some of the Λ_b baryons are produced indirectly through the decays of heavier states $\Sigma_b \to \Lambda_b \pi$, $\Sigma^*_b \to \Lambda_b \pi$. Thus, the observed Λ_b polarisation will be diluted and, according to the present models, the dilution factor is expected to be in the range 0.34–0.67 [17-52]. The lower value corresponds to the case in which the polarisations of the Λ_b, Σ_b and Σ^*_b are in the relation $P_b = P(\Sigma_b) = -P(\Sigma^*_b)$, and the upper limit corresponds to $P_b = -P(\Sigma_b) = P(\Sigma^*_b)$.

The large Λ_b sample, characterised by a small background, can be used for a precise determination of the Λ_b lifetime. The maximum-likelihood fit, taking into account the proper decay time resolution and assuming a single exponential for the background with mean decay time the same as for the neutral *B* hadrons, gives a statistical precision of 0.3%.

17.6 Conclusions on the *B*-physics potential

The expected *B*-physics performance of ATLAS is summarised in the Table 17-21. High-statistics studies of *CP* violation in various *B*-decay channels will give measurements of the unitarity-triangle angles α and β, and will search for deviations from the Standard Model. These measurements will be complemented by the measurement of the B_s-oscillation parameter Δm_s. Several other measurements will be made with the B_s and Λ_b, thus complementing the data from e^+e^- *B*-factories. Finally, very rare *B* decays will be accessible as well.

Table 17-21 Summary of the *B*-physics potential. The assumed integrated luminosity is 30 fb^{-1}, except for the rare dimuon decays, where 130 fb^{-1} is assumed.

Observable	Expected accuracy or value	World data (situation in 1999)
$\sin 2\alpha$	$\delta_{stat}(\alpha) \approx 2°$	Estimated to be in the range $\sin 2\alpha = -0.26^{+0.29}_{-0.28}$ [17-11]
$\sin 2\beta$	$\delta_{stat}(\sin 2\beta) = 0.010$	$\sin 2\beta = 0.79^{+0.41}_{-0.44}$ [17-10]
Angle γ		Estimated to be in the range $\gamma = (59.5^{+8.5}_{-7.5})°$ [17-11]
$\xi = 2\lambda \sin\gamma \lvert V_{ub}\rvert / \lvert V_{cb}\rvert$	$\delta(\xi)$=0.03 (stat.)	ξ = 0.024–0.054 [17-32]
Δm_s	Measured up to 38.5 ps^{-1}	Δm_s > 12.4 ps^{-1} [17-31]
$\tau(B_s^0)$	$\delta\Gamma_s/\Gamma_s$=0.7% (stat.)	$\tau(B_s^0) = 1.54 \pm 0.07$ ps [17-32]
$\Delta\Gamma_s$ in the B_s-meson system	$\delta(\Delta\Gamma_s)/\Delta\Gamma_s$=12% (stat.)	$\Delta\Gamma_s/\Gamma_s$ < 0.83 [17-53]
$\lvert V_{td}\rvert / \lvert V_{ts}\rvert$ from rare decays	$\delta(\lvert V_{td}\rvert / \lvert V_{ts}\rvert)$=14% (stat.)	$\lvert V_{td}\rvert / \lvert V_{ts}\rvert$ < 0.27 [17-32]
$\tau(\Lambda_b)$	$\delta(\tau(\Lambda_b))/\tau(\Lambda_b)$ =0.3% (stat.)	$\tau(\Lambda_b) = 1.24 \pm 0.08$ ps [17-32]
$Br(B_s^0 \to \mu\mu)$	4.3σ signal (SM)	Not measured yet
$Br(B_d^0 \to \mu\mu)$	Upper limit 3x10^{-10} (SM)	Not measured yet
A_{FB} of muons in rare semileptonic decays	$\delta(A_{FB})$< 5%(stat.)	Not measured yet

17.7 References

17-1 M. Mangano, ‘Heavy Flavour Production’, talk given at the LHCC Workshop ‘Theory of LHC processes’, CERN, 9–13 February 1998.

17-2 B. L. Combridge, J. Kripfganz and J. Ranft, Phys. Lett. **B70** (1977) 234;
R. Cutler, D. Sivers, Phys. Rev. **D17** (1978) 196;
H. U. Bengtsson, Computer Physics Communications **31** (1984) 323.

17-3 T. Sjostrand, ‘PYTHIA 5.7 and JETSET 7.4: Physics and manual’, LU-TP-95-20 (1995).

17-4 P. Eerola, ‘The inclusive muon cross-section in ATLAS’, ATLAS Internal Note ATL-PHYS-98-120 (1998);
S. P. Baranov and M. Smizanska, ‘Beauty production overview from Tevatron to LHC’, ATLAS Internal Note ATL-PHYS-98-133 (1998).

17-5 A. Dell’Acqua, ‘DICE manual version 0.10’, ATLAS Internal Note ATL-SOFT-95-011 (1995).

17-6 E. Richter-Was, D. Froidevaux and L. Poggioli, ‘ATLFAST 2.0 a fast simulation package for ATLAS’, ATLAS Internal Note ATL-PHYS-98-131 (1998).

17-7 E. J. Buis *et al.*, ‘Update of Inner Detector performance parameterisations’, ATLAS Internal Note ATL-INDET-98-215 (1998).

17-8 M. Smizanska *et al.*, ‘Overview of simulations for ATLAS *B*-physics studies in period 1996-1999’, ATLAS Internal Note ATL-COM-PHYS-99-042 (1999).

17-9 ATLAS Collaboration, Trigger performance status report, CERN / LHCC / 98-15 (1998).

17-10 CDF collaboration, 'A Measurement of sin2β from $B \to J/\psi K^0_S$ with the CDF Detector'. CDF internal note CDF/PUB/BOTTOM/CDF/4855, Feb 1999.

17-11 F. Parodi, P. Roudeau and A. Stocchi, 'Constraints on the parameters of the CKM matrix by end 1998', hep-ex/9903063 (1999).

17-12 P. F. Harrison (ed.) *et al.*, BaBar Collaboration, 'The BaBar Physics Book: Physics at an Asymmetric *B* Factory', SLAC-R-0504, Oct 1998.

17-13 M. Gronau, A. Nippe and J. L. Rosner, Phys. Rev. **D47** (1993) 1988.

17-14 ATLAS Collaboration, Technical Proposal, CERN/LHCC/94-43 (1994).

17-15 R. Fleischer and T. Mannel, Phys. Lett. **B397** (1997) 269.

17-16 D. Rousseau and P. Sherwood, 'Measurement of sin(2α) in the $B^0_d \to \pi\pi$ channel', ATLAS-COM-PHYS-99-012 (1999).

17-17 R. Godang *et al.*, CLEO Collaboration, Phys. Rev. Lett. **80** (1998) 3456.

17-18 D. Buskulic *et al.*, ALEPH Collaboration, Phys. Lett. **B384** (1996) 471.

17-19 R. Fleischer, CERN-TH/98-60 (1998), to appear in Eur. Phys. J. **C.**

17-20 A. Ali and D. London, 'Profiles of the Unitarity Triangle and CP-violating Phases in the Standard Model and Supersymmetric Theories', DESY preprint 99-042, UdeM-GPP-TH-99-58, hep-ph/9903535 (1999).

17-21 M. Beneke, G. Buchalla and I. Dunietz, Phys. Rev. **D54** (1996) 4419;
M. Beneke *et al.*, 'Next-to-leading order QCD corrections to the lifetime differences of B_s mesons', CERN-TH 98-261 (1998).

17-22 I. Dunietz, Phys. Rev. **D52** (1995) 3048;
A. S. Dighe *et al.*, 'Angular distributions and lifetime differences in $B_s \to J/\psi\phi$ decays', FERMILAB-PUB 95-345 T (1995);
A. S. Dighe, I. Dunietz and R. Fleischer, 'Resolving a discrete ambiguity in the CKM angle β through $B_{(u,\,d)} \to J/\psi K^*$ and $B_s \to J/\psi\phi$ decays', CERN-TH 98-85 (1998).

17-23 B. Cano-Coloma and M. A. Sanchez-Lozano, Nucl. Phys. **B508** (1997) 753.

17-24 E. J. Eichten, C. H. Hill and C. Quigg, Phys. Rev. Lett. **71** (1993) 4116;
E. J. Eichten, C. H. Hill and C. Quigg, 'Orbitally Excited Heavy-Light Mesons Revisited', FERMILAB-CONF-94/118-T (1994).

17-25 M. Smizanska, 'Determination of $\Delta\Gamma_s$ by ATLAS and the impact of non-zero $\Delta\Gamma_s$ on other B^0_s studies', ATLAS Internal Note ATL-PHYS-99-003 (1999).

17-26 CDF Collaboration, Phys. Rev. Lett. **75** (1995) 3068.

17-27 G. Barenboim, J. Bernabeu, J. Matias and M. Raidal, '*CP* asymmetries in B_s decays and spontaneous *CP* violation', hep-ph/9901265 (1999).

17-28 G. Barenboim, J. Bernabeu and M. Raidal, Phys. Rev. Lett. **80** (1998) 4625.

17-29 I. Dunietz, Phys. Lett. **B270** (1991) 75.

17-30 LHCb Collaboration, Technical Proposal, CERN/LHCC/98-4 (1998).

17-31 The LEP *B* Oscillation Working Group, 'Combined Results on B^0 oscillations: Results for Summer 1998 Conferences', LEPBOSC 98/3 (1998).

17-32 C. Caso *et al.*, Particle Data Group, Eur. Phys. J. **C3** (1998) 1.

17-33 D. Buskulic *et al.*, ALEPH Collaboration, Eur. Phys. J. **C7** (1999) 553.

17-34 H. G. Moser and A. Roussarie, Nucl. Instr. and Methods **A384** (1997) 491.

17-35 A. Ali, 'Flavour changing neutral current processes and CKM phenomenology', DESY preprint 97-256 (1997), hep-ph/9801270. To be published in the Proceedings of the First APCTP Workshop Pacific Particle Physics Phenomenology, Oct. 31- Nov. 2, 1997, Seoul, South Korea.

17-36 B. Grinstein, M. B. Wise and M. J. Savage, Nucl. Phys. **B319** (1989) 271.

17-37 D.Melikhov, N.Nikitin and S.Simula, Phys. Rev. **D57** (1998) 6814.

17-38 A.Ali, '*B* Decays, Flavour Mixings and *CP* Violation in the Standard Model', DESY preprint 96-106 (1996), hep-ph/9606324. Published in the Proceedings of the XX International Nathiagali Summer College on Physics and Contemporary Needs, Bhurban, Pakistan, June 24–July 13, 1995, eds. Riazuddin, K.A. Shoaib *et al.*; Nova Science Publishers, New York.

17-39 P. Cho, M. Misiak and D. Wyler, Phys. Rev. **D54** (1996) 3329.

17-40 D. Melikhov, N. Nikitin and S.Simula, Phys. Lett **B430** (1998) 332.

17-41 A. Ali, Nucl. Instr. and Methods **A384** (1996) 8.

17-42 D. Melikhov *et al.*, 'Studying the physics beyond the Standard Model in rare semileptonic *B*-decay $B \to K^* \mu^+ \mu^-$ with ATLAS detector', ATLAS Internal Note PHYS-98-123 (1998).

17-43 T. M. Aliev, C. S. Kim and M. Savci, Phys. Lett. **B441** (1998) 410.

17-44 D. Melikhov, N. Nikitin and S. Simula, Phys. Lett **B410** (1997) 290.

17-45 F. Albiol *et al.*, 'Searching for B_c mesons in ATLAS', ATLAS Internal Note ATL-PHYS-94-058 (1994).

17-46 M. Galdon and M. A. Sanchis-Lozano, Z. Phys. **C71** (1996) 277.

17-47 M. A. Sanchis-Lozano, Nucl. Phys. **B440** (1995) 251.

17-48 M. Lusignoli and M. Masetti, Z. Phys. **C51** (1991) 549.

17-49 CDF collaboration, Phys. Rev. **D55** (1997) 1142.

17-50 T.A. De Grand and H.I. Miettinen, Phys. Rev. **D24** (1981) 2419;
Y. Hama and T. Kodama, Phys. Rev. **D48** (1993) 3116;
J. Ellis, D. Kharzeev and A. Kotzinian, Z. Phys. **C69** (1996) 467;
W.G.D. Dharmaratna and G.R. Goldstein, Phys. Rev. **D53** (1996) 1073.

17-51 J. Lach, 'Hyperon polarisation: an experimental overview', FERMILAB-CONF-92-378, Dec 1992. Invited talk given at International Workshop on Flavour and Spin in Hadronic and Electromagnetic Interactions, Turin, Italy, 21-23 Sep 1992.

17-52 J. Hrivnac, R. Lednicky and M. Smizanska, J. Phys. **G21** (1995) 629.

17-53 CDF collaboration, 'Measurement of the B_s^0 meson lifetime using semileptonic decays', to be published in Phys. Rev. **D59** (1999).